SIMULATION OF TUNNEL EXCAVATIONS

IN SQUEEZING GROUND

By

EZZAT A. HANAFY, B.Sc.(Eng.), M.Eng.

A Thesis

Submitted to the School of Graduate Studies

in Partial Fulfilment of the Requirements

for the Degree

Doctor of Philosophy

McMaster University

March 1981

DOCTOR OF PHILOSOPHY (1981)   McMASTER UNIVERSITY
(Civil Engineering)   Hamilton, Ontario

TITLE: Simulation of Tunnel Excavations in Squeezing Ground

AUTHOR: Ezzat Ahmed Dia Eldin Hanafy
      B.Sc. (Eng.) (Cairo University)
      M.Eng. (McMaster University)

SUPERVISORS: Dr. J.J. Emery and
      Dr. Y.P. Vaid

NUMBER OF PAGES: xiii, 182

ABSTRACT

Empirical, analytical, and semi-rational methods for the stability analysis and design of underground openings are generally not adequate to consider the major design parameters for tunnels in squeezing ground. Tunnel construction in squeezing ground and the increasing North American use of the precast concrete segmental liners were the prime motivation for developing an elastic-plastic-creep simulation of tunnel excavation and liner placement.

Based on the finite element method, the simulation method incorporates: the primary state of stress; excavation in stages; liner placement delay; and determination of the elastic-plastic-creep response for each stage of construction, including ground-interface-support system interaction for both plane strain (two-dimensional) and advancing face (three-dimensional) conditions. Construction sequences of excavation and support placement are simulated using 'deactivation' and 'reactivation' operations on the stiffness matrix terms corresponding to the selected rate of face advance. Incorporation of the inelastic behaviour of both ground yielding and time-dependent deformations is based on the initial stress and initial strain methods, respectively. The three-dimensional stress analysis near the advancing face is based on an axisymmetric approach and Fourier series approximation that allows the non-symmetric radial and axial loadings due to the primary state of stress to be considered. The axisymmetric approach is also extended to include inelastic ground behaviour.

A comprehensive design for a tunnel in a formation that may exhibit squeezing is given. Using this typical field problem, several parametric studies are presented. It is shown that the elastic deformations are only significant near the advancing face and their influence is very minor at a distance of about two times the tunnel diameter. The consideration of the actual advancing face condition, lining placement delay, and the use of a soft backing can significantly reduce the design stresses developed in the liner.

The simulation method presented can be used to develop improved ground characterization through the monitoring of tunnel convergence followed by back analysis.

ACKNOWLEDGEMENTS

TABLE OF CONTENTS

TABLE OF CONTENTS (Cont'd)

LIST OF TABLES

ix

LIST OF FIGURES

x

LIST OF FIGURES (Cont'd)

LIST OF FIGURES (Cont'd)

xii

CHAPTER 1

INTRODUCTION

1.1 TUNNEL DESIGN

The analysis of underground openings and their support systems involves the consideration of ground-structure interaction, and it is essential to recognize this coupling in developing safe and economic designs. The ground-structure interaction is particularly important for underground openings in weak formations and/or formations having pronounced time-dependency such as 'squeezing ground'. Terzaghi (1946) referred to the squeezing ground condition as one in which the loading on a tunnel support system is likely to increase after construction to values many times higher than the initial loading. Recently, this term has been applied rather broadly to describe ground yielding (Lane, 1975) and time-dependent deformations (Myer et al., 1977) due to: relief of stress concentrations; simple swelling related to moisture changes; and progressive ground movements accompanied by a gradual build up of loads on the support system (Lee and Lo, 1976).

In this study, both ground yielding and time-dependency of deformations, and their influences on underground opening and support system integrity, are of major concern. Typical examples of damage and time-dependent convergence for construction in squeezing ground in Southern Ontario, the area of main interest herein, are given in Table 1.1.

1

TABLE 1.1

TYPICAL EXAMPLES OF DAMAGE TO TUNNELS
AND OPEN EXCAVATIONS IN SOUTHERN ONTARIO
'SQUEEZING GROUND'

EXAMPLE 1 : Thorold Tunnel

Intense cracking in a 1.80 m thick concrete wall observed several years after construction near the end of the Thorold Tunnel under the Welland Canal that was excavated as a 5 x 5 m open trench through horizontally bedded dolomite (Lee and Lo, 1976; Franklin and Hungr, 1978).

EXAMPLE 2 : Hamilton Sewer Trench

Damage to a 6 m wide culvert constructed near Hamilton by open trenching into horizontally bedded dolomite and limestone (Franklin and Hungr, 1978).

EXAMPLE 3 : Milton Quarry

Pressure ridges (pop-ups) of about 1 m developed in the floor of a limestone/dolomite quarry near Milton that is underlain by shale (Franklin and Hungr, 1978).

EXAMPLE 4 : Niagara Turbine Wheel Pits

Convergence (inward movement) in excess of 80 mm recorded in the turbine wheel pits excavated as vertical deep shafts of 125 m into horizontally bedded dolomite and shale rocks of the Niagara Gorge in 1903. Such convergence has caused alignment dislocation (Lee and Lo, 1976; Franklin and Hungr, 1978).

EXAMPLE 5 : Toronto Water Intake Tunnel

Continuing convergence and liner pressure increases in a water intake tunnel constructed near Toronto. For example, after four months the monitored liner stresses were four times the initial values following installation (Franklin Trow Associates Limited, Personal Communication, 1978).

These case records cover recent engineering practices and indicate that the designs often failed to rationally account for potential squeezing ground behaviour that influences excavation-support system performance. This deficiency makes the determination of a safety factor for such ground conditions extremely difficult, particularly if long term time-dependency is involved.

The overall design parameters involved in tunnelling are summarized in Table 1.2. Consideration of these parameters is vital in judging the suitability of the tunnel and liner system proposed for a given site, and potential associated geotechnical problems. Also, they strongly influence the overall stability of the excavation during construction and the magnitude and time-dependency of support loadings for liner design (Peck, 1969; Egger, 1974; Ward, 1978). A comprehensive design method that takes into account the range of tunnel design parameters involved is not currently available. (A brief review of available tunnel design method is presented in Section 1.3.) With the increasing use of underground space involving excavations in weak formations and/or formations having pronounced time-dependency, a systematic design method is necessary to overcome deficiencies in current procedures. In order to develop a method for determining the stresses and deformations for tunnel-support systems in squeezing ground, it is necessary to understand the key parameters involved.

TABLE 1.2

DESIGN PARAMETERS FOR UNDERGROUND CONSTRUCTION

1. Overall Ground Conditions

    a. Geological

    b. Hydraulic

2. Mechanical Properties of Formation

    a. Strength and deformation parameters
       (both intact rock and discontinuities)

    b. Time-dependency

    c. Post-failure behaviour

3. Primary State of Stress

    a. Magnitude

    b. Orientation

4. Underground Layout

    a. General layout

    b. Orientation

    c. Shape

5. Construction

    a. Excavation method

    b. Construction sequence

    c. Support system

1.2 IMPORTANT FACTORS FOR TUNNEL DESIGN IN SQUEEZING GROUND

The factors that are considered most important to tunnel design, particularly in squeezing ground, are: the primary state of stress; potential ground yielding and time-dependent behaviour; ground-structure interaction; the construction sequence; and three-dimensional influences near the tunnel face.

1.2.1 Primary State of Stress

One of the important factors which influences potential ground movements is the primary state of stress prior to excavation, particularly the existence of high horizontal (lateral) in situ stresses. In formations with high lateral stress unloading due to excavation, creep and/or sliding over planes of weakness can cause large support system loadings resulting in failure or intolerable deformations. Stress measurements, the monitored behaviour of tunnels and excavations, and recent folding and faulting of near surface formations indicate that high lateral stresses exist near the ground surface in many areas of Canada and around the world. They also indicate that at shallow depths (less than 500 metres) these horizontal stresses can be significantly greater than the vertical stress, and are much higher than expected from simple overburden and elasticity considerations. For depths in excess of about one kilometre, the average horizontal stress and vertical stress tend to equalize (Brown and Hoek, 1978).

For Southern Ontario, the existence of high lateral stresses is now recognized and accounted for through various methods in recent designs

(Franklin and Hungr, 1978). The major principal stress is in a north-east to easterly direction, and only a small difference in magnitude between the two horizontal principal stresses is found, except where the stresses are influenced by major topographic features such as the Niagara Gorge. The measured vertical stresses were generally close to the estimated overburden stresses. The average stress ratio K (between the horizontal and vertical stresses) varies considerably at shallow depths, reaching values as high as ten (Franklin and Hungr, 1978). There are at least two possible explanations for high horizontal stresses that have been advanced: a direct consequence of tectonic forces on a major scale (for example, a north-east to easterly trending maximum compressive stress in Southern Ontario that is probably of much larger extent); or erosional unloading processes in which, due to lateral confinement, the horizontal stresses are reduced much less than the vertical stress (Sbar and Sykes, 1973; Herget, 1974; Lo and Morton, 1976; Franklin and Hungr, 1978).

Regardless of the causative mechanism(s), it is important that sites with potentially high horizontal stresses be recognized early in the design stage for underground openings, and adequate measures taken to avoid adverse effects due to creep and/or movement along planes of weakness. In many cases, it is difficult to assess fully the primary state of stress from stress monitoring at the site in advance of construction, so that initial designs should reflect conservative assumptions regarding lateral stresses. The importance of monitoring during actual tunnel excavation and liner placement to check design assumptions cannot be overemphasized.

1.2.2　Ground Yielding and Time-Dependent Behaviour

Potential ground yielding and time-dependent behaviour are important factors influencing tunnel designs in squeezing ground. Damage, and even failure, of underground openings in squeezing ground of the type outlined in Table 1.1 indicates the importance of this time-dependency. Typical ground movements are illustrated in Figure 1.1 which gives time-convergence (diametral closure) measurements at two different sections (profiles) during excavation of an underground opening. This tunnelling example was selected since the field measurements are available, and the methods described herein were used during the tunnel's design and construction. The water intake tunnel constructed near Toronto is 4 metres in diameter at a depth of approximately 60 metres in horizontally bedded shale. High horizontal stresses exist in this area and the average stress ratio K is likely to be equal to, or slightly greater than, unity at depth of interest. Each asterisk on Figure 1.1 corresponds to a face advance of approximately 2.5 metres and the instrumentation was initially installed close to the face at an average distance of 2.5 metres. It can be seen that the convergence rates are very high following each successive blast as the face is advanced and they then decrease with time. The convergence for this example is apparently mainly elastic, or elastic-plastic, with a fairly small time-dependent creep component. It can also be seen that the convergence of the vertical spans (1-5) is greater than for the horizontal spans (3-7). This is probably due to bedding influences (transverse isotropy) and the high lateral stresses resulting in some crown separation.

8
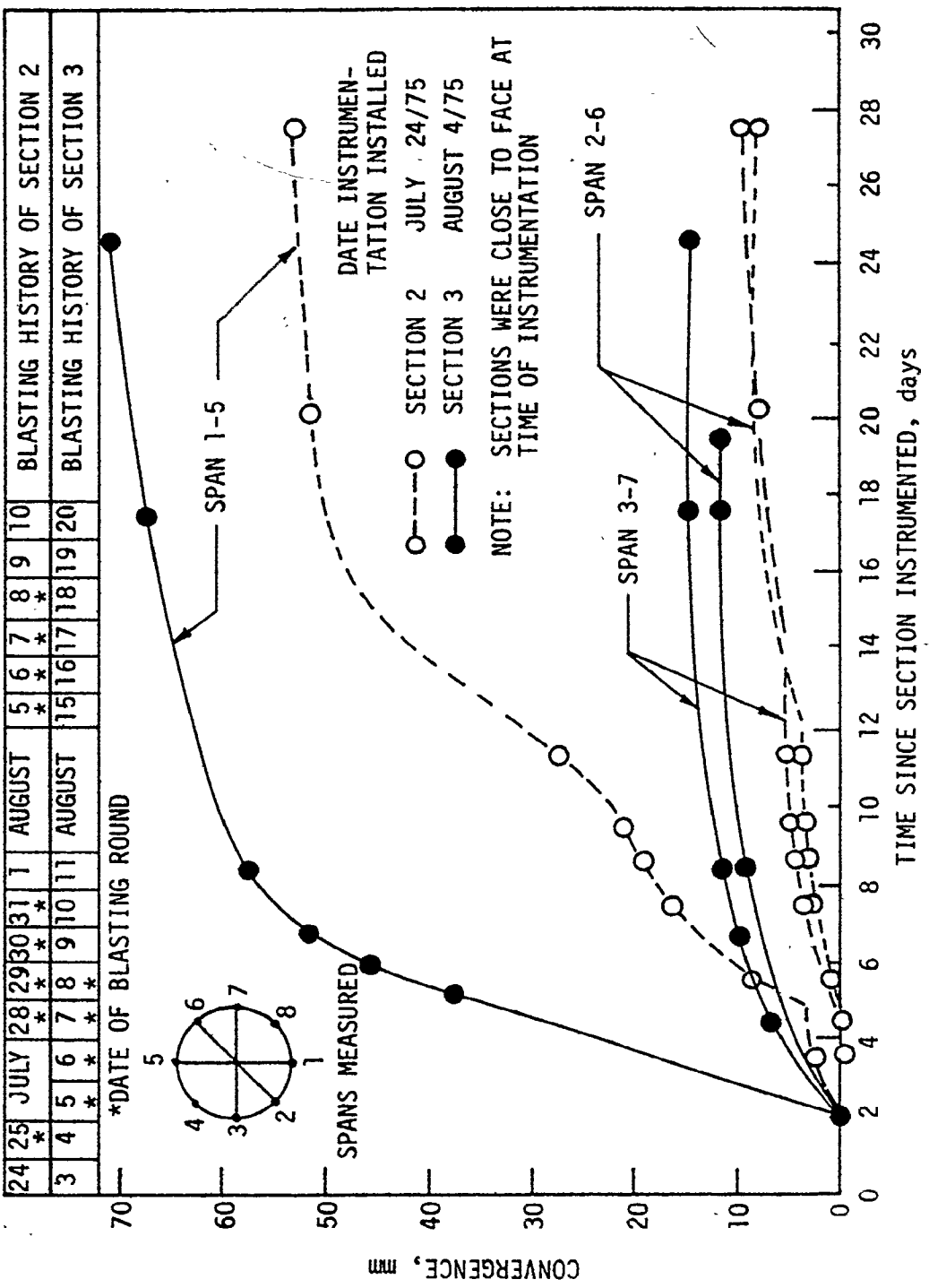
FIGURE 1.1   TYPICAL FIELD CONVERGENCE MEASUREMENTS DURING EXCAVATION OF A WATER TUNNEL, NEAR TORONTO, ONTARIO (FRANKLIN-TROW ASSOCIATES LIMITED, PERSONAL COMMUNICATION, 1979)

Similar behaviour is observed during creep testing, even at low stress levels (Robertson, 1963; Boresi and Deere, 1963; Hobbs, 1970; Afrouz and Harvey, 1974) which fall into the range of stresses encountered in the vicinity of many underground openings (Lo and Morton, 1976). The typical creep behaviour observed for many materials under compressive loading is shown schematically in Figure 1.2. The total strain (elastic and creep components) at any time t for a particular stress level may be represented by:

$$\varepsilon(t) = \varepsilon_0 + \varepsilon_p(t) + \varepsilon_s(t) + \varepsilon_T(t) \qquad\qquad 1.1$$

where ε_0 is the instantaneous strain; $\varepsilon_p(t)$ is the primary creep; $\varepsilon_s(t)$ is the secondary creep or 'steady state' creep; and $\varepsilon_T(t)$ is the tertiary creep. Through the empirical approach, which appears to have gained the widest acceptance to describe creep, parameters such as strain and strain rate are measured experimentally in terms of time, stress and temperature. These values are then used to develop creep relationships.

1.2.3 Ground-Support Interaction

Ground-support interaction is the predominant factor governing tunnel designs in squeezing ground. Stresses within the tunnel support system generally depend on the ground-support interaction, and in particular on: the time of installation; distance of support system from tunnel face during installation; and support system rigidity relative to the formation. Installation delay (time or space, or both) and/or soft backings have a dramatic effect in reducing the stress build-up.
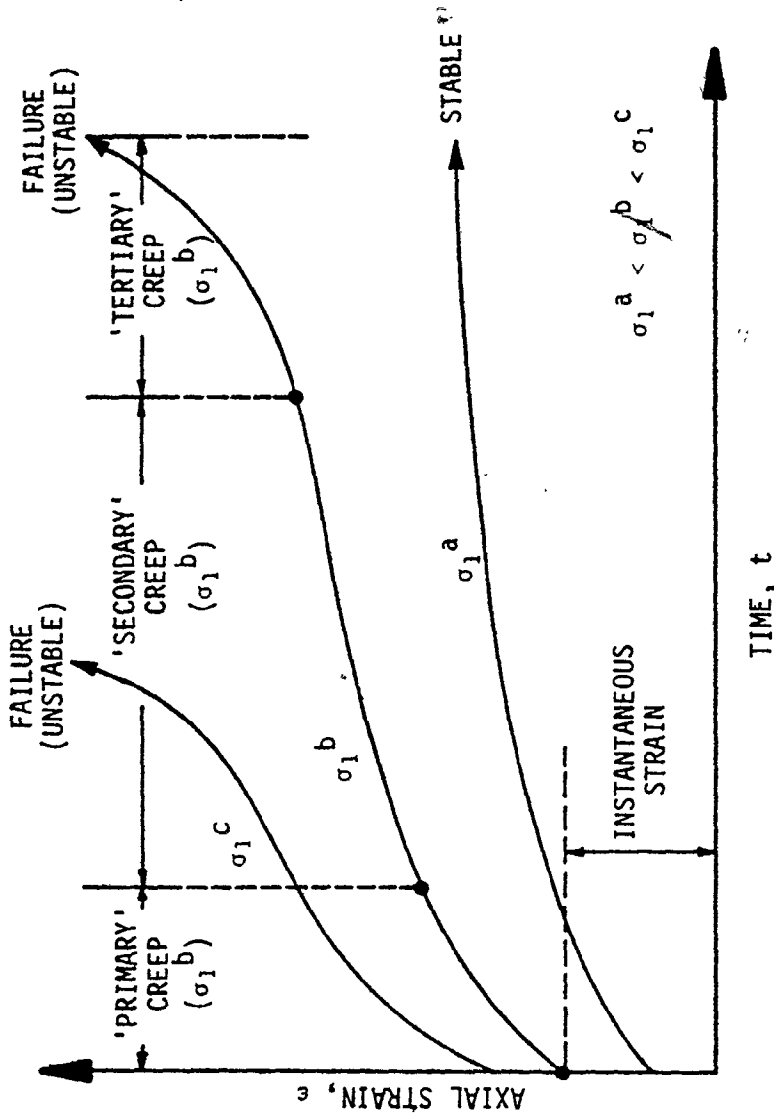
FIGURE 1.2 TYPICAL CREEP BEHAVIOUR FOR DIFFERENT UNIAXIAL COMPRESSIVE STRESS LEVELS

1.2.4 Construction Sequence

In order to take into account the full ground-support inter-
action, the construction sequence has to be considered. Conventioanl
construction of tunnel support systems in North America typically com-
bines two systems of support - primary and secondary linings - each re-
quiring very different construction techniques and equipment. It has
been long recognized that the primary support is often adequate for load
carrying purposes and the secondary lining may not be loaded to any ex-
tent (Peck, 1969). For this reason, and for improved construction eco-
nomics, single support systems have been widely used in Europe. One
such system, precast segmental concrete liners, has now gained attention
in North America with a number\of recent applications, as it couples
ease of construction with improved support system economics.

During excavation, when the tunnel face is being advanced, the
precast concrete segments are usually installed up to some construction
limited distance from the face. The typical sequence of tunnel excava-
tion and support placement to be simulated in any analysis is shown in
Figure 1.3. The tunnel zone of length ℓ_u near the advancing face is
assumed to be unsupported after the last ring of support segments has
been installed. This ring of segments and the face position are shown
in Figure 1.3 a. For a new round of excavation, the tunnel face will ad-
vance and reach the position shown in Figure 1.3 b. Then a new ring of
segments as shown in Figure 1.3 c is installed and the construction
cycle is repeated.

TUNNEL ADVANCING
.FACE

D = TUNNEL DIAMETER
ℓ_u = UNSUPPORTED LENGTH PRIOR
TO EXCAVATION
t_r = RIGID SUPPORT
THICKNESS
t_s = SOFT BACKING THICKNESS

(a) TUNNEL FACE AND THE
UNSUPPORTED SECTION JUST
PRIOR TO FACE ADVANCE

ADVANCE

(b) TUNNEL FACE ADVANCING DURING A NEW
EXCAVATION STEP

SUPPORT SEGMENT
PLACED

(c) NEW SUPPORT SEGMENT INSTALLATION
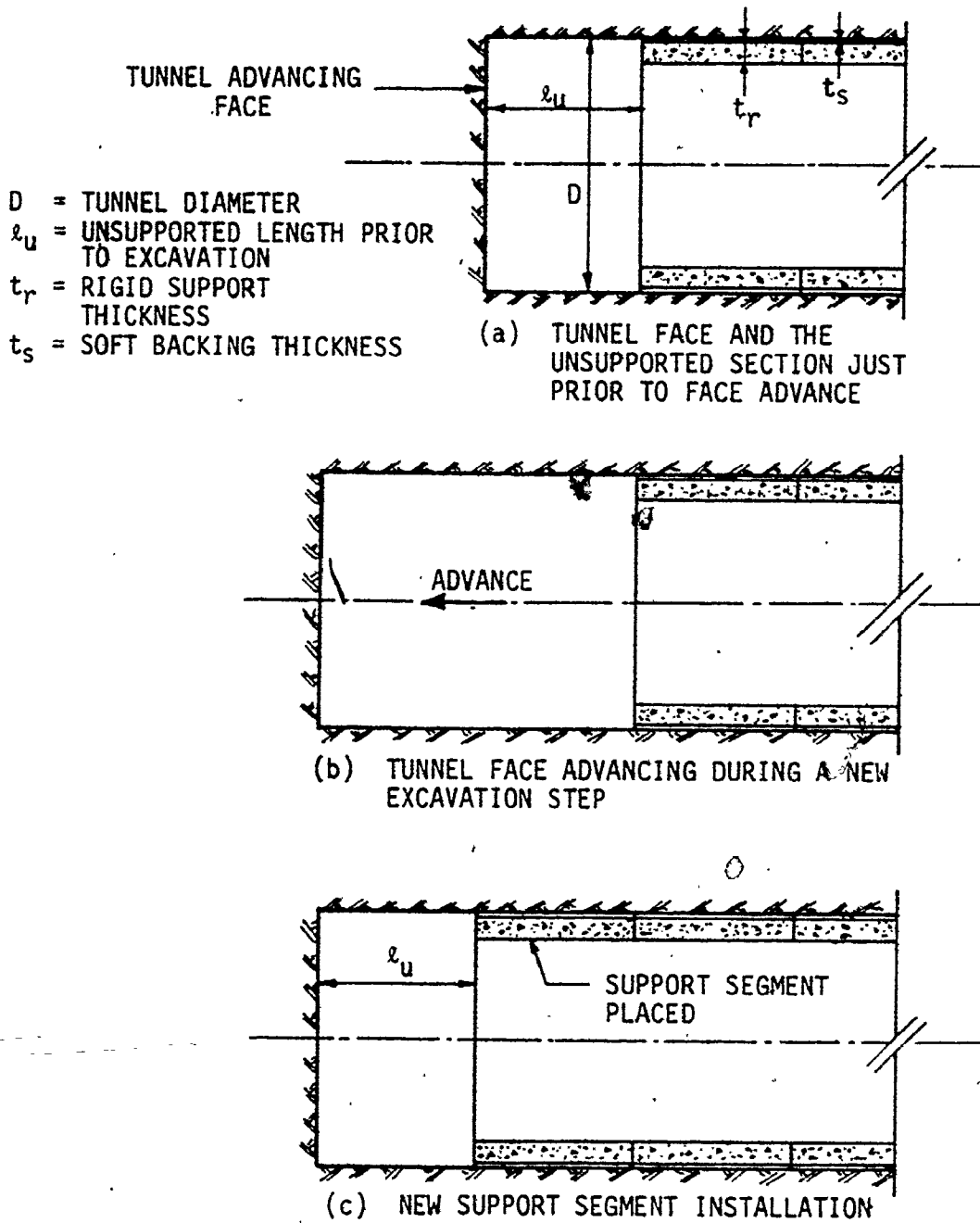
FIGURE 1.3   TUNNEL EXCAVATION AND SUPPORT INSTALLATION

Following excavation, there will be a change in the stress field and a load redistribution around the tunnel. Much of the redistributed load is transferred to the tunnel support already in place, particularly the last ring of segments installed. A significant portion of the load is also transferred to the unexcavated ground ahead of the advancing face. This load redistribution will cause a 'complex' three-dimensional pattern of movements within the ground mass (Einstein and Schwartz, 1978).

1.2.5 Three-Dimensional Influence

If the support system is installed near the advancing face, i.e. within the zone of three-dimensional influence , prediction of lining stresses becomes a complicated problem, and the three-dimensional influences must be taken into consideration during design.

Although the primary emphasis in this study was directed towards the aspects of tunnelling in squeezing ground summarized above, it is recognized that other parameters are significant such as bedding, anisotropy and discontinuities.

1.3 REVIEW OF AVAILABLE PROCEDURES FOR TUNNEL DESIGN

The available methods for tunnel design may be classified into three general groups: empirical; semi-rational; and analytical. In the empirical methods (Szechy, 1973) several design procedures have been established to estimate the load acting on the support system based on the ground characteristics and the dimensions of the opening (Terzaghi's

method, for instance). These methods do not generally account for ground-support interaction. In addition, these empirical methods can only be justified for shallow tunnels and formations with no significant time-dependency (Lombardi, 1974). Semi-rational design methods (Tunnelling Technology, 1976) are based on case records of existing practice and various ground classification systems in an attempt to relate support requirements to ground characteristics. The limitations on this approach are perhaps best given in Ward's Rankine Lecture: "This approach unfortunately perpetuates existing practice, and does not necessarily distinguish conservative work, or even perhaps unsatisfactory practice. It takes no account of the complex rock-support interaction mechanics or the fact that the same support can be both satisfactory and unsatisfactory in the same rock conditions depending on construction procedure." (Ward, 1978). Analytical methods (Obert and Duvall, 1967) based on elastic theory are directly applicable only to formations which can be considered linearly elastic at stress levels below failure, and without time-dependent behaviour. Thus, they are quite limited in their applicability. In addition, they do not take ground-structure interaction into account (Lombardi, 1974).

Although these design methods may achieve their intended goal, when used with good engineering judgement within limited ranges of applicability for which experience is available, often they cannot be easily extended or generalized. In some cases, particularly for tunnels in squeezing ground, their use is generally not acceptable.

Improved analytical and numerical solutions for tunnel design

have recently become available. Ladanyi (1976) introduced a complete plane strain solution for a circular opening in an infinite, non-linear, elastic-plastic medium subjected to uniform internal pressure. The procedure is most relevant to the design of pressurized tunnels. Lombardi (1973, 1974) developed a design method which can be employed near the tunnel face by introducing assumptions of axial symmetry and plane deformations. Florence and Schwer (1978) presented a stress analysis solution for a circular opening in the idealized plane strain condition. This analysis allows for a failure criterion and assumes an ideally plastic post-failure behaviour. Krenk (1978) developed a solution taking creep into consideration in order to estimate the convergence around spherical and cylindrical cavities. These solutions are quite useful for unlined openings subjected to uniform axisymmetric stresses.

Two-dimensional, plane strain, finite element solutions have been extensively used (for example, Pariseau, Voight and Dahl, 1970; Shieh and Sandhu, 1970; Meek, 1973; Zienkiewicz, 1977) to predict the deformations and stresses within the excavation vicinity and the support system in elastic-plastic mediums. Recently, three-dimensional analyses have been performed using both the finite element and boundary integral equation methods. The finite element method was used for an unlined tunnel in an elastic medium (Descoeudres, 1974), and for a lined tunnel in an elastic-perfectly plastic medium (Wittke and Pierau, 1976). The boundary integral equation method was used for unlined tunnels in an infinite, homogeneous, isotropic, linear elastic medium (Hocking, 1976). This method is well suited to some problems of the type mentioned above.

However, the important time-dependency of deformations was not considered in these tunnelling simulation analyses.

1.4 PRIMARY OBJECTIVE OF THE STUDY

The primary objective of this study was to develop a practical method for simulating tunnelling that can be systematically applied to the analysis and design of underground openings in squeezing ground. Based on the previous review of factors influencing tunnel and support system behaviour, the following features were considered important: ability to predict stresses and deformations in the ground-support system; ability to consider ground and support system as a composite unit, so that important interaction effects can be accounted for; ability to consider potential ground yielding and time-dependency so that, in addition to any elastic response, plastic and viscous behaviour can be incorporated; versatility to cover both two-dimensional plane strain conditions (far from the advancing face) and three-dimensional influences (near the advancing face); and ability to include the independent parameters for any idealized tunnel system (geometry, material properties, primary state of stress and construction sequence).

1.5 SIMULATION APPROACH ADOPTED

Given the 'complexity' of tunnelling simulation, the general approach adopted herein is based on the finite element method (Desai and Abel, 1972; Zienkiewicz, 1977) which seems to be the most realistic approach available at this time. Using the finite element method, the

primary factors influencing tunnel design in squeezing ground can be considered and readily incorporated into the simulation. The finite element method simulation is divided into two approaches or conditions: the plane strain (far from the tunnel face) and the three-dimensional (near the advancing face) cases. Incremental techniques are adopted to simulate the construction sequences of excavation and support placement, and to allow the incorporation of the inelastic ground behaviour of yielding and creep. Deactivation and reactivation processes on the element stiffness matrices are used for excavation and support placement simulation, respectively. The initial strain and initial stress methods (Zienkiewicz, 1977) are used for the creep and yielding analyses, respectively, adopting the explicit approach (Zienkiewicz and Cormeau, 1974).

The simulation approach is still based on a fair amount of idealization and several assumptions. Adopting the continuum mechanics approach the ground, which is actually anisotropic and discontinuous on both the micro- and macro-scales, is replaced by an idealized isotropic continuum (Zienkiewicz, 1968; Daemen, 1975). However, major discontinuities such as jointing can be readily incorporated in the analysis using elements such as the linear joint element developed by Goodman et al (1968). This has been described in detail previously and does not form part of the study (Hanafy, 1976). This idealized ground medium is assumed to deform linearly elastic under loading or unloading with constant moduli up to a certain limit of the stress state at which plastic or permanent deformations become possible. This stress state limit is

defined by an appropriate yield function such as the von Mises or the extended von Mises (Mohr Coulomb) criteria. The ground medium at this limit is assumed to be a perfectly plastic material. It is also assumed that the yielding behaviour can be equated to ductile behaviour and using the rules of plasticity a stress redistribution process is formulated. The time-dependent deformations are assumed to have elastic and non-recoverable components in which the non-recoverable components are determined from the appropriate nonlinear time-dependent creep relationship. These are the general assumptions involved, and they will be discussed in detail along with supplementary assumptions in the following chapters.

It should be noted that while these idealizations and assumptions are involved, the great 'flexibility' of the finite element method allows the incorporation of more realistic assumptions as the necessary characterization information becomes available.

In Chapter 2, a finite element method approach for excavation and support placement simulation is developed for the idealized plane strain ground medium condition.

In the second approach to the problem, a solution technique is developed in Chapter 3 using the axisymmetric finite element method to formulate the problem of the three-dimensional behaviour of cylindrical openings considering tunnel advancement.

In both approaches, the sequence of incremental excavation, support liner installation and time-dependent creep analysis have been

modelled in such a way that any sequence of processes can be performed. Simple finite element mesh generating programs for underground excavation and support installation analyses have also been developed to considerably decrease the overall time for mesh and input data preparation.

The application of the finite element method simulation approach developed is demonstrated for typical underground cavities in two-dimensional plane strain and three-dimensional axisymmetric situations in Chapters 4 and 5, respectively. Particular attention is given to the effect of high initial lateral stresses and the effect of the squeezing condition on the deformations and stresses in both the ground and support system. The results are reported in a format useful for future design implementation purposes.

CHAPTER 2

PLANE STRAIN SIMULATION OF UNDERGROUND OPENINGS

2.1 INTRODUCTION

The underground openings simulation presented in this chpater is based on assuming a plane strain condition in which there is no strain along the opening axis (i.e. $\varepsilon_z = 0$). This plane strain simulation is based on the finite element method using triangular, linear displacement, constant strain elements.

The main features of the simulation procedure are presented in following sections, starting from the initial in situ stress field prior to excavation. The 'deactivation' and 'reactivation' processes used for excavation and support placement simulation, respectively, are then explained (i.e. staged construction). The incremental initial stress and incremental initial strain methods for nonlinear stress analysis have been adopted for the time-independent yielding and time-dependent creep response, respectively. With the aid of a mesh generation program developed for simple circular openings, the effects of boundary location and condition on the deformations and stresses have been considered. Finally, the advantages and limitations of the plane strain simulation approach are discussed in preparation for the advancing face simulations discussed in the following chapter. The accuracy of both the solution procedure and

20

the computer program developed have been verified through comparisons with closed form solutions, where possible. Some typical field cases involving tunnels excavated in various formations are discussed later in Chapter 4 to demonstrate the program's capabilities.

2.2 EXCAVATION SIMULATION

The single step, finite element method, excavation simulation program, developed previously (Hanafy, 1976) has been extended and modified to simulate excavation in stages and to permit an incremental load analysis. This analysis is based on the general numerical procedure developed by Goodman and Brown (Desai and Abel, 1972) for simulating embankment construction and excavation problems in geotechnical engineering. The main aspects of the excavation simulation approach are shown in Figure 2.1. The final stresses after excavation are the sum of two cases: the initial stresses at the site prior to excavation; and the perturbation stresses resulting from the application of 'release forces' acting around the opening to give a stress-free excavated surface (Meek, 1973; Kulhawy, 1974). The steps in the analysis can be summarized as follows:

1. Determining the initial in situ element stresses $\{\sigma_0\}_e$ in terms of the site overburden conditions and free field transverse stress ratio K_t:

$$\sigma_v = \gamma h \qquad\qquad 2.1$$

$$\sigma_h = K_t \sigma_v \qquad\qquad 2.2$$

$$\tau_{vh} = \tau_{hv} = 0 \qquad\qquad 2.3$$
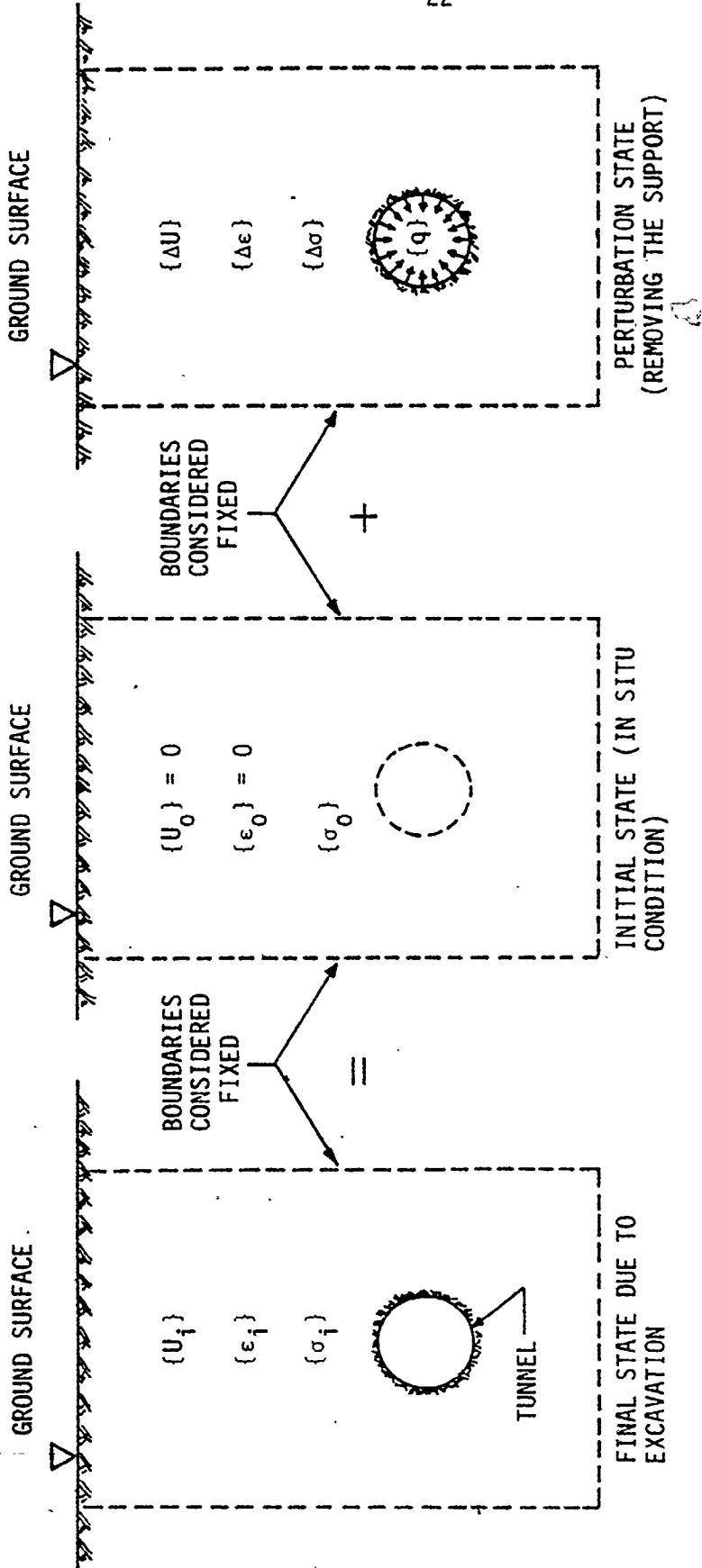
FIGURE 2.1 EXCAVATION SIMULATION

(assuming level ground, no residual shear stresses and the plane strain condition) where σ_v is the vertical stress at depth h; γ is the unit weight of the ground; σ_h is the horizontal stress; and τ_{vh}, τ_{hv} are the shear stresses. Near the surface, the initial state of stress varies considerably with the depth D of the element centroid (i.e., considering shallow tunnels). However, in the case of deep tunnels, the initial state of stress can be considered constant with depth. In this case, D is taken as the depth of the tunnel axis below the ground surface.

2. Removing the influence of the elements contained in the excavation stage by reducing their stiffness matrix coefficients to very small values with respect to their initial values prior to excavation. The factor $x\ 10^{-6}$ was found (Kulhawy, 1974) to be appropriate to ensure that these excavated elements do not influence the succeeding computations. This process is called 'deactivation'.

3. Computing the equivalent nodal forces $\{q\}_e$ for the stresses within the 'excavated' elements which have common boundaries with the unexcavated elements (i.e. at excavation boundary). To obtain these forces, the simplest procedure is to impose a virtual displacement at the nodes of the excavated elements and to equate the external work done by the forces and the strain energy recovered during that displacement:

$$\{q\}_e = \int_{vol} [B]_e^T \{\sigma_o\}_e \, dv \qquad\qquad 2.4$$

where [B] is the strain-displacement matrix. This load, with opposite sign, represents the equivalent nodal forces to be applied at the excavated boundary to simulate excavation of the element.

4. Assembling the nodal forces acting only at the excavated boundaries. The resulting load vector gives 'the release forces' {Q} required to produce the 'stress free' excavation surface.

5. Computing the perturbation stresses {Δσ} resulting from the application of the release forces {Q}, totally or incrementally, on the finite element configuration obtained in Step 2.

6. Determination of the final stresses {σ_f} for this excavation step by adding the perturbation stresses to the initial in situ stresses. In the case of incremental loading, Steps 5 and 6 are repeated until the total forces {Q} are applied.

7. For each excavation stage, Steps 2 to 6 are repeated until the excavation is completed.

It should be noted that the above general approach is often used in excavation simulations based on the finite element method. The various methods are basically the same except:

1. The 'excavated' elements either have their stiffnesses reduced to very small values relative to initial values, or are removed completely from the mesh configuration. Both methods are accurate and similar in formulation. Using the reduced stiffness

approach has the fundamental advantage that these elements then remain available for use in representing further construction stages such as lining placement as explained in Section 2.3.

2. The equivalent boundary nodal forces $\{q\}_e$ should be determined from the stresses at the 'excavated' surface. For constant strain elements, where the resulting constant stresses are usually considered to act at the centroids, two major methods have been proposed (Clough and Duncan, 1969; Christian and Wong, 1973) to determine boundary stresses. The first method (Clough and Duncan, 1969; Meek, 1973; and Kulhawy, 1974) involves determination of the equivalent boundary forces directly from the excavated elements adjacent to the excavation boundaries, while the second (Clough and Mana, 1976) involves determination of these forces from both the adjacent excavated and unexcavated elements. The first method is adopted throughout this study, with the provision that the thickness of the excavated layer adjacent to the excavation boundaries should be minimized. This ensures the desired accuracy in boundary stresses and nodal forces.

2.2.1 Plane Strain Analysis Capability Verification

Following development of the finite element program, runs were completed to verify the accuracy of both the excavation procedure and actual program. This involved comparing computed results for the problem of a uniformly stressed continuum with a cylindrical hole, to closed form solutions from linear elasticity (Obert and Duvall, 1967). Details

of the problem are given in Figure 2.2.

Two different checks were completed: treating the problem as an initially unstressed medium subjected to external uniform boundary stresses with a circular opening made up of elements with very low stiffness values relative to the surrounding medium ($\times 10^{-6}$); and starting from a uniformly stressed medium, completing one and three stage excavations to form the circular opening, as shown in Figure 2.3. Since the problem being considered is linear elastic, either simulation should give the same results. The first type of check was performed to determine if the presence of low stiffness elements in the excavated zone influences the predicted results as this is an important aspect of the excavation simulation routine adopted. The second type of check allows the actual excavation in stages aspects to be checked.

The finite element mesh used in all studies is shown in Figure 2.4, and the checks confirmed that:

1. The 'deactivation' process is a satisfactory procedure since the reduced stiffness elements have no noticeable influence on the results.

2. The results for the one and three stage excavations are identical as anticipated for the linear elastic assumption.

3. All of the finite element method (FEM) results are very close to the closed form solution as indicated for the radial and tangential stresses in Figure 2.5.
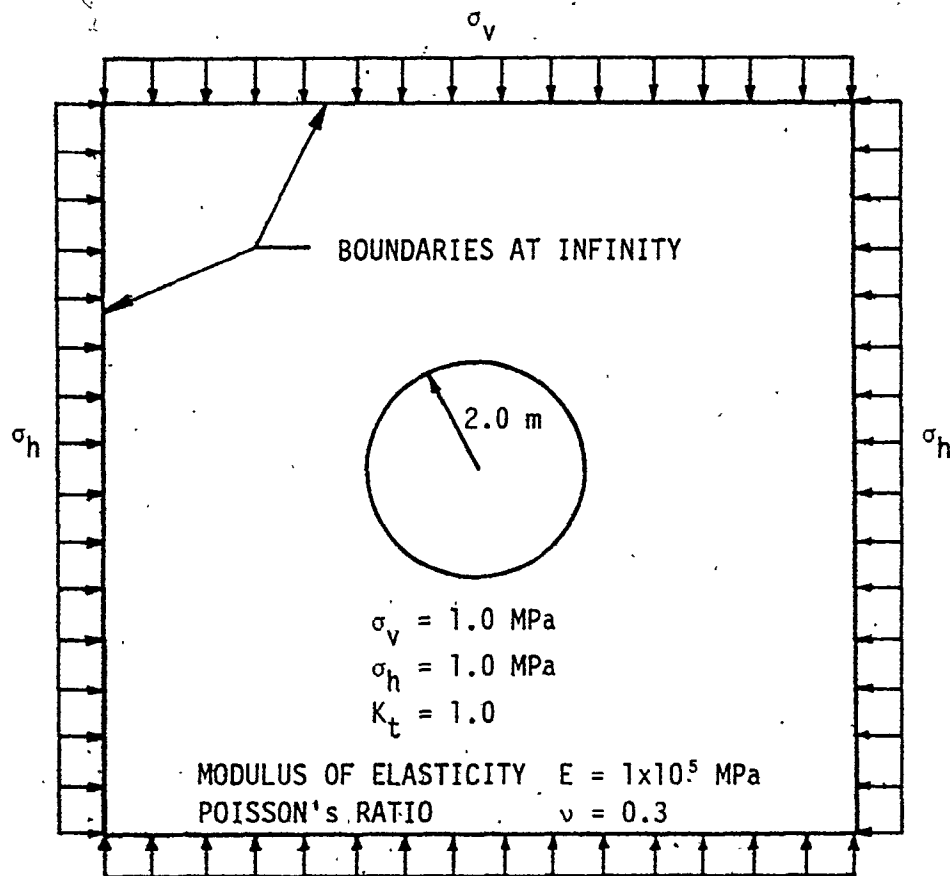
FIGURE 2.2   PROBLEM WITH AVAILABLE CLOSED FORM
SOLUTION USED DURING PLANE STRAIN
PROGRAM VERIFICATION

ONE-STEP EXCAVATION

REMOVED IN ONE STEP

0.0   1.0   2.0
      Metres

THREE-STEP EXCAVATION

REMOVED IN 3RD STEP

REMOVED IN 2ND STEP

REMOVED IN 1ST STEP

0.0   1.0   2.0
      Metres
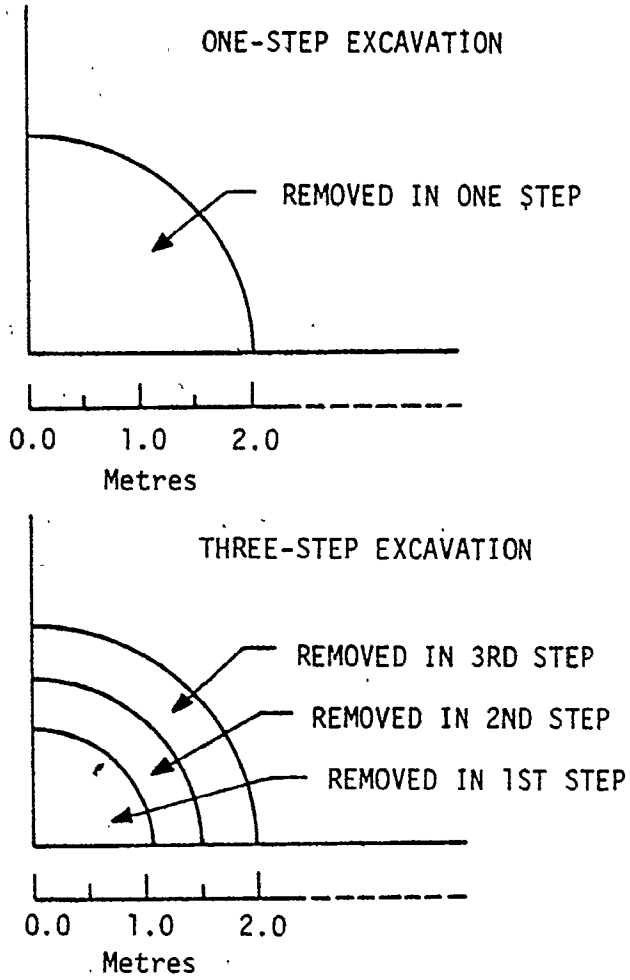
FIGURE 2.3   ONE AND THREE STAGE EXCAVATION SIMULATIONS
              USED DURING PLANE STRAIN PROGRAM VERIFICATION
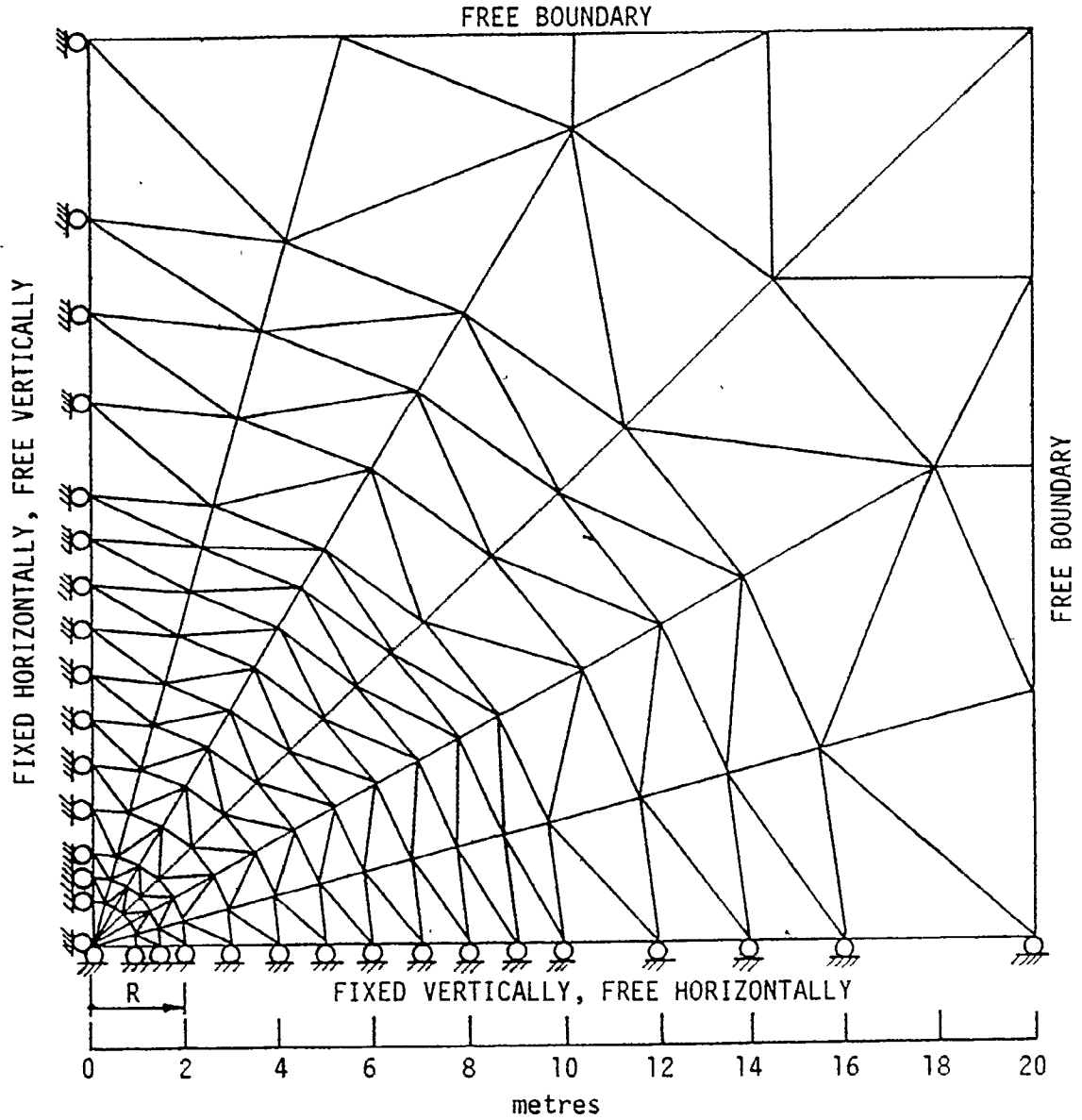
FIGURE 2.4 FINITE ELEMENT MESH USED DURING PLANE STRAIN
PROGRAM VERIFICATION (SIMULATION OF FIGURE 2.2)
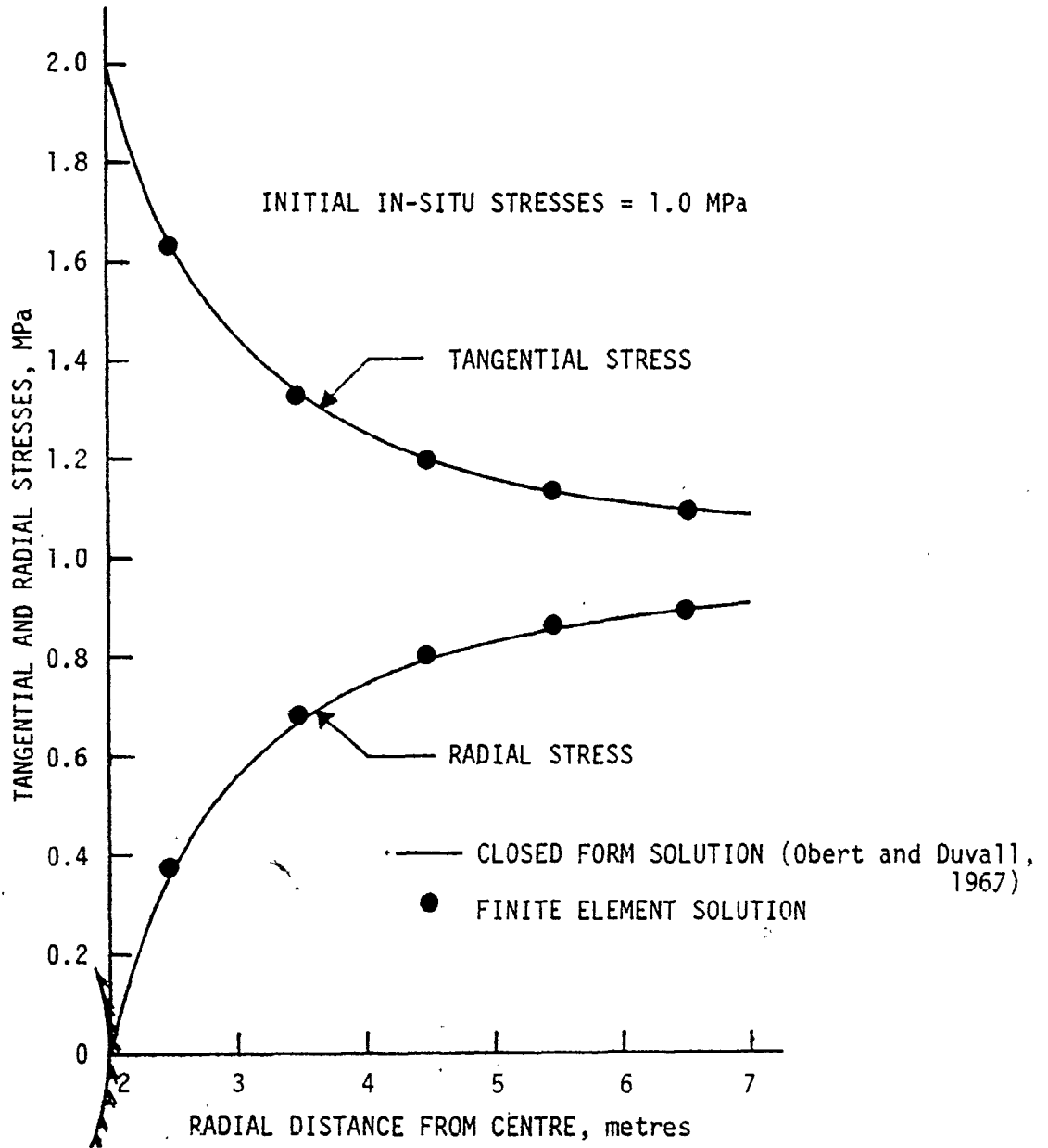
FIGURE 2.5   TANGENTIAL AND RADIAL STRESS DISTRIBUTIONS
AROUND A CIRCULAR OPENING.   COMPARISON OF
CLOSED FORM AND FEM SOLUTIONS

2.3 YIELDING GROUND ANALYSIS

The principal feature of any yielding ground stress analysis associated with excavations is the elastic-plastic post-yielding behaviour. The solution of such problems requires a yield criterion and a constitutive relationship for post-yielding.

Experimentally, it is known that yielding can occur only if the stresses $\{\sigma\}$ satisfy the general yield criterion (Mendelson, 1970):

$$F(\{\sigma\}, K) = 0 \qquad\qquad 2.5$$

which is an hypothesis giving a relationship between stresses and material properties at the limit of elastic behaviour. The three most common criteria used in geotechnology have been the Mohr-Coulomb, von Mises, and Tresca (Pariseau, 1972). In their original form, the von Mises and Tresca criteria were developed to study the yielding of metals and only account for deviatoric stress components. For porous materials such as rock, soil and concrete, it is known that yielding depends not only on the deviatoric components of stress, but also on the hydrostatic components. The Mohr-Coulomb criterion was originally developed for soils and provides for internal friction or dependence of the yield strength on confining stress. It does not, however, include any influence of the intermediate principal stress on yield. For this reason, Drucker-Prager (1952) developed a generalized version of the Mohr-Coulomb criterion or an extended von Mises criterion which is that most accepted for rock and soils:

$$F = \alpha I_1 + \sqrt{J_2} - K \qquad\qquad 2.6$$

where α and K are the yield parameters which are related to the Mohr-Coulomb C and ϕ parameters used in geotechnology. I_1 is the first invariant of the stress tensor and J_2 is the second invariant of the deviatoric stress tensor (Fung, 1965). This yield function (Equation 2.6) differs from the von Mises criterion by the addition of the αI_1 term. When $\alpha = 0$, i.e. a perfectly plastic material, the function is identical to the von Mises criterion (Pariseau et al, 1970).

The major concern in using any failure criterion for geotechnology problems is to relate the material constants α and K in the yield function to the material parameters ϕ and C obtained in standard laboratory shear testing. A constitutive relationship for post-yielding is also required for plastic analyses. Such a constitutive relationship, though idealized, is used to relate the strain and stress increments in the plastic region.

2.3.1   Idealization

In the elastic range, the strains are related to the stresses by the generalized Hooke's law for linear elastic, isotropic materials (Zienkiewicz, 1977). The general elasticity matrix for this case $[D^E]$ is given in Appendix A.

To relate increments of strain to increments of stress in the plastic region, major assumptions normally adopted in plasticity of metals analyses are also assumed to be valid in the simulation approach:

1. The ground is assumed to be an elastic-perfectly plastic material

in which no strain-hardening is anticipated. The stress-strain curve idealization for loading and unloading is shown in Figure 2.6.

2. The von Mises yield criterion which is equivalent to the generalized Mohr-Coulomb yield criterion (extended von Mises) for the special case of elastic-perfectly plastic materials is assumed to be applicable.

3. The Prandtl-Reuss condition (components of plastic strain increments are proportional to, and parallel to, the corresponding stress deviator with no volume change due to plastic deformation) is assumed to be applicable. Then, the increments of plastic strain components $\Delta\varepsilon_{ij}^P$ are determined using the Prandtl-Reuss equation:

$$\Delta\varepsilon_{ij}^P = \frac{3}{2}\frac{\Delta\varepsilon_e^P}{\sigma_e} S_{ij} \qquad\qquad 2.7$$

where $\Delta\varepsilon_e^P$ is the equivalent plastic strain increment, σ_e is the equivalent stress and S_{ij} are the deviatoric stresses.

4. Dorn's definitions for the equivalent strain and equivalent stress are adopted (Lubahn and Felgar, 1961). In these definitions, the equivalent strain increment is related to the octahedral shear strain increment, and the equivalent stress is related to the octahedral shear stress:

$$\Delta\varepsilon_e^P = \frac{1}{\sqrt{2}}\Delta\gamma_{oct}^P \qquad\qquad 2.8$$
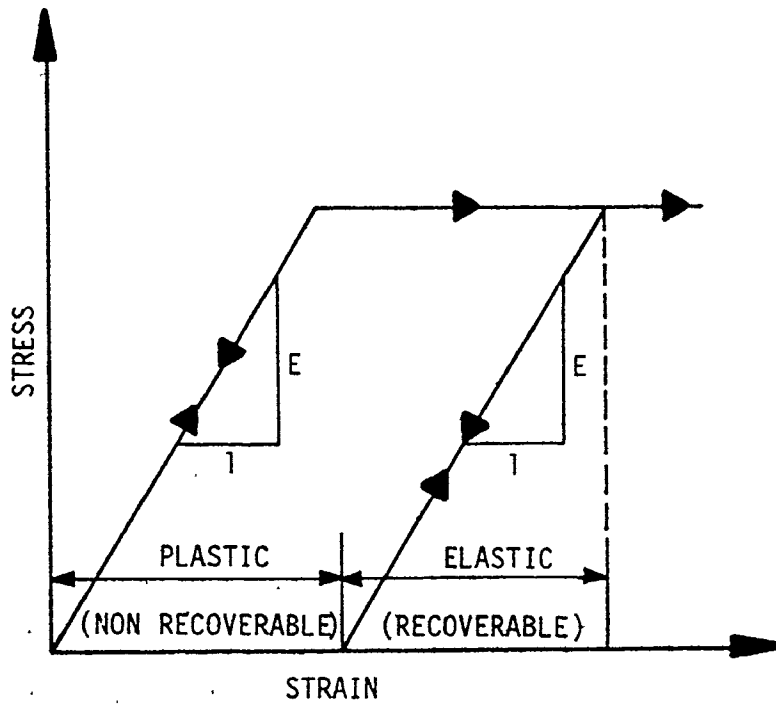
FIGURE 2.6   ELASTIC-PERFECTLY PLASTIC STRESS-
             STRAIN RELATIONSHIP IDEALIZATION
             ADOPTED TO REPRESENT GROUND
             YIELDING

and $\sigma_e = \dfrac{3}{\sqrt{2}} \tau_{oct}$ 2.9

5. The associated flow rule (Mendelson, 1970), which implies the
    normality principal, is adopted to determine the accumulated
    plastic strain. Geometrically, this implies the normality of
    strain increment vectors to the yield surface in the stress
    space. The plasticity matrix based on the von Mises yield cri-
    terion is given in Appendix A.

Some of these assumptions were made to simplify the overall ana-
lysis. The inclusion of more refined plasticity idealizations such as
strain-hardening will be the subject of future research.

In order to obtain the full constitutive equations, a lengthy
process is involved. Derivations for the von Mises and Drucker-Proger
yield criteria are given in detail in the literature and will not be re-
peated here (Reyes and Deere, 1966; Marcal and King, 1967; Yamada et
al, 1968; Zienkiewicz et al, 1977; and Shieh and Sandhu, 1970). The
final yielding ground plastic constitutive equations based on the von
Mises yield criterion are given in Appendix A. The appropriate consti-
tutive relationship is then used to form the stiffness matrix depending
on whether the element is behaving elastically or plastically.

2.3.2   Plastic Analysis: Incremental Intitial Stress Method

To incorporate the potential plastic response of the opening in
the staged excavation and creep simulation analyses, a numerical tech-
nique compatible with incremental loading must be adopted. Various

approaches have been proposed, and are available for use in nonlinear finite element problems (Desai and Abel, 1972; Zienkiewicz, 1977): the incremental elasticity method (variable stiffness method); the initial strain method; and the initial stress method. Understanding the limitations of each method helps when selecting the most appropriate method for use in the analysis.

In the incremental elasticity method (variable stiffness method) (Marcal and King, 1967; Yamada et al, 1968), the nonlinear analysis is completed by using small load increments. For each load increment, the material is considered to be elastic with a variable stiffness. There are two serious disadvantages with this method: excessive computer time required for changing the element stiffness matrices at each step to take into account the plastic deformation through a new tangent (or secant) modulus; and changing material properties which are not appropriate with the creep analysis. For these reasons, the initial strain and initial stress methods have been developed. Both of these methods use the same technique to approach the solution of a nonlinear problem using small load increments (Zienkiewicz, 1977). For each load increment, the material is treated as an elastic material with a constant stiffness. If the stress-strain level reached is higher than the true stress-strain level, a correction must be made to bring this point to its actual position. In the initial stress method, the stresses are brought down to the correct level by introducing an initial stress $\Delta\sigma$, while in the initial strain method, the strains are adjusted by introducing an initial strain, $\Delta\varepsilon$. A set of body forces equilibrating these initial

values can be applied to the structure (without changing the elastic properties) to deform it further, resulting in an additional set of strains and corresponding stress increments. If the final stress-strain level exceeds that permitted for the nonlinear relationship, the cycle has to be repeated using the new initial values.

In problems where the stress levels can be determined for given strains, the initial stress method can be used. This method is particularly useful when the strains increase rapidly with increasing stress. Typical example problems for this method are when the degree of hardening is small, or if the material behaves in an elastic-perfect plastic manner.

In some problems such as creep where there are residual (locked in) stresses, the stress levels cannot be explicitly determined in terms of strains. On the other hand, it is possible to determine strains in terms of stresses. In these cases, the initial strain method offers significant advantages.

In this study, the initial stress method and the initial strain method have been used in the elastic-plastic and creep analyses, respectively. A computer program for the plastic analysis of plane strain situations has been developed based on the general procedure outlined by Zienkiewicz (1977) using the initial stress method. The main steps in this procedure are:

1. Applying the first load increment and determining increments of elastic strain $\{\Delta\varepsilon\}$ and corresponding elastic stress $\{\Delta\sigma\}$ using

the elasticity matrix $[D^E]$.

2. Obtaining the final stress-strain level existing at the end of this increment:

$$\{\sigma'\} = \{\sigma_0\} + \{\Delta\sigma\} \qquad\qquad 2.10$$

and $\{\epsilon'\} = \{\epsilon_0\} + \{\Delta\epsilon\}$ \qquad\qquad 2.11

where $\{\sigma_0\}$ and $\{\epsilon_0\}$ are the initial stress and strain at the beginning of this increment (if any).

3. Checking the yield condition using the final stress level reached:

   (a) if $F(\{\sigma'\}) < 0$, the element is still elastic and no plastic process is needed. Apply the next load increment (if any) and proceed from Step 1.

   (b) if $F(\{\sigma'\}) > 0$ (mathematically only, since $F > 0$ is undefined) and $F(\{\sigma_0\}) = 0$ (this means that the element goes into yield at the beginning of this increment), use the elastic-plastic matrix $[D^{EP}]$ (computed with $\{\sigma_0\}$, where $[D^{EP}] = [D^E] - [D^P]$) to find the correct stress increment $\{\Delta\sigma'\}$:

   $$\{\Delta\sigma'\} = [D^{EP}] \{\Delta\epsilon\} \qquad\qquad 2.12$$

   (c) if $F(\{\sigma'\}) > 0$ (mathematically only) and $F(\{\sigma_0\}) < 0$, find the intermediate stress-strain level ($\{\sigma^*\}$ and $\{\epsilon^*\}$) at which yield begins. The difference between the final and the intermediate stress-strain levels gives the elastic

stress and strain increments, above the yield point, which have to be adjusted:

$$\{\Delta\sigma^*\} = \{\sigma'\} - \{\sigma^*\} \qquad\qquad 2.13$$

$$\{\Delta\varepsilon^*\} = \{\varepsilon'\} - \{\varepsilon^*\} \qquad\qquad 2.14$$

Then find the correct stress increment with the elastic-plastic matrix $[D^{EP}]$:

$$\{\Delta\sigma'\} = [D^{EP}] \{\Delta\varepsilon^*\} \qquad\qquad 2.15$$

4. Computing the initial stress which has to be redistributed by a set of forces:

$$\text{in case (3-b)} \quad \{\Delta\sigma''\} = \{\Delta\sigma'\} - \{\Delta\sigma\} \qquad\qquad 2.16$$

$$\text{and in case (3-c)} \quad \{\Delta\sigma''\} = \{\Delta\sigma'\} - \{\Delta\sigma^*\} \qquad\qquad 2.17$$

Obtain current stress-level

$$\{\sigma\} = \{\sigma'\} - \{\Delta\sigma''\} \qquad\qquad 2.18$$

$$\{\varepsilon\} = \{\varepsilon'\} \qquad\qquad 2.19$$

5. Computing the residual nodal forces using:

$$\{q\}_e = \int_{vol} [B]_e^T \{\Delta\sigma''\}_e \, dv \qquad\qquad 2.20$$

6. Applying these residual forces and obtaining a new elastic solution ($\{\Delta\sigma\}$ and $\{\Delta\varepsilon\}$) using the original elastic properties.

7. Repeating Steps 2 to 6.

The process is stopped if the residual forces obtained in any iteration are small relative to the applied external forces and the

system can then take the next load increment. If this is not achieved in a reasonable nubmer of iterations, a collapse condition has been reached and the process is stopped.

2.3.3 Vertification of the Plastic Analysis

A thick-walled cylinder under incremental, increasing internal pressure was used to verify the accuracy of the elastic-plastic analysis developed. This particular example was chosen since the closed form solution has been given by Prager and Hodge (1951). Their solution was obtained for the plane strain situation and the assumption that the material is elastic-perfectly plastic following the von Mises yield criterion. In the finite element solution, the same assumption of ideal plasticity was made, again using the von Mises yield criterion. A quarter of this thick-walled cylinder as shown in Figure 2.7 was used because of the symmetry of the problem. The internal pressure was applied in small increments of 34.475 kPa. When the internal pressure reached 344.75 kPa, the stresses near the inner radius started to exceed the yield stress, and the stress redistribution stage of the plastic analysis was automatically initiated. Eventually, with the iteration process and increasing pressure increments, the thick-walled cylinder yielded completely as anticipated. The spread of the plastic zones is given in Figure 2.8.

The computed tangential stress distributions for different elastic-plastic boundaries are compared with the closed form solution in Figure 2.9. The finite element method results also showed that the

MODULUS OF ELASTICITY $E = 689.5 \times 10^3$ kPa
POISSON'S RATIO $\nu = 0.3$
COHESION $C = 689.5$ kPa
ANGLE OF INTERNAL FRICTION $\phi = 0°$

INCREMENTAL
INTERNAL
PRESSURE

25.4 mm

25.4 mm

50.8 mm

144 ELEMENTS AND 91 NODES
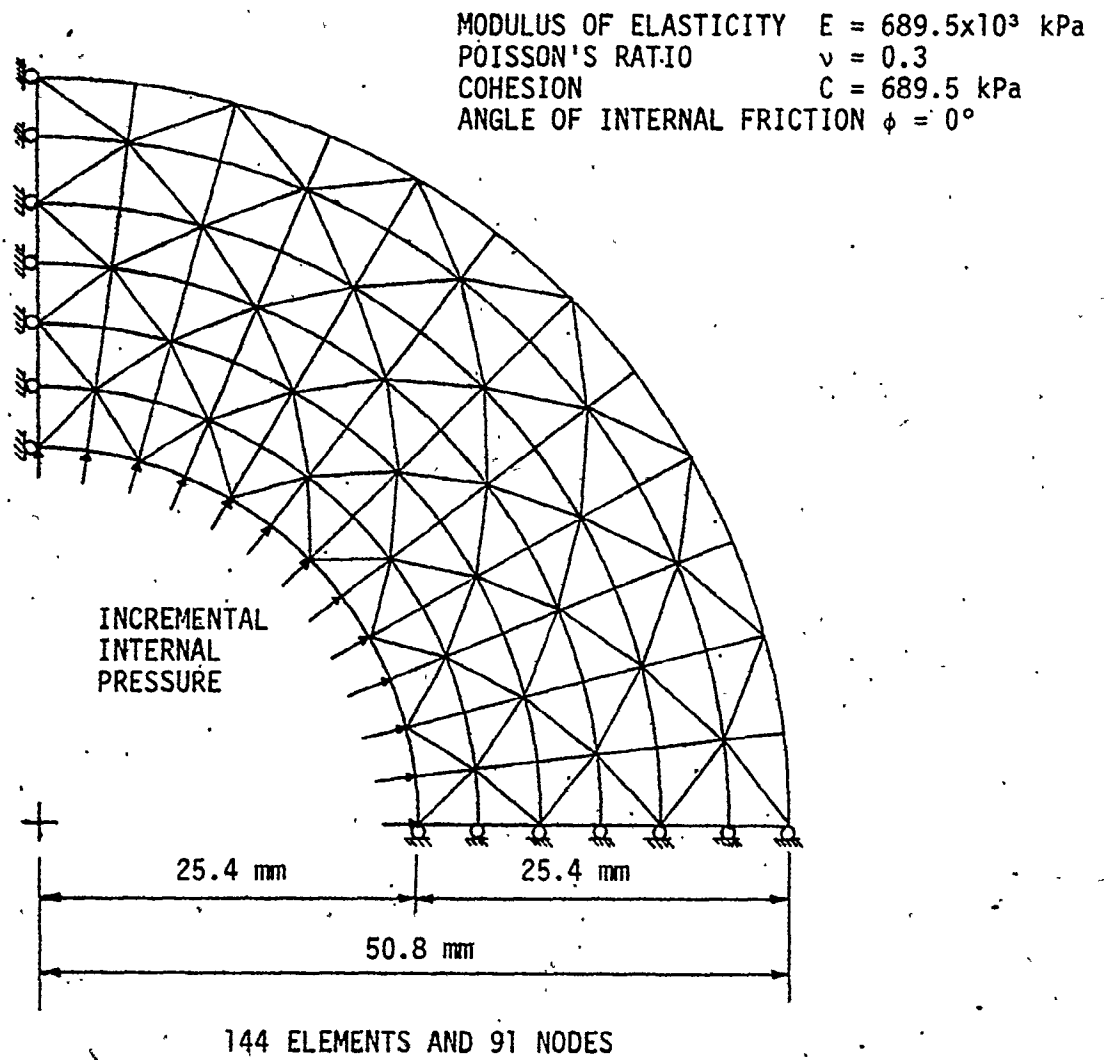
FIGURE 2.7 FINITE ELEMENT MESH REPRESENTATION
OF A THICK-WALLED CYLINDER

	INC	ITR	P, kPa
	2	6	344.75
	3	11	379.225
	4	18	413.70
	5	16	448.175
	6	13	482.65
	7	29	517.125
	8	19	551.6
	8	40	551.6
	9	15	586.075

INC = INCREMENT
ITR = ITERATION
 P = INTERNAL PRESSURE
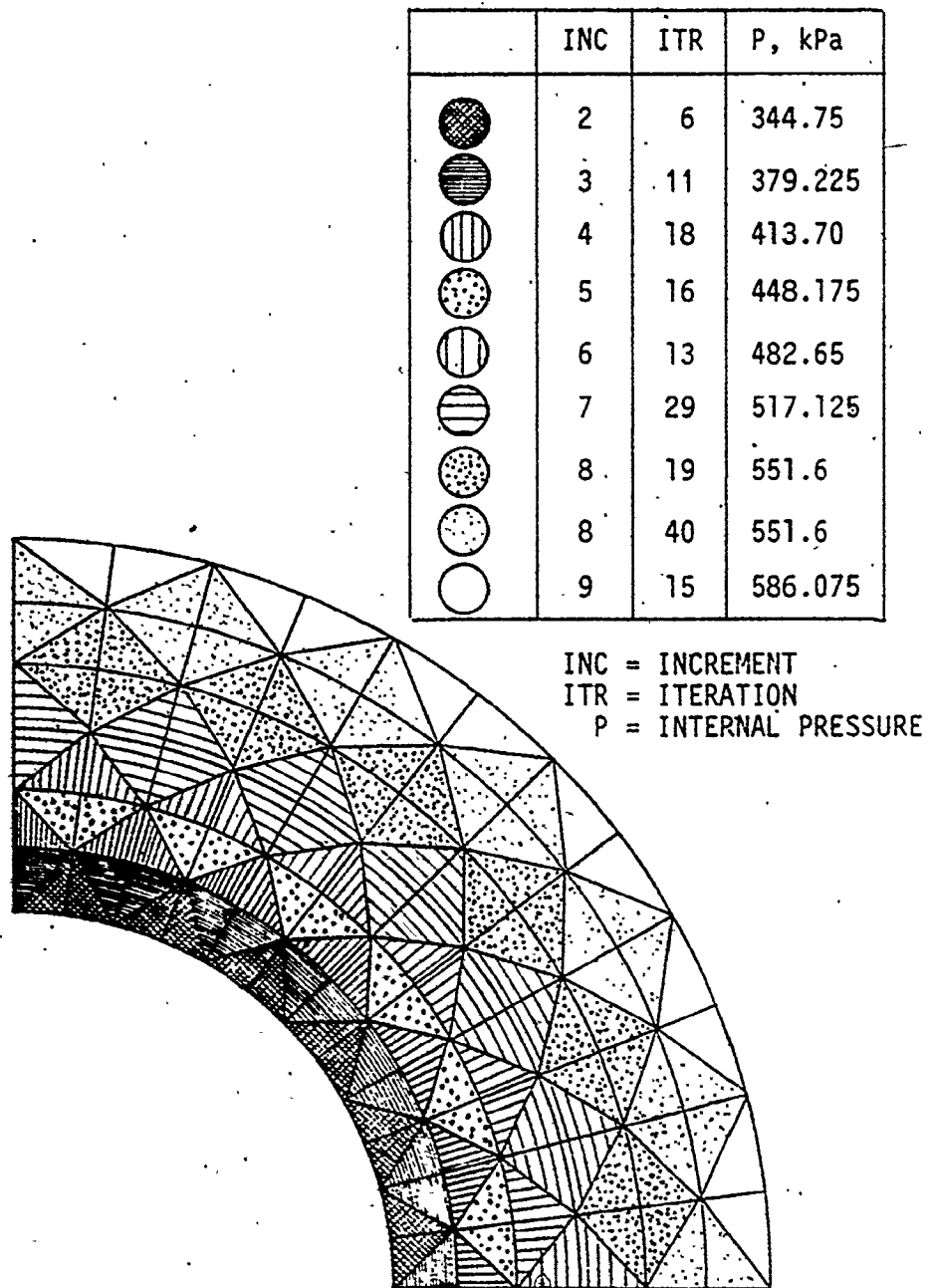
FIGURE 2.8   PROGRESSIVE GROWTH OF PLASTIC DOMAINS
IN THE THICK-WALLED CYLINDER WITH IN-
CREMENTAL INTERNAL PRESSURE, FEM
SOLUTION
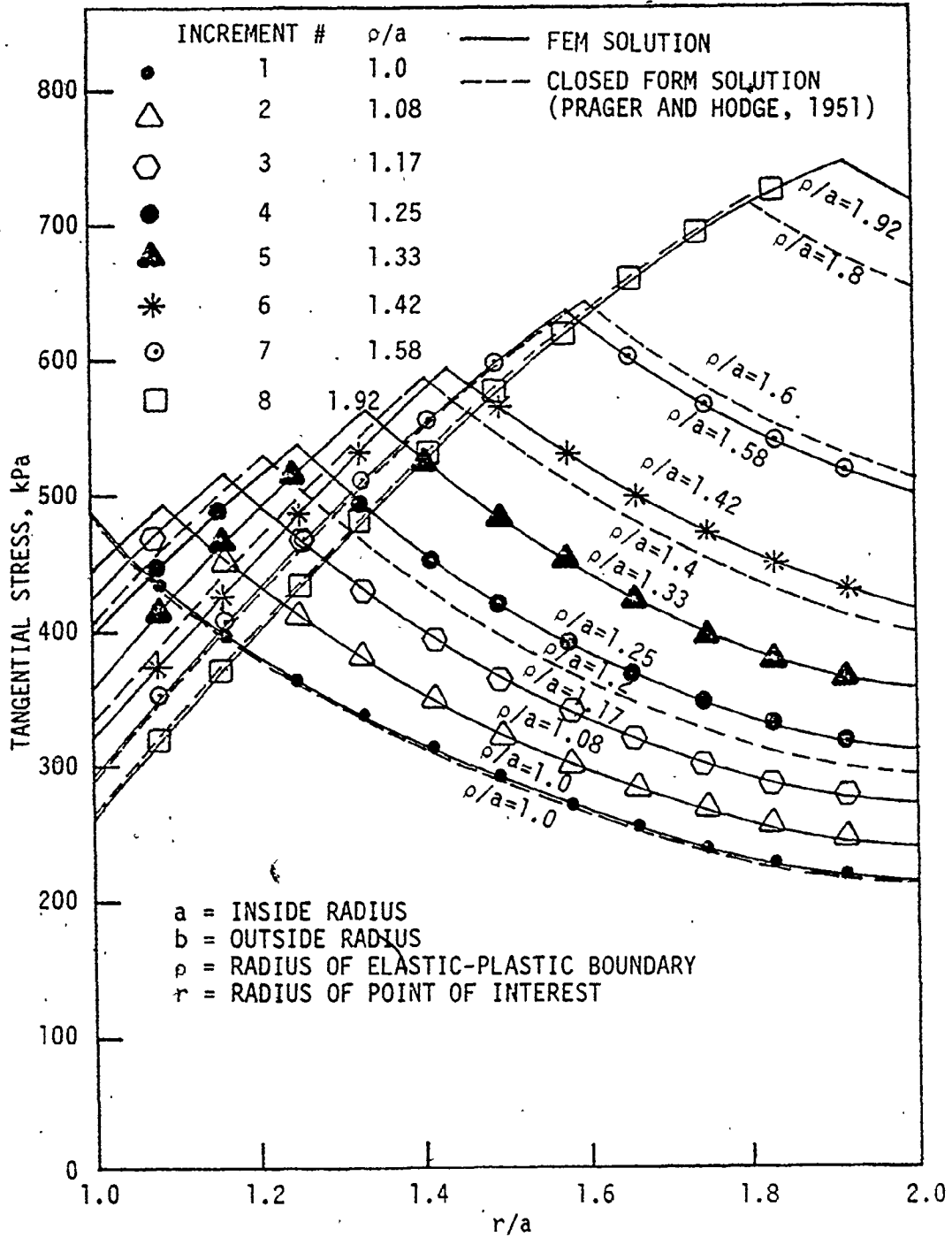
FIGURE 2.9   DISTRIBUTION OF TANGENTIAL STRESSES FOR A·THICK-
WALLED CYLINDER FOR VARIOUS ELASTIC-PLASTIC
BOUNDARIES, FEM SOLUTION AND CLOSED FORM SOLUTION

radial displacements are in excellent agreement with the closed form
solution.

2.4 CREEP ANALYSIS

The analysis of the time-dependent behaviour of excavations re-
quires the selection of an appropriate constitutive relationship that
adequately describes the material behaviour involved. Further, the sel-
ected constitutive relationship should be in a form that can be incor-
porated in the selected solution method (Emery, 1978). In order to de-
velop such a relationship, there are three general approaches available
in geomechanics (Emery, 1971): the fundamental or micromechanistic
approach; the phenomenological or rheological model approach; and the
empirical approach. In the fundamental approach, the strain rate equa-
tions for creep are developed directly from considerations of micro-
mechanistic behaviour. This approach provides an insight into the bond-
ing mechanicsms and shear resistance on the molecular scale that contri-
bute to creep movements (Hirst and Mitchell, 1968), but is difficult to
apply at the macro level. In the rheological model approach, a mathe-
matical description of creep behaviour can be developed using physical
models (springs, dashpots and sliders) that are assumed to behave, under
loading and unloading, in a similar manner to the actual material. The
adequacy of the final solution lies in how well the rheological model
represents the actual material. The constitutive equations based on
linear rheological models, which have been used extensively in flow
problems, represent an idealized condition since the creep response for

most soils and rock is significantly nonlinear (Hirst and Mitchell, 1968). Such behaviour may be best categorized by the empirical approach (Robertson, 1963; Hirst and Mitchell, 1968). In the empirical approach,. parameters such as strain and strain rate are measured experimentally in terms of time, stress and temperature, under controlled conditions. The results may then be used to develop constitutive relationships representing the material's creep behaviour. While the empirical approach was adopted in this study, the other two methods can be incorporated with some modifications.

A creep relationship must satisfy several criteria before being applied to an excavation problem: it must describe the anticipated creep behaviour for the stress paths involved; it must be applicable over the stress ranges anticipated; the parameters must be readily determined; and it must be in a form suitable for the solution method adopted. Most available creep relationships are based on uniaxial, constant load, compressive testing. Therefore, they must be extended through some idealization to describe the multiaxial changing stress state that is representative of the actual field conditions.

2.4.1 Multiaxial Creep Behaviour Idealization

Based on the following three major assumptions, a suitable multiaxial idealization can be achieved:

1. Adopting certain definitions to relate the actual creep strain increments and stresses to equivalent corresponding values. These are then directly compared to the uniaxial creep strain

increment and stresses in any creep relationship. The most
appropriate definitions are those given by Dorn (Lubahn and
Felgar, 1961), where the equivalent creep strain increment is
related to the octahedral creep shear strain increment and the
equivalent stress is related to the octahedral shear stress by
the equations:

$$\Delta\varepsilon_e^c = \frac{1}{\sqrt{2}} \Delta\gamma_{oct}^c \qquad\qquad 2.21$$

and, $$\sigma_e = \frac{3}{\sqrt{2}} \tau_{oct} \qquad\qquad 2.22$$

where $\Delta\varepsilon_e^c$ is the equivalent creep strain increment; $\Delta\gamma_{oct}$ is
the octahedral creep shear strain increment; σ_e is the equiva-
lent stress; and τ_{oct} is the octahedral shear stress.

2. Assuming the Prandtl-Reuss condition (the components of creep
   strain increments are proportional to, and parallel to, the
   corresponding stress deviator with no volume change due to
   creep) is applicable. Then, the increments of creep strain
   components, $\Delta\varepsilon_{ij}^c$, are determined using the equation:

$$\Delta\varepsilon_{ij}^c = \frac{3}{2} \frac{\Delta\varepsilon_e^c}{\sigma_e} S_{ij} \qquad\qquad 2.23$$

where S_{ij} are the deviatoric stresses. This equation is ana-
logous to the Prandtl-Reuss equation of plasticity (Lubahn and
Felgar, 1961).

3. Adopting a cumulative rule to determine the accumualted creep
   strains when the stresses are changing. The appropriate one

which has been widely adopted is the strain-hardening cumulative strain rule. This rule states that the component of strain rate depends only on the current creep strain and current stress, the effect of previous strain rates being negligible. The rule is shown schematically in Figure 2.10 and is often referred to as a mechanical equation of state (Lubahn and Felgar, 1961).

It should be noted that this generalization from the uniaxial to the multiaxial case is based on various assumptions from the theory of plasticity and the validity of these assumptions in geotechnology is still an open question which requires further research. However, the strain-hardening approach is supported by considerable data reported in the literature (Emery, 1971).

2.4.2 Creep Analysis: Incremental Initial Strain Method

In general, an incremental procedure is adopted for the creep analysis in which the final solution is determined by solving a number of linearized problems distributed between the initial and final desired time. The components of the creep strain increment for each time interval are assumed to be given by Equation 2.23. During creep, the stresses will be changing with time and can be represented by the typical smooth stress-time curve shown in Figure 2.11. The creep strain increments are assumed to follow the strain-hardening cumulative creep law. The analysis is simplified by considering incremental creep strains in a constant stress time interval Δt, followed by an instantaneous stress increment. The error introduced through keeping the stresses constant in the time interval Δt decreases as the time interval is decreased (Greenbaum, 1966;

48

FIGURE 2.11 APPROXIMATION OF A SMOOTH STRESS-STRAIN CURVE BY A SERIES OF STEPS (EMERY, 1971)
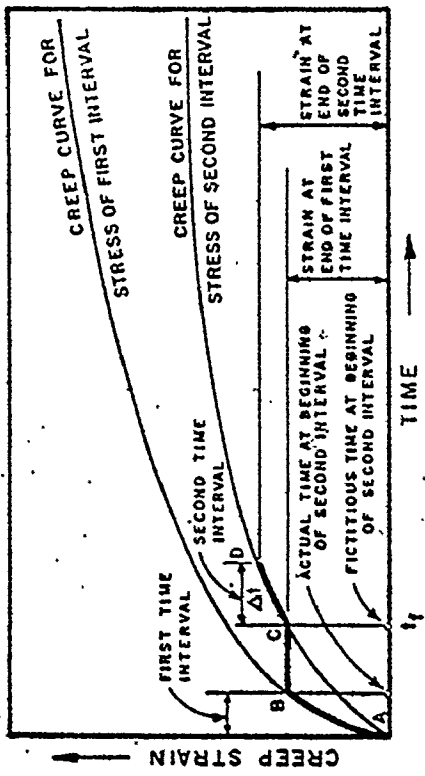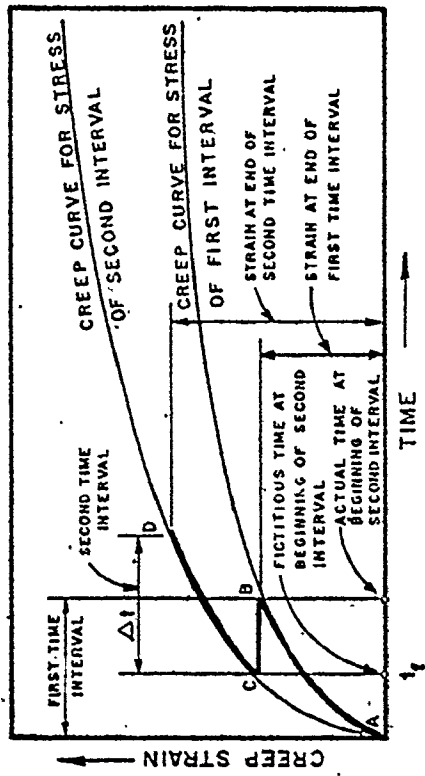
FIGURE 2.10 SCHEMATIC SHOWING HOW TO DETERMINE THE INCREMENT OF CREEP STRAIN WITH CHANGING STRESS (EMERY, 1971)

Emery, 1971).

At the beginning of each time interval the stresses, and elastic and creep strains, will be known from the calculations for the preceding time interval. For the first creep increment, there are no creep strains so that the elastic solution is the starting point. The incremental procedure can be summarized as:

1. Determining the equivalent stress value σ_e from the stresses obtained at the end of the preceding time interval.

2. Calculating the equivalent creep strain increment $\Delta\sigma_e^C$ for this time interval from the appropriate selected uniaxial creep relationship using the equivalent stress obtained in Step 1. Since the equivalent stress will usually change for each time interval, the strain-hardening cumulative creep law shown in Figure 2.10 is used to determine the fictitious time t_f at the beginning of this interval. Then, t_f, Δt and σ_e can be used in the creep relationship to determine $\Delta\varepsilon_e^C$.

3. Calculating the components of the creep strain increment $\Delta\varepsilon_{ij}^C$ using Equation 2.23, with σ_e and $\Delta\varepsilon_e^C$ obtained in Steps 1 and 2, respectively.

4. Calculating the accumulated creep strains at the end of this time interval by adding the creep strain increments $\Delta\varepsilon_{ij}^C$ obtained in Step 3 to the creep strains at the beginning of the time interval.

5. Calculating the stress increment $\Delta\sigma_{ij}$ at the end of the time interval using the creep strain increments obtained in Step 3 together with the constitutive, kinematic, and equilibrium equations and boundary conditions for the particular problem.

The previous steps are repeated for each time interval up to the final desired elapsed time. In the present analysis, there are no internal interactions to improve the solution accuracy using the stresses determined at the end of the time interval. However this could be done, if desired, in a similar manner to the plastic analysis explained previously. Generally, as shown by Greenbaum (1966) the time intervals can be selected sufficiently small to yield the desired accuracy without iterations.

2.4.3 Determination of Time Increments

In the incremental procedure for nonlinear creep problems, the time intervals selected must be small enough to ensure the stability of the solution process. Greenbaum (1966) studied this time interval selection and suggested the following limits in order to ensure stability:

$$\Delta\varepsilon_e^C / \varepsilon_e^E \leq 1/25 \qquad\qquad 2.24$$

where $\Delta\varepsilon_e^C$ is the equivalent creep strain increment, and ε_e^E is the equivalent elastic strain, and

$$\Delta t_{j+1} \leq 1.2 \, \Delta t_j \qquad\qquad 2.25$$

The computer program for creep analyses based on the above procedures, and developed by Emery (1971), was incorporated as a sub-

program in the present analysis after completing any necessary modifications. Further details on the methods adopted are given by Greenbaum (1966) and Emery (1971).

2.4.4 Verification of the Creep Analysis

A thick-walled cylinder under a constant internal pressure of 2.5 MPa was used to check the accuracy of the creep analysis since the closed form solutions are available for this problem (Greenbaum, 1966). Due to symmetry, a quadrant of the cross-section was used (boundary condition restriction) to obtain the radial deformations and stress distributions in the cylinder using the finite element method. The same mesh idealization shown in Figure 2.7 was used with inside radius 4.064 mm and outside radius 6.350 mm. The creep relationship used was:

$$\varepsilon = 6.4 \times 10^{-18} \sigma^{4.4} t \qquad\qquad 2.26$$

where ε is the creep strain, σ is the stress in psi, and t is the time in minutes. Figure 2.12 gives a comparison of the finite element method solution with the closed form solution for the stresses in the thick-walled cylinder for both the elastic and steady state creep conditions, while Figure 2.13 gives the computed radial creep deformations compared to the finite element solution obtained by Greenbaum (1966). It can be seen that there is a close agreement between all of these solutions.
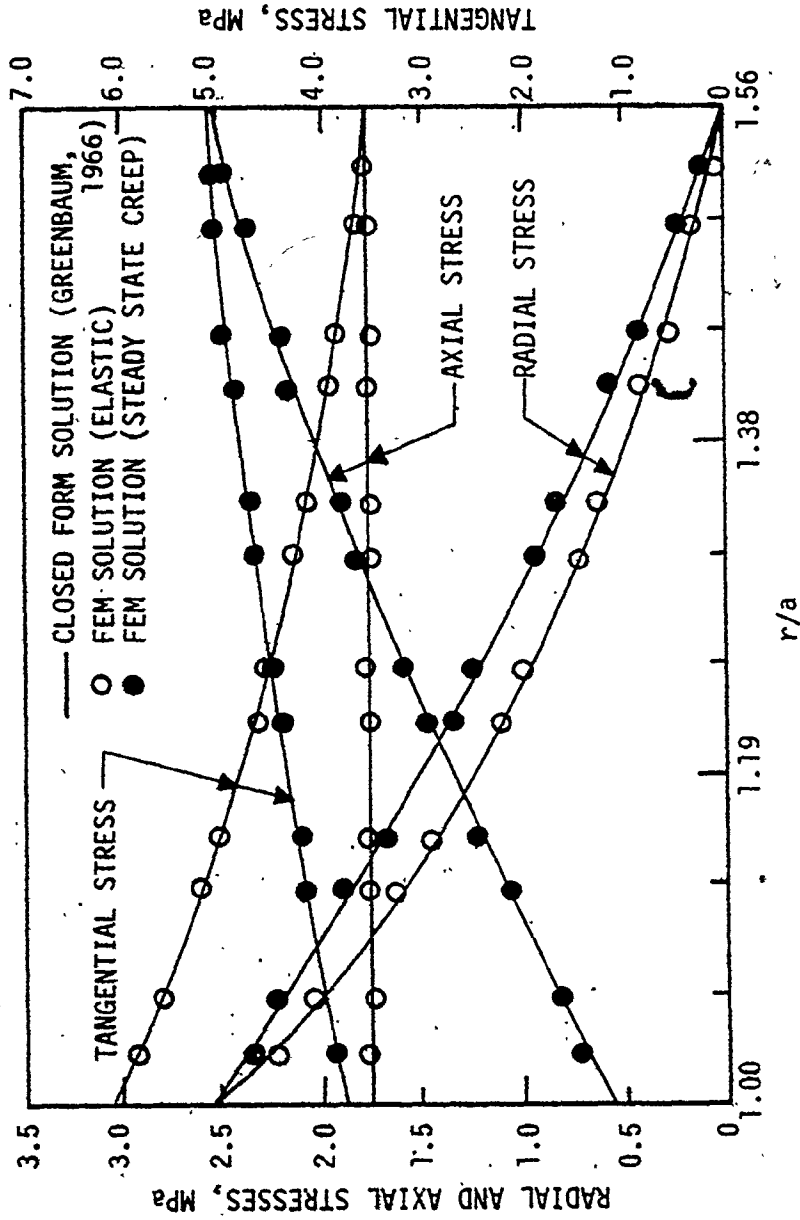
FIGURE 2.12   ELASTIC AND STEADY STATE STRESS DISTRIBUTION IN THE THICK-WALLED CYLINDER, COMPARISON OF CLOSED FORM AND FEM SOLUTIONS
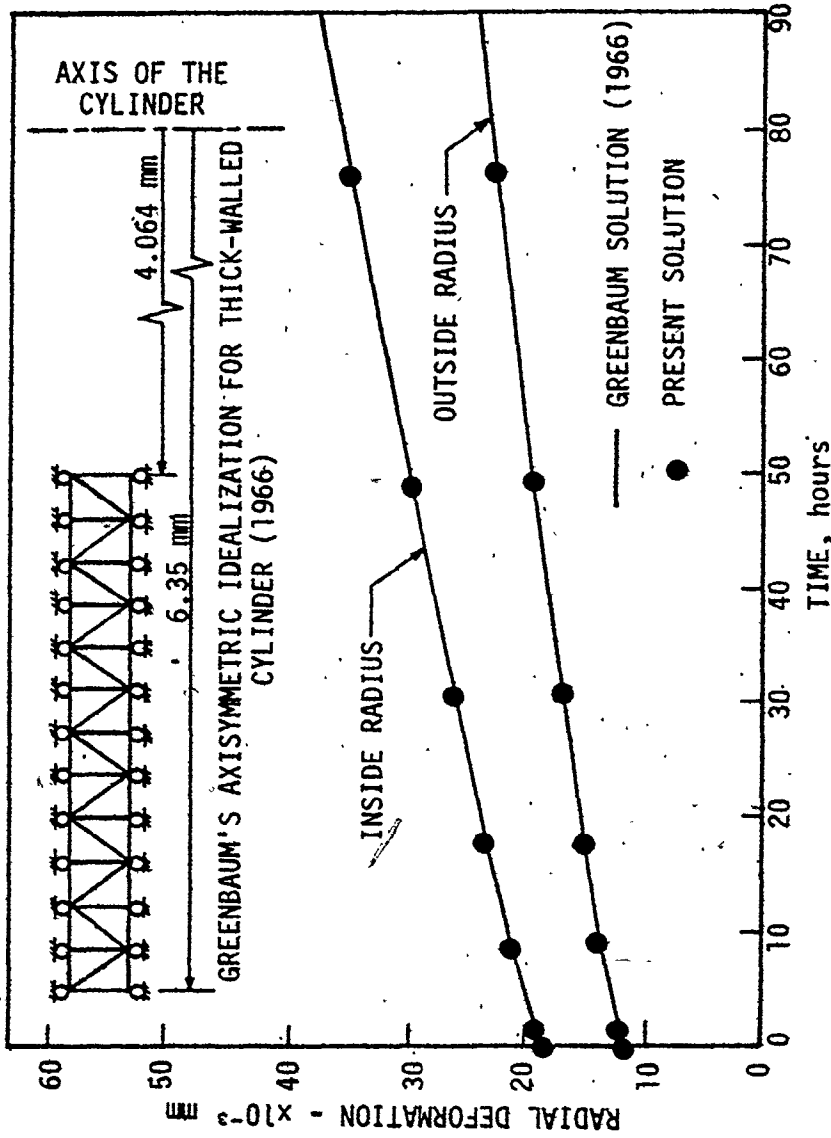
FIGURE 2.13 RADIAL CREEP DEFORMATION OF THE THICK-WALLED CYLINDER

2.5 SIMULATION OF TUNNEL SUPPORT INSTALLATION

The tunnel support installation is simulated by reactivating the elements which were deactivated during the excavation simulation. The reactivation process has been formulated by adjusting the appropriate modulii for elements representing the liner and including them in the global stiffness matrix. Stresses and strains within these liner elements and their nodal displacements are set to zero to obtain elements free of stresses, strains and displacements after installation and before any kind of loading. The tunnel support can be a rigid, or soft-rigid, liner. The rigid liner, with a stiffness generally greater than that of the ground, can be represented by one or more layers of elements. The soft-rigid support, which consists of a rigid liner and a soft backing between the liner and the ground, is constructed from two materials. Each of these materials can be represented by one or more layers of elements. The soft backing should have a very low stiffness with respect to the ground and rigid part of the liner as its function is to reduce stress build-up by readily deforming under time-dependent loadings.

Although the liner has been treated as a linear elastic, isotropic material having no time-dependency, the analysis does allow the incorporation of liner time-dependency if desired.

For a more detailed stress distribution in the liner, a refined mesh for the liner can be used separately, and the stresses obtained by imposing the appropriate displacements from the coarser mesh as boundary conditions.

2.6 FINITE ELEMENT METHOD COMPUTER PROGRAM AND GENERAL DESCRIPTION

A plane strain, small linear displacement, triangular finite element computer program has been developed using the approach described previously. The resulting computer program, PSEA, (Plane Strain Excavation Analysis) developed for homogeneous or nonhomogeneous isotropic, linear elastic-perfectly plastic media having time-dependent characteristics can simulate the following conditions:

1. excavation in-stages for any shape of opening and incremental loadings;

2. support placement delay to allow the major time-dependent deformations to occur if significant creep behaviour is involved;

3. support placement simulation with, or without, soft backing;

4. elastic-plastic analysis following any change in the stress state as a limiting stress condition;

5. creep analysis after support installation to predict the long term behaviour of the support system and the maximum stress developed.

2.7 MESH GENERATION PROGRAM

A mesh generation program has been developed for circular openings to provide the input data for the finite element excavation program. The mesh and the input data cards are generated automatically by the computer using only two input data cards. Several hundred data cards describing nodal fixidity conditions, nodal coordinates, and element coding, as well as a general mesh plot are provided. This program

considerably decreases the overall time for mesh and input data preparations. It minimizes the errors due to key punching. Also, it will help in cases where parametric studies or detailed stress analyses for the tunnel support are required. This program can be used as a subroutine in any other finite element program with a few modifications in notations.

Due to the symmetry of the geometry and the loading about the vertical axis, one half of the region is selected for the analysis when the initial in situ stress field increases with depth. If these stresses do not vary with the depth, one quarter of the region is required for the analysis. The boundary was chosen as a 'semi' circle at a distance from the tunnel face. The mesh consists of triangular elements formed by 'semi' circles, located at increasing distances apart, with a number of radials. The excavated elements can be represented by one or more layers as shown in Figure 2.14. These excavated elements will then be used later to represent the tunnel support as explained before.

To investigate mesh refinement influences on the predicted results, several cases were investigated for a circular opening in a radially uniform in situ stress field. These cases were varied from coarse to fine meshes with the boundary located 10 radii from the tunnel centre. The results show that with an increasing number of elements, the results approach the closed form solution. It was also found that meshes with a minimum of 160-180 elements would provide a reasonable idealization for plane strain excavation analyses where only one half of the medium is simulated.

OUTSIDE BOUNDARY CAN
BE FREE OR FIXED

R_b

R

ELEMENTS
TO BE EX-
CAVATED
(ALSO RE-
PRESENTING
FUTURE
LINER)

R = TUNNEL RADIUS

R_b = OUTSIDE BOUNDARY
RADIUS

192 ELEMENTS AND 117 NODES
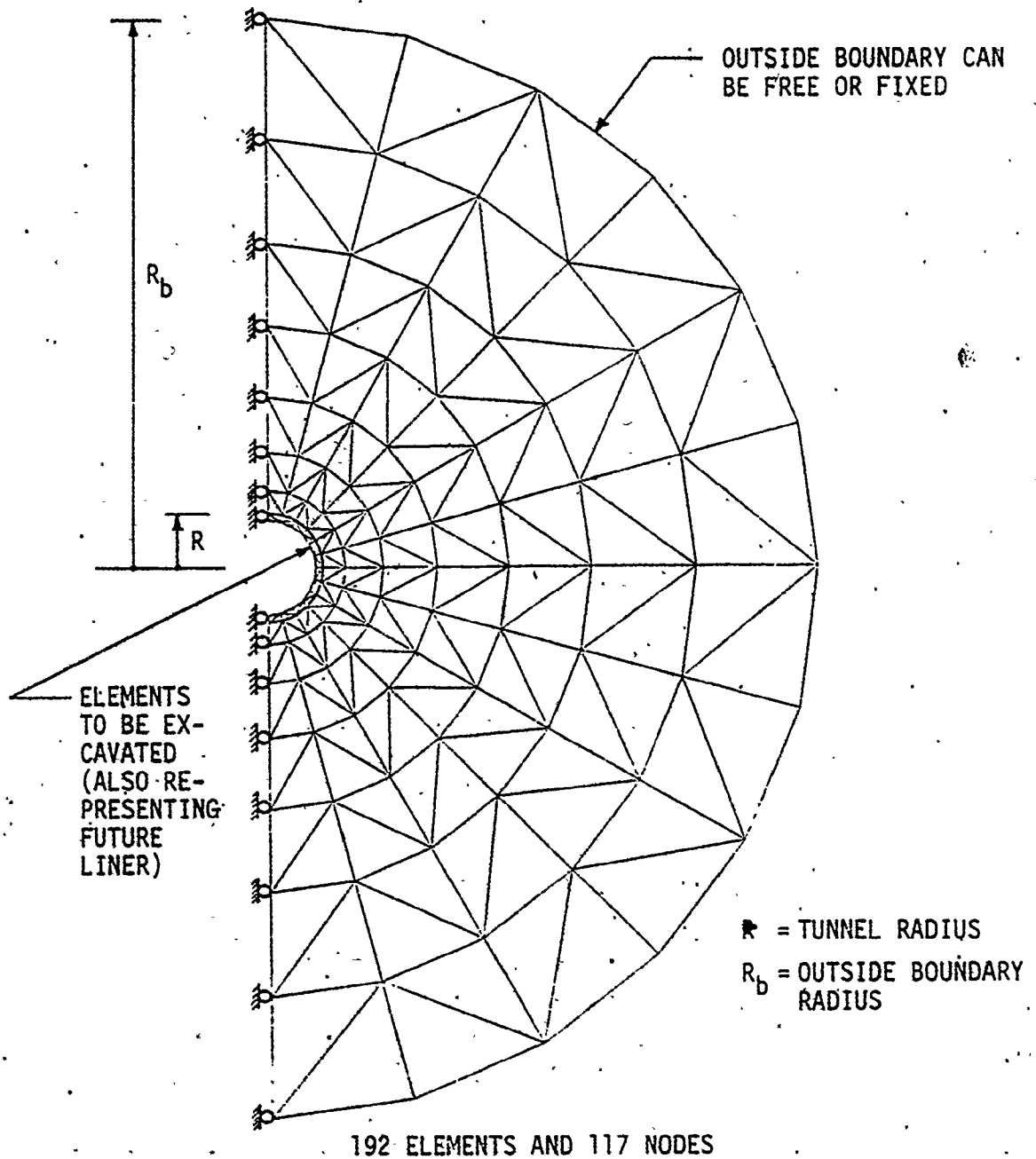
FIGURE 2.14   TYPICAL MESH GENERATED FOR UNDERGROUND
EXCAVATION AND LINER PLACEMENT SIMULATION,
PLANE STRAIN CONDITION

2.8 BOUNDARY CONDITION INFLUENCES

Since the finite element method involves a 'truncation' of the medium to a finite size, a boundary located near the opening will influence the computed results. The boundaries must be located far enough from the opening to not only minimize the boundary location influences, but also to ensure results independent of the boundary condition chosen. The question of the boundary condition influences has been raised since there are two boundary idealizations that can be adopted: fixed (no displacement); and free boundaries. To investigate the difference between both boundary idealizations, a number of excavation analyses for a circular cavity having radially uniform in situ stresses, with different boundary locations for both boundary conditions were conducted. The other boundaries were located at 3 to 10 times the tunnel radius away from the tunnel axis. Half the mesh shown in Figure 2.14 was used (since uniform stresses were involved) for all cases with the same number of elements and nodes (96 elements and 63 nodes). The results are plotted in Figure 2.15. The results show that if the boundary is sufficiently distant, whether it is fixed or free, the analysis gives results which are not significantly different. For example, if the boundary is located between 7 and 10 times the tunnel radius away from the opening, the results obtained from both boundary condition idealizations are within 2% of each other and approaching the closed form solution. Also, these results can be improved if the number of elements is increased.
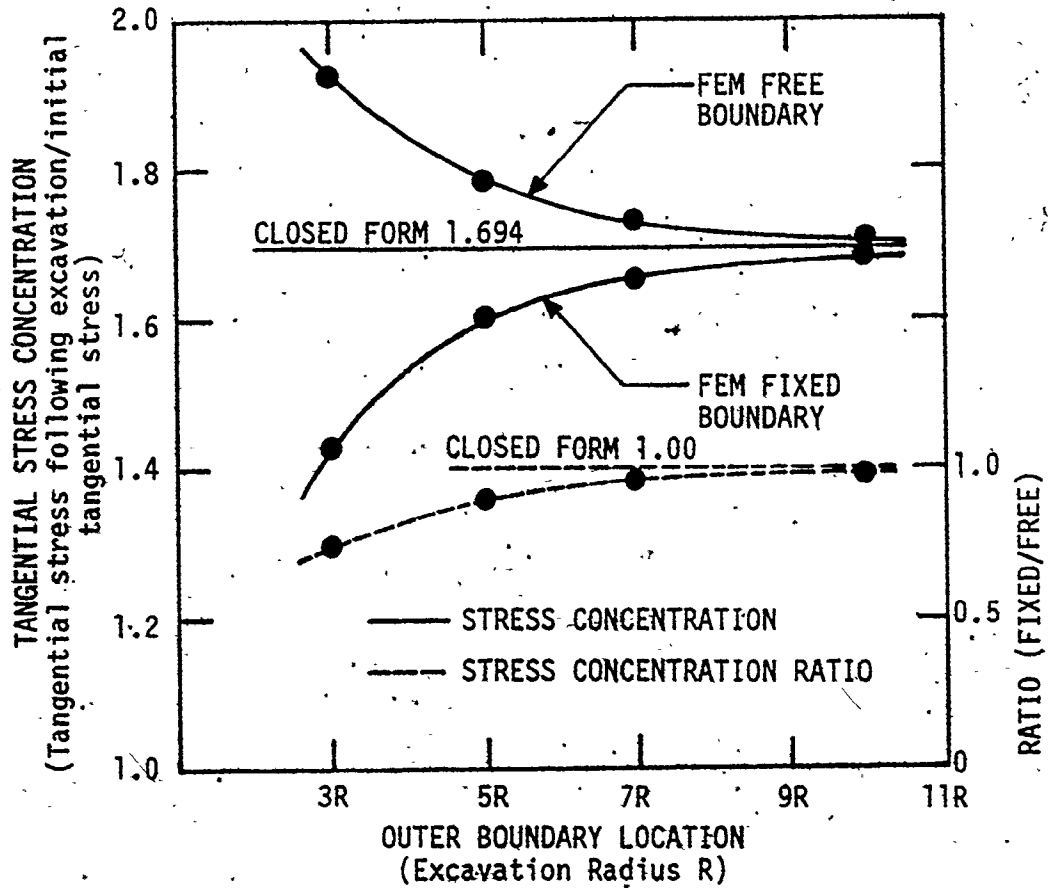
FIGURE 2.15. BOUNDARY CONDITION INFLUENCES ON THE
STRESS CONCENTRATION AT A DISTANCE 1.2R
FROM THE TUNNEL AXIS (R = TUNNEL RADIUS)

2.9 ADVANTAGES AND LIMITATIONS OF THE PLANE STRAIN ANALYSIS

The two-dimensional plane strain analysis of excavations has inherent advantages which make it popular, and it is still widely used in practice. It is simple and economic when compared with three-dimensional stress analysis. It can accommodate any shape of excavation, and can be used for nonhomogeneous ground conditions. It can handle boundary conditions such as loads or displacements, and discontinuities can be incorporated without difficulty. Moreover, using a two-dimensional plane strain analysis for designing tunnel support systems is generally satisfactory if the support system will be placed some distance from the advancing face.

However, a two-dimensional plane strain analysis is not applicable for simulating excavation (face advancement) and support placement near the advancing face where the three-dimensional deformations and stresses must be considered. In addition, such a stress analysis cannot be used to simulate the progressive interaction during face advancement and support placement. To remove these limitations, a three-dimensional axisymmetric approach has been adopted to deal more correctly with the problems cited. This approach is explained in Chapter 3.

CHAPTER 3

THREE-DIMENSIONAL SIMULATION OF CYLINDRICAL TUNNEL EXCAVATIONS FOR AXISYMMETRIC OR NON-AXISYMMETRIC STRESS STATES NEAR THE ADVANCING FACE

3.1 INTRODUCTION

The two-dimensional (plane strain) simulation of tunnel excavation and liner placement presented in Chapter 2 was extended through an axisymmetric approach to include the full representation of the actual three-dimensional behaviour near the advancing tunnel face. As mentioned previously, tunnelling in squeezing ground and the increasing use of precast concrete segmental liners were the prime motivation for developing the three-dimensional simulation.

The axisymmetric approach was adopted to consider the two most common loading conditions due to axisymmetric and non-axisymmetric initial in situ stress states. The first case is limited to axisymmetric tunnel structures and axisymmetric loadings due to a uniform radial stress condition. For this case, the transverse stress ratio K_t (ratio between the lateral and vertical stresses) is equal to unity. The finite element formulation for this case is then similar to that for plane strain analyses.

Since K_t is not generally equal to unity, the more important second case of axisymmetric tunnel structures subjected to non-axisymmetric loadings due to non-uniform radial stress condition

61

($K_t \neq 1$) was also considered. This generalization requires separation of
the variables by expanding them into Fourier series with respect to the
angular direction θ: The approach is thus identical to the analysis of
solids of revolution subjected to non-axisymmetric loadings (Zienkiewicz,
1977).

The axisymmetric approach used is restricted to axisymmetric
structures whose geometry and material properties do not vary with the
angular direction θ. In other words, it is applicable to cylindrical
cavities constructed in isotropic, homogeneous media. The analysis pre-
sented here is also restricted to cases where one of the in situ principal
stress directions coincides with the tunnel's axial direction. (This
aspect of the analysis is discussed in Section 3.2.) While discontinu-
ities (joints, bedding, faults) and individual liner segment joints cannot
be considered in the axisymmetric simulation, the importance and potential
behaviour of these features can be considered with supplementary plane-
strain analyses of the type presented in the previous chapter. This
typically involves the use of displacement boundary conditions from the
axisymmetric simulation in conjunction with the plane strain analyses.

The axisymmetric simulation has been developed in the form of a
general finite element program which can be used during engineering design.
It can be applied to simulate the following conditions involved during
tunnelling processes:

1. Excavation of the full tunnel cross section in stages to simulate
   face advancement (incremental advance).

2. Installation of the tunnel support system, with or without soft backing, at a selected distance from the advancing face.

3. Support installation delay to allow most of the time-dependent displacements to occur if creep behaviour is involved.

4. Elastic-plastic analysis following any change in the stress state.

5. Creep analysis after support installation to determine the maximum stresses developed in the liner.

Excavation and support placement are simulated using the deactivation and reactivation operations during the analysis. Simulation of the incremental advance of the tunnel face is thus possible by deactivating each 'round' of elements sequentially.

Details of the axisymmetric simulation procedures and methodology (axisymmetric finite element method, initial in situ stresses, excavation simulation, ground yielding, creep analysis, and tunnel liner placement) are described in following sections of this chapter. Simplified flow diagrams are given along with a mesh generation program developed for ease of data input. A typical underground opening problem selected to compare the axisymmetric simulation method results with other methods is then described. The results from this analysis are also reported to demonstrate the capability of the proposed axisymmetric simulation method. Further applications of the three-dimensional (axisymmetric) simulation method are given as a series of examples in Chapter 5.

3.2 AXISYMMETRIC FINITE ELEMENT METHOD

A typical axisymmetric, triangular, finite element of the type adopted in the analysis is shown in Figure 3.1. The triangular cross section of the element 'ijk' is rotated about the Z-axis forming a complete axisymmetric solid ring element concentric with the Z-axis. In the case of axisymmetric solids, it is convenient to work with cylindrical coordinates, i.e. the angular direction θ and two coordinates r,z in the R-Z plane shown in Figure 3.1. The corners of this element are nodal circles, each with three degrees of freedom (i.e. motion in the r,z and θ directions is permitted), and a three-dimensional stress analysis is involved.

The radial, axial, and circumferential load and displacement components are P_r, P_z and P_θ, and u, v and w in the r, z and θ directions, respectively:

$$\{P\}^T = \{P_r \; P_z \; P_\theta\} \tag{3.1}$$

$$\{U\}^T = \{u \; v \; w\} \tag{3.2}$$

The strain components, which correspond to these displacements, are:

$$\{\epsilon\}^T = \{\epsilon_r \; \epsilon_z \; \epsilon_\theta \; \gamma_{rz} \; \gamma_{r\theta} \; \gamma_{z\theta}\} \tag{3.3}$$

where
$$\epsilon_r = \frac{\partial u}{\partial r}$$

$$\epsilon_z = \frac{\partial v}{\partial z}$$

$$\epsilon_\sigma = \frac{1}{r}\left(\frac{\partial w}{\partial \theta} + u\right) \tag{3.4}$$
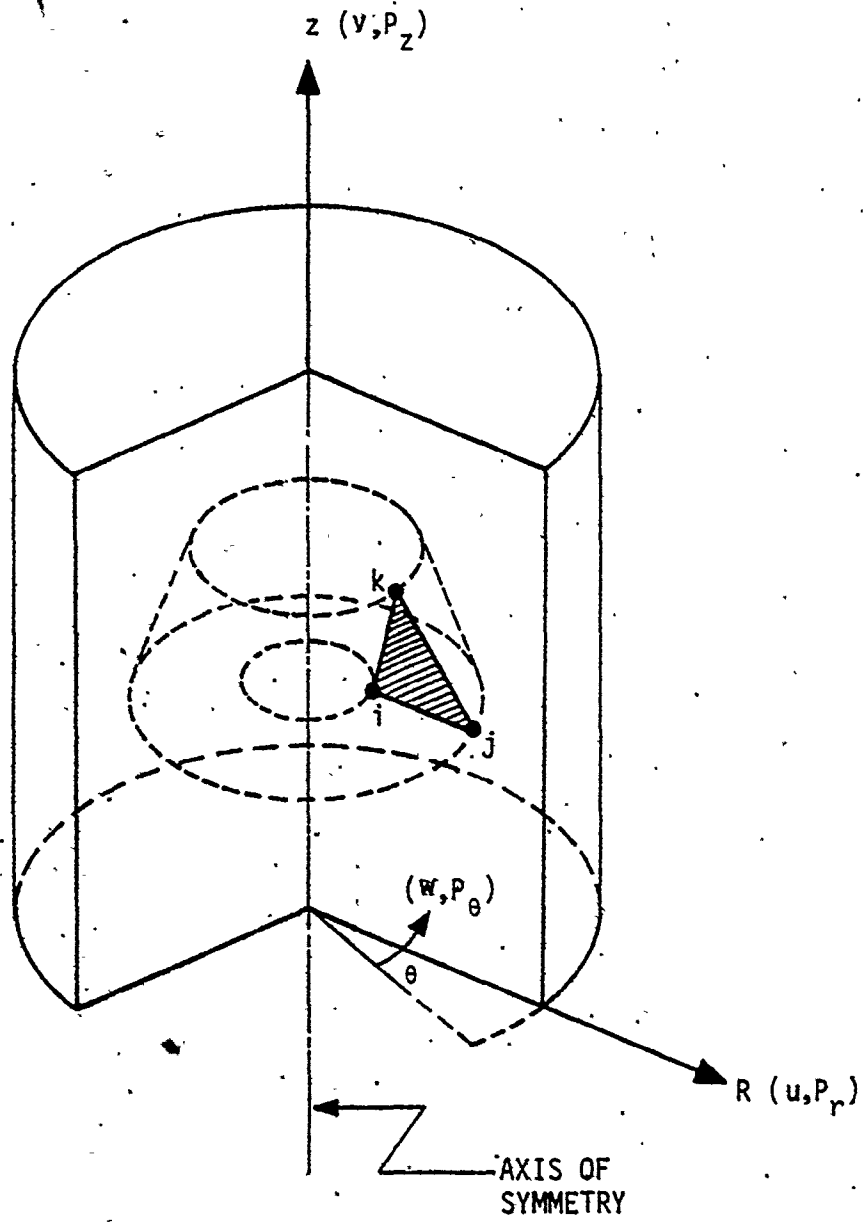
FIGURE 3.1   TYPICAL AXISYMMETRIC, TRIANGULAR, FINITE
ELEMENT OF AN AXISYMMETRIC SOLID

$$\gamma_{rz} = \frac{\partial u}{\partial z} + \frac{\partial v}{\partial r}$$

$$\gamma_{r\theta} = \frac{1}{r} \left(\frac{\partial u}{\partial \theta} - w \right) + \frac{\partial w}{\partial r}$$

$$\gamma_{z\theta} = \frac{\partial w}{\partial z} + \frac{1}{r} \frac{\partial v}{\partial \theta}$$

and the corresponding stress components are:

$$\{\sigma\}^T = \{\sigma_r \ \sigma_z \ \sigma_\theta \ \tau_{rz} \ \tau_{r\theta} \ \tau_{z\theta}\} \qquad (3.5)$$

While a 'simple' element has been adopted, the analysis can be made more sophisticated in this regard. The full finite element formulation for the axisymmetric case of loading is very similar to that for the plane strain and plane stress cases and will not be repeated here (Desai and Abel, 1972; Zienkiewicz, 1977). However, it should be noted that lengthy expressions (see Appendix B) are involved when exact integrations are adopted for any expression involving radial terms. It is also possible to use an approximate procedure (Nair, 1975) to evaluate such expressions for the centroidal points as an average of the nodal element coordinates (see Figure 3.1):

$$\bar{r} = \frac{1}{3} (r_i + r_j + r_k) \qquad (3.6)$$

$$\bar{z} = \frac{1}{3} (z_i + z_j + z_k) \qquad (3.7)$$

While reasonably accurate results are achieved using this approximate procedure, exact integrations have been adopted throughout. Further details on these integrations are given in Appendix B.

Combining all of the elements representing the excavation problem, using the displacement method, yields the general equation to be solved:

$$[K]\{u\} = \{P\} \tag{3.8}$$

where $[K]$ is the global stiffness matrix assembled from all elements, $\{u\}$ is the vector of unknown nodal displacements and $\{P\}$ is the nodal loading vector due to excavation.

The major change in this approach from the plane strain case is in the load vector formulation (Equation 3.8). In the axisymmetric case, the nodal forces represent the combined effect of the forces acting along the circumference of the circle forming the element node. The load vector then becomes:

$$\{P\} = 2\pi \iint [B]^T \{\sigma_0\} \, r \, dr \, dz \tag{3.9}$$

where $\{\sigma_0\}$ is the vector of total stresses within the removed element.

The most general case of non-axisymmetric loading can be resolved into two components: symmetric and antisymmetric modes with respect to the plane containing the $\theta = 0$ axis, as shown in Figure 3.2. Expansion for a number of harmonics in both the symmetric and antisymmetric modes then gives a full Fourier series representation.

As stated previously, the present analysis is restricted to cases where one of the in situ principal stress directions coincides with the tunnel's axial direction. For example, this situation is shown in Figure 3.3 for a horizontal tunnel. The Z-axis (see Figure 3.1), which is the

Prn cos nθ
Pzn cos nθ

-Pθn sin nθ

(a) nth SYMMETRIC MODE

Prn sin nθ
Pzn sin nθ

Pθn cos nθ

(b) nth ANTISYMMETRIC MODE
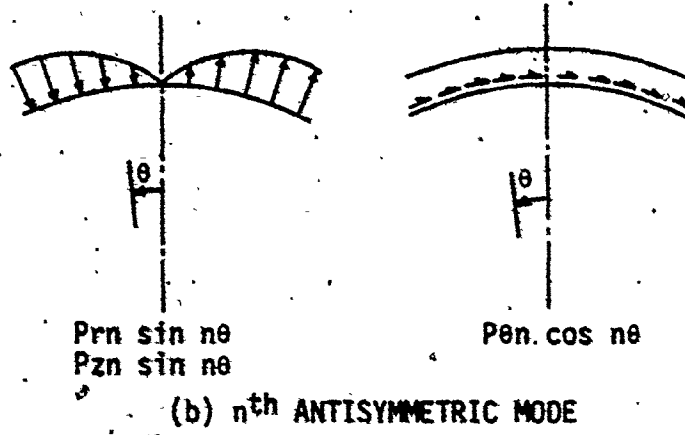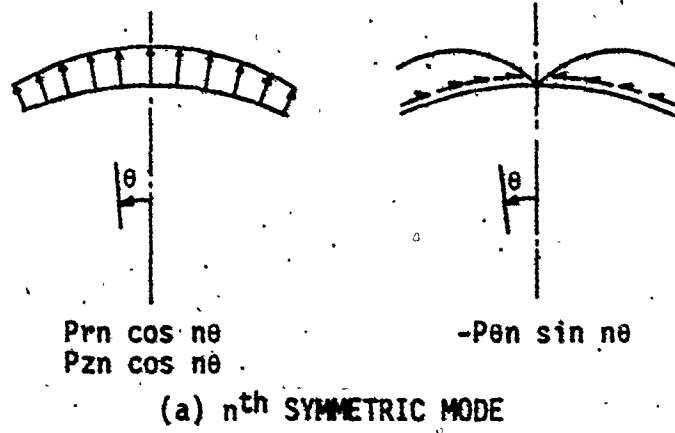
FIGURE 3.2   FOURIER SERIES REPRESENTATION
OF THE APPLIED LOADING
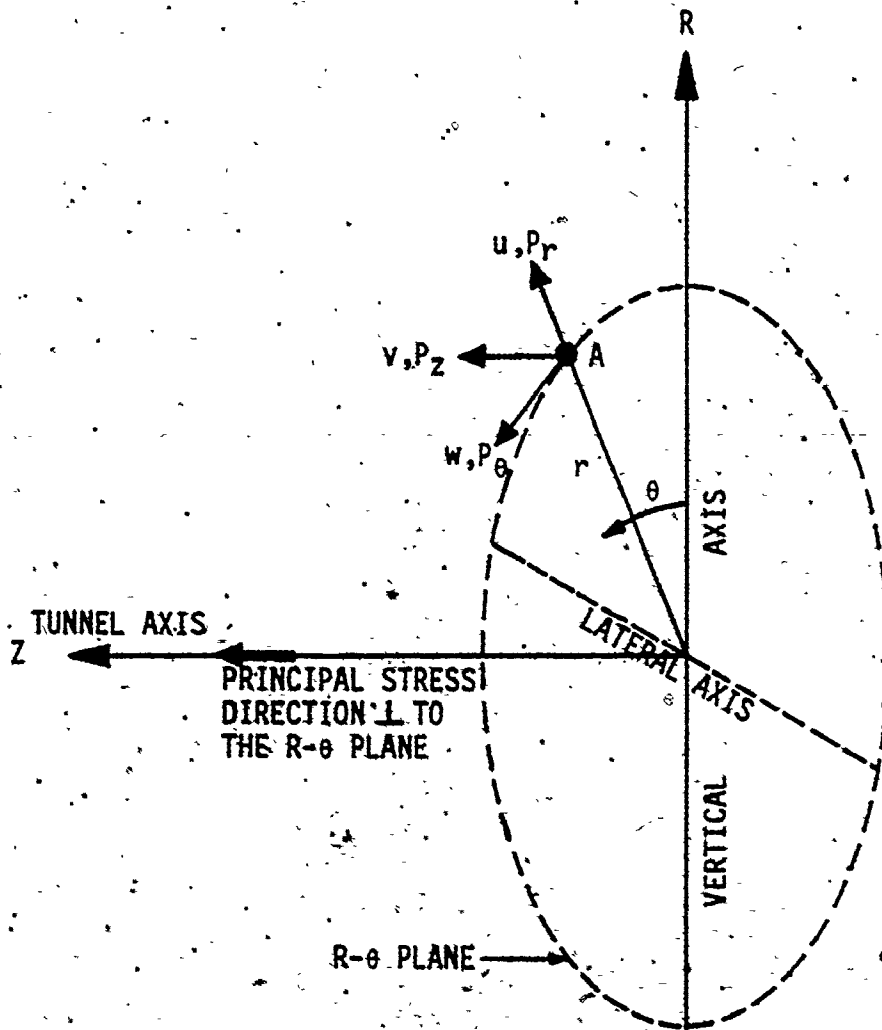
FIGURE 3.3   VERTICAL, LATERAL AND TUNNEL AXIS REFERENCE
DIRECTIONS FOR A HORIZONTAL TUNNEL

axis of revolution for the axisymmetric elements and the tunnel axial direction, coincides with one of the in situ principal stress directions. This axis is also directed towards the direction of excavation and face advancement. Figure 3.2 also shows the vertical and lateral directions which are the directions of the other in situ principal stresses in the R - θ plane. In the case of a vertical shaft being excavated downwards, the Z-axis will be downward and the R-θ plane will be in the horizontal plane containing the major and minor horizontal in situ stresses.

Since most tunnels and shafts involve this situation of a plane of symmetry in the radial in situ stress conditions, the necessity of considering the antisymmetric modes shown in Figure 3.2 is eliminated. For this reason, and to limit computer core and time requirements, only symmetric modes of the type shown in Figure 3.2 were considered in the present analyses. However, for special stress conditions, the more general case with both symmetric and antisymmetric modes can be readily developed using the existing program. In this case, a full three-dimensional analysis using three-dimensional elements and representation of discontinuities may be more appropriate from a computer time and cost point of view.

For the case where symmetric modes are adequate, the applied loads and the nodal circle displacements are expanded in a Fourier series for symmetric modes as follows:

loads -

$$P_r(r,z,\theta) = \Sigma P_{rn}(r,z) \cos n\theta$$

$$P_z(r,z,\theta) = \Sigma P_{zn}(r,z) \cos n\theta \qquad (3.10)$$

$$P_\theta(r,z,\theta) = \Sigma_{\theta n}(r,z) \sin n\theta$$

displacements -

$$u(r,z,\theta) = \Sigma u_n(r,z) \cos n\theta$$

$$v(r,z,\theta) = \Sigma v_n(r,z) \cos n\theta \qquad (3.11)$$

$$w(r,z,\theta) = \Sigma w_n(r,z) \sin n\theta$$

where $P_{rn}(r,z)$, $P_{zn}(r,z)$ and $P_{\theta n}(r,z)$ are the known load amplitudes and $u_n(r,z)$, $v_n(r,z)$ and $w_n(v,z)$ are the unknown displacement amplitudes for a particular harmonic n.

The strains corresponding to the displacements of Equation 3.4 can also be expanded as a Fourier series of strain amplitudes given by:

$$\varepsilon_r = \Sigma \varepsilon_{rn} \cos n\theta$$

$$\varepsilon_z = \Sigma \varepsilon_{zn} \cos n\theta$$

$$\varepsilon_\theta = \Sigma \varepsilon_{\theta n} \cos n\theta \qquad (3.12)$$

$$\gamma_{rz} = \Sigma \gamma_{rzn} \cos n\theta$$

$$\gamma_{r\theta} = \Sigma \gamma_{r\theta n} \sin n\theta$$

$$\gamma_{z\theta} = \Sigma \gamma_{z\theta n} \sin n\theta$$

Thus, the strain amplitudes can also be obtained in terms of nodal circle displacements. Using the constitutive equation, element stress amplitudes

can be readily evaluated as functions of element strain amplitudes.

The number of harmonics selected for the analysis must be suffi-
cient to represent adequately the applied loading shape or the initial in
situ stress state (Wilson, 1965).

The finite element formulation and derivations adopted for the
analysis follow the general procedures outlined by Wilson (1965). The
element stiffness matrix is evaluated using standard energy principles
(Fung, 1965; Zienkiewicz, 1977) for the harmonic n. Knowing the global
stiffness matrix for the entire continuum, the unknown displacement
amplitudes for each harmonic can then be evaluated. Using such an axi-
symmetric approach, the three-dimensional analysis is reduced to a set
of uncoupled two-dimensional analyses in which the total number of problems
is equal to the number of harmonics being used, i.e. one for each Fourier
index n (Wilson, 1965; Brebbia and Conner, 1974; Zienkiewicz, 1977).
Summation then yields the final solution for the non-axisymmetric loading
case (Zienkiewicz, 1977; Brebbia and Conner, 1974).

3.3 DETERMINATION OF THE IN SITU STRESS FIELD

The in situ stresses must be known for each element. This requires
knowing the Fourier coefficients of the stress field and the minimum num-
ber of harmonics required to adequately represent the stress field. These
data can be obtained if the in situ stresses are known numerically at a
set of points with varying angular direction θ as a function of the over-
burden vertical stress.

73

The initial state of stress is expressed in terms of the vertical, transverse and longitudinal (axial) stresses, typically as ratios of the overburden vertical stress at the tunnel centre line:

$$\sigma_{yy} = \gamma h$$

$$\sigma_{xx} = K_t \, \sigma_{yy}$$

$$\sigma_{zz} = K_\ell \, \sigma_{yy} \tag{3.13}$$

$$\tau_{xy} = \tau_{yz} = \tau_{zx} = 0$$

where: σ_{yy} is the vertical stress at depth h; γ is the unit weight of the ground; σ_{xx} is the transverse (lateral) stress in terms of the transverse stress ratio K_t; σ_{zz} is the axial stress in terms of the longitudinal (axial) stress ratio K_ℓ; and the shear stresses τ_{xy}, τ_{yz}, τ_{zx} are assumed to be zero. For this case, σ_{yy}, σ_{xx} and σ_{zz} are principal in situ stresses.

In the present case of symmetric modes of the non-axisymmetric loading, the stress components given by Equation 3.13 are determined for each element only at a set of points, M', spaced along a semi circle as shown in Figure 3.4. These circles represent the paths of the element centroidal points at which stresses are specified for the constant stress elements adopted. The number of points (M') selected is somewhat arbitrary and depends upon the desired accuracy in representing the 'stress shape' using the Fourier series approach. Using the Fourier expansion (as a numerical method of approximation) with sine and cosine functions which satisfy the orthogonality relationships with respect to summation over
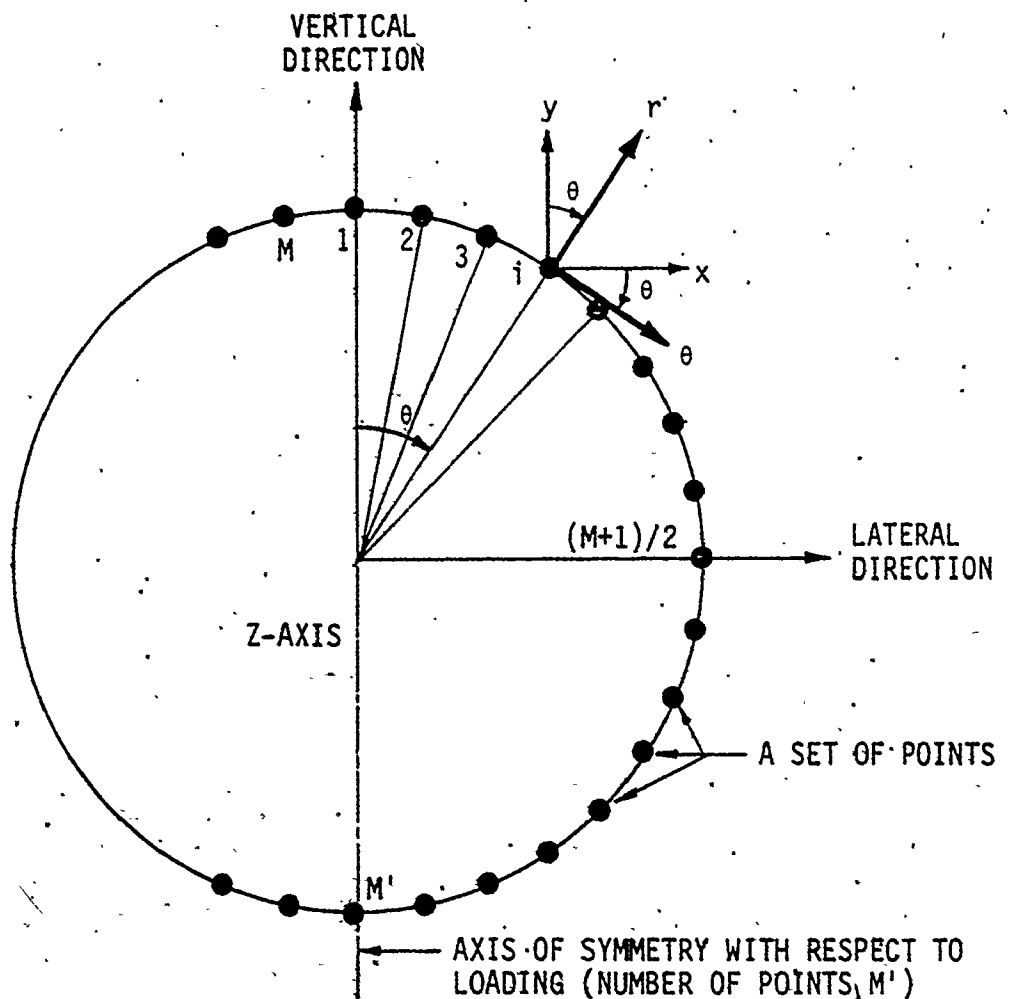
FIGURE 3.4   SET OF POINTS SPACED ALONG A CIRCLE AT WHICH
STRESSES CAN BE SPECIFIED TO REPRESENT THE
STRESS DISTRIBUTION USING FOURIER SERIES

the points, the complete in situ stress functions for each ring element are obtained.

3.4 DETERMINATION OF FOURIER COEFFICIENTS

The in situ stress field σ, with varying angular direction θ, can be approximated using the Fourier expansion of function $\sigma*$:

$$\sigma(\theta) \approx \sigma*(\theta) = A_0 \phi_0(\theta) + A_1 \phi_1 + \ldots, + A_n \phi_n(\theta) \qquad (3.14)$$

where: $\phi_0, \phi_1, \phi_2 \ldots, \phi_n$ are functions chosen in advance depending on whether symmetric or antisymmetric harmonics are involved, and $A_0, A_1, \ldots, A_n$ are expansion or Fourier coefficients (i.e. amplitudes) which are to be determined.

For the present case of only symmetric modes, the stresses are:

$$\sigma_r(\theta) \approx \sigma_r^*(\theta) = \Sigma \, \sigma_{rn} \cos n\theta$$

$$\sigma_z(\theta) \approx \sigma_z^*(\theta) = \Sigma \, \sigma_{zn} \cos n\theta$$

$$\sigma_\theta(\theta) \approx \sigma_\theta^*(\theta) = \Sigma \, \sigma_{\theta n} \cos n\theta$$

$$\tau_{rz}(\theta) \approx \tau_{rz}^*(\theta) = \Sigma \, \tau_{rz}(\theta) \cos n\theta \qquad (3.15)$$

$$\tau_{r\theta}(\theta) \approx \tau_{r\theta}^*(\theta) = \Sigma \, \tau_{r\theta}(\theta) \sin n\theta$$

$$\tau_{z\theta}(\theta) \approx \tau_{z\theta}^*(\theta) = \Sigma \, \tau_{z\theta}(\theta) \sin n\theta$$

where $n = 0, 2, 4 \ldots N$, and N is the total number of harmonics selected. It is necessary to determine the stress amplitudes so that $\sigma*(\theta) = \sigma(\theta)$ holds exactly, or as closely as possible, at all points M'. This condition leads to a set of linear equations with N number of unknowns and M'

equations (i.e. N equals the total number of harmonics and M' equals the total number of points spaced along the semi circle, Figure 3.4. The radial stress is given to demonstrate the analysis used:

$$\sigma_r(\theta_0) = A_0 + A_2 \cos 2\theta_0 + A_4 \cos 4\theta_0 + \ldots$$

$$\sigma_r(\theta_1) = A_0 + A_2 \cos 2\theta_1 + A_4 \cos 4\theta_1 + \ldots$$

$$\sigma_r(\theta_2) = A_0 + A_2 \cos 2\theta_2 + A_4 \cos 4\theta_2 + \ldots$$

$$(3.16)$$

$$\sigma_r(\theta_m) = A_0 + A_2 \cos 2\theta_m + A_4 \cos 4\theta_m + \ldots$$

or in matrix form:

$$\{\sigma(\theta_m)\}_{M'} = [\cos(n\theta)]_{M' \times N} \{A_n\}_N \qquad (3.17)$$

where m = M'-1 and N is the total number of harmonics.

To solve Equation 3.16 in order to obtain the unknown coefficients $(A_0, A_2, A_4 \ldots)$, two cases must be considered:

1. If M' = N. The number of points equals the number of harmonics. This indicates that the number of unknowns equals the number of equations. Then, the above system of equations has exactly one solution. In this case, the method of determination of $\sigma^*(\theta)$ is called interpolation (Dahlquist and Björck, 1974). Equation 3.14 can be directly solved using a suitable numerical method such as

the Gauss elimination method (Conte and Boor, 1972).

2. If $M' > N$. This is the common case where the number of points is greater than the number of harmonics. This indicates that the system has more equations than the number of unknowns, i.e. it is overdetermined. In such a case, the function obtained $\sigma^*(\theta)$ is satisfied only approximately. In some cases, $\sigma^*(\theta) = \sigma(\theta)$ at all points can be obtained depending on the shape of the stress function and the number of harmonics used. An important method for the treatment of overdetermined linear equation systems is the least squares method (Conte and Boor, 1972). To solve the system of overdetermined equations, the following procedure was used:

$$\{S\}_{M'} = [C]_{M' \times N} \{A\}_N \qquad (3.18)$$

where $\{S\}$ and $[C]$ are known and $\{A\}$ is unknown. Then, multiplying both sides of Equation 3.16 by $[C]^T$ yields:

$$[C]^T_{N \times M'} \{S\}_{M'} = [C]^T_{N \times M'} [C]_{M' \times N} \{A\}_N \qquad (3.19)$$

i.e.
$$[CS]_N = [C^T C]_{N \times N} \{A\}_N \qquad (3.20)$$

where $[C^T C]$ is a symmetric matrix. Equation 3.17 gives a set of N linear equations for the N unknown coefficients of $A_0, A_2, A_4, \ldots A_n$ and it can be solved by a suitable numerical method such as the Gauss elimination method.

The analysis described above has been used for all the stress components to obtain the stress amplitudes for each ring element for a number

of harmonics. This part of the analysis has been formulated in a sub-program called FCS (Fourier Coefficients for Stresses). The output is given for each computation step in tabular form as well as in figures (curves). Plots for each individual harmonic, summation of harmonics and comparisons with the actual stress functions are also provided. The programming for this analysis has been tested using the examples presented at the end of this chapter.

3.5 EXCAVATION SIMULATION

The simulation of circular tunnel and shaft excavations, and the face advance of cylindrical cavities, which are three-dimensional analyses, can be simplified by taking advantage of the axial symmetry of these structures. The axisymmetric excavation simulation method used in the advancing face analysis follows the general procedure described in Chapter 2 for the plane strain condition using the deactivation process. Two major assumptions must be made and recognized at this stage in order to adopt the axisymmetric approach. First, the ground is considered to be a homogeneous and isotropic medium. Secondly, the excavation process is assumed to proceed across the full circular cross section in single or multiple drifts. With the trend to tunnelling machines, this can be considered a reasonable assumption.

The excavation simulation for axisymmetric structures subjected to non-axisymmetric initial in situ stress fields using axisymmetric ring finite elements and the deactivation process is summarized by the simplified flow diagram given in Figure 3.5. To illustrate the simulation of an

EVALUATION OF THE INITIAL STATE OF STRESS AND STRAIN AT PRESELECTED LOCATIONS WITH VARYING ANGLE OF ROTATION θ

DETERMINATION OF THE STRESS AMPLITUDES, FOR THE ELEMENTS EVENTUALLY TO BE REMOVED IN THE CURRENT EXCAVATION STAGE, BY EXPANDING THE STRESSES WITHIN THESE ELEMENTS INTO A NUMBER OF HARMONICS USING FOURIER SERIES APPROXIMATION

DETERMINATION OF THE NODAL FORCE AMPLITUDES, REPRESENTING THE RE-MOVAL OF THE SUPPORTING GROUND AND USING THE STRESS APLITUDES PRE-VIOUSLY CALCULATED, FOR EACH FOURIER INDEX

ELIMINATION OF THE CONTRIBUTION OF THE ELEMENTS, TO BE REMOVED IN THE CURRENT EXCAVATION STAGE, FROM THE GLOBAL STIFFNESS MATRICES

DETERMINATION OF THE NODAL DISPLACEMENT AMPLITUDES BY IMPOSING THE EQUIVALENT NODAL FORCE AMPLITUDES AT THE EXCAVATION BOUNDARY AND SOLVING THE EQUATIONS OF EQUILIBRIUM

DETERMINATION OF THE STRAIN AND STRESS INCREMENT AMPLITUDES USING THE COMPATIBILITY AND CONSTITUTIVE EQUATIONS

EVALUATION OF THE DISPLACEMENT, STRAIN AND STRESS INCREMENTS AT THE PRESELECTED LOCATIONS WITH VARYING ANGLE OF ROTATION θ, FOR EACH FOURIER INDEX

SUMMATION OVER THE HARMONICS FOR THE DISPLACEMENT, STRAIN AND STRESS INCREMENTS WITH THE CORRESPONDING INITIAL VALUES YIELDS THE FINAL SOLUTION AT THE END OF THE CURRENT EXCAVATION STAGE

THE PREVIOUS PROCEDURE IS REPEATED UNTIL THE SPECIFIED TOTAL NUMBER OF EXCAVATION STAGES IS COMPLETED

FIGURE 3.5   SIMPLIFIED "FLOW" DIAGRAM FOR THE EXCAVATION ANALYSIS OF AXISYMMETRIC STRUCTURES SUBJECTED TO NON-AXISYMMETRIC INITIAL IN SITU STRESS ꓹYMMETRIC RING FINITE ELEMENT AND THE DEACTI-

underground excavation near the advancing face, consider the finite element mesh shown in Figure 3.6. The elements shown in this figure by broken lines are the elements to be excavated. The procedure then consists of the following steps:

1. Determination of the in situ stresses within the excavation vicinity (see Section 3.3) in order to initiate the excavation simulation. This requires evaluation of the initial state of stress (and strain) at preselected locations with varying angle of rotation θ.

2. Determination of the stress amplitudes for the specified elements to be eventually removed in the current excavation stage, by expanding the stress within these elements into a number of harmonics using the Fourier series approximation described in Section 3.4.

3. Determination of the nodal force amplitudes for each Fourier index using equation 3.9 at the excavation boundaries. These nodal forces represent the removal of the supporting ground and are equivalent to the stress amplitudes previously calculated within the elements to be removed.

4. Elimination of the contribution of the elements, to be removed in the current excavation stage, from the global stiffness matrix by reducing their coefficients by 1×10^6 for each Fourier index. These reduced stiffness elements are retained to represent any further construction steps such as tunnel support placement through reactivation.

81
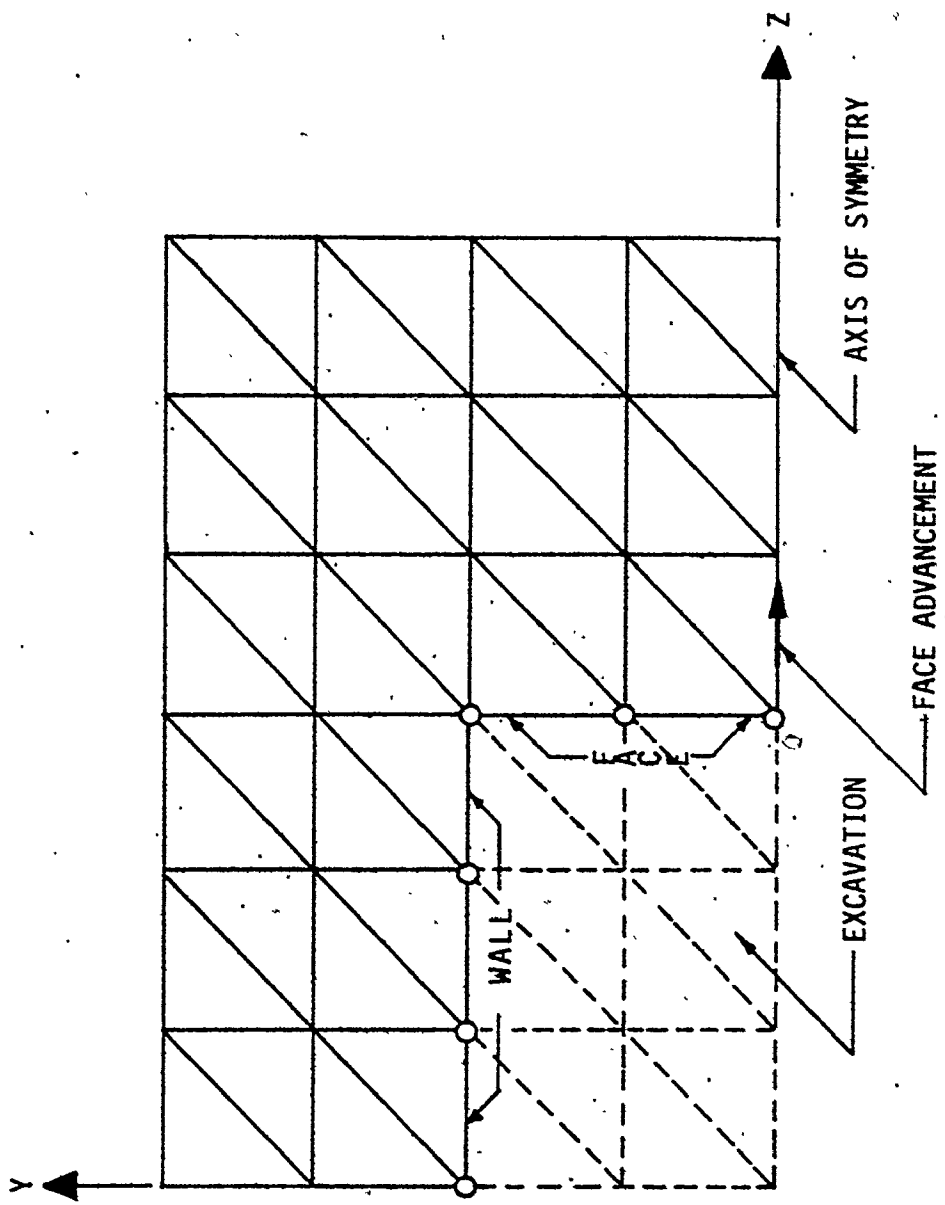
FIGURE 3.6   SIMULATION OF EXCAVATION STEPS USING THE AXISYMMETRIC APPROACH

5. Determination of the nodal displacement amplitudes by imposing the equivalent nodal force amplitudes at the excavation boundaries and solving the equations of equilibrium. The calculated equivalent nodal forces are applied only to the corresponding nodal points on the excavation boundaries to give the desired stress-free condition.

6. Determination of the strain and stress increment amplitudes using the compatibility and constitutive equations.

7. Evaluation of the displacement, strain and stress increments at the pre-selected locations with varying angle of rotation θ, for each Fourier index.

8. Summation over the harmonics for the displacements, strain and stress increments with the corresponding initial values yields the final solution at the end of the current stage. These values are considered the initial state for a further excavation step.

9. The previous procedure is repeated until the specified total number of excavation steps is completed.

If the ground is assumed to behave in a linearly elastic manner, the previous procedure for excavation simulation analysis is followed. In the case of stresses above the yield stress (termed 'excessive' stresses), ground yielding may occur and the analysis is modified to include this condition.

3.6 GROUND-YIELDING ANALYSIS

The plastic analysis during the axisymmetric excavation and advancing face simulation of cylindrical cavities subjected to non-axisymmetric in situ stresses, which are symmetric about a plane containing the axis of revolution, is similar to the method previously adopted for the plane strain conditions. The initial stress method adopted for plastic analyses is still appropriate for non-axisymmetric yielding. In the case of a uniform axisymmetric in situ stress condition (K_t = 1), which is a special case, yielding occurs uniformly and in complete rings around the circular opening. In the case of non-axisymmetric in situ stresses, yielding does occur non-uniformly around a circular opening. Yielding may occur at the springline if in situ overburden vertical stresses are greater than the horizontal stress components or may occur at the crown if horizontal stress components are greater than the overburden vertical stresses, to relieve the high tangential stresses around the opening.

In the initial stress method, which seems to be the best available for the axisymmetric approach, there is no need to change the material properties due to plastic yielding during the iterative procedure. Fictitious equivalent forces are used to let the excavation vicinity deform to simulate yielding and to redistribute the excessive stresses around the opening. (This method is also consistent with the creep analysis since the material properties are assumed to be constant during creep.) This general plastic analysis method is explained in Chapter 2 and will not be repeated here. Only the additional features to incorporate the plastic

analysis into the three-dimensional simulation using the axisymmetric approach will be given.

The method also involves the expansion of the excessive stresses above the elastic stress limit into Fourier series with the assumption that the ground is a linearly elastic-perfectly plastic material. In the computation, pseudo forces equivalent to the excessive stresses are determined and the stiffnesses of the elements that have yielded are unchanged. The general procedure for the ground yielding analysis is given in simplified form in Figure 3.7. The overall procedure is repeated until the specified convergence criteria are achieved. The best stress criterion used is that the equivalent stress during yielding is within 0.2 to 0.5% of the limiting stress state with a limitation on the number of iterations of 10 to 20 to achieve this condition. The plastic analysis is formulated in a subprogram and incorporated into the excavation simulation analysis to handle ground yielding for the three-dimensional stress analysis near the advancing face.

It should be mentioned that the analysis has been checked for the special case of an axisymmetric loading with the same problem given in Section 2.3. The results are in excellent agreement with both the closed form solution and plane strain analysis. Typical results for the general case are given in Chapter 5 where actual example problems are analyzed.

In order to consider creep behaviour, the analysis is extended and modified to incorporate time-dependent deformations as described in the next section.

EVALUATION OF THE INITIAL STATE OF STRESS AND STRAIN AT PRESELECTED LOCATIONS WITH VARYING ANGLE OF ROTATION θ

DETERMINATION OF THE EXCESSIVE STRESS INCREMENTS, ABOVE THE SPECIFIED ELASTIC STRESS LIMIT, AT THE SAME PRESELECTED LOCATIONS WITH VARYING ANGLE OF ROTATION θ

DETERMINATION OF THE EXCESSIVE STRESS INCREMENT AMPLITUDES BY EXPAND-ING THE EXCESSIVE STRESS INCREMENTS INTO A NUMBER OF HARMONICS USING FOURIER SERIES APPROXIMATION

DETERMINATION OF THE NODAL FORCE AMPLITUDES FOLLOWING THE INITIAL STRESS METHOD AND USING THE STRESS AMPLITUDES PREVIOUSLY CALCULATED, FOR EACH FOURIER INDEX

DETERMINATION OF THE NODAL DISPLACEMENT AMPLITUDES BY IMPOSING THE EQUIVALENT NODAL FORCE AMPLITUDES AT THE CORRESPONDING NODES AND SOLVING THE EQUATIONS OF EQUILIBRIUM

DETERMINATION OF THE STRAIN AND STRESS INCREMENT AMPLITUDES USING THE COMPATIBILITY AND CONSTITUTIVE EQUATIONS

EVALUATION OF THE DISPLACEMENT, STRAIN AND STRESS INCREMENTS AT THE PRESELECTED LOCATIONS WITH VARYING ANGLE OF ROTATION θ, FOR EACH FOURIER INDEX

SUMMATION OVER THE HARMONICS FOR THE DISPLACEMENT, STRAIN AND STRESS INCREMENTS WITH THE INITIAL CORRESPONDING VALUES YIELDS THE FINAL SOLUTION AT THE END OF THE CURRENT PLASTIC ITERATION

THE PREVIOUS PROCEDURE IS REPEATED UNTIL THE SPECIFIED CONVERGENCE CRITERIA ARE ACHIEVED

FIGURE 3.7   SIMPLIFIED "FLOW" DIAGRAM FOR THE PLASTIC ANALYSIS OF AXISYMMETRIC STRUCTURES SUBJECTED TO NON-AXISYMMETRIC INITIAL IN SITU STRESS FIELD USING THE AXISYMMETRIC RING ELEMENT AND THE INITIAL STRESS METHOD

3.7 CREEP ANALYSIS

In excavation design cases where the time-dependent stress-strain behaviour of the ground mass is relevant, a creep analysis must be considered within the excavation analysis performed near the advancing face. Such an analysis is essential to cover five major questions:

1. The effect of face progression on tunnel inward displacements;

2. The appropriate time-delay before any support system (liner) is placed to limit stress development;

3. How far back from the advancing face the liner must be installed to both limit stress development and potential yielding;

4. The necessary thickness of the soft backing between the rock and the rigid support system to limit stress development; and

5. The maximum stresses developed in the liner due to the long-term time-dependent creep response.

These major questions must be answered before starting construction since in some cases, the support must be placed as close as possible to the tunnel face if limiting the tunnel closure is critical. In other cases, the support must be placed at a distance from the advancing face and/or a time-delay is required to attenuate the ground displacements and minimize the required support thickness. For the general case of non-axisymmetric stress field, closure due to creep will not be uniform around the opening as compared to the special case of an axisymmetric stress field.

The nonlinear creep analysis during the excavation and face advance simulation of cylindrical cavities subjected to non-axisymmetric in situ

stresses, which are symmetric about a plane containing the axis of revolution, was based on the initial strain method. This approach is common in the numerical analysis of creep problems. The general procedure is similar to that developed by Samuelson (1970) who analyzed the creep behaviour of cylindrical shell under arbitrary loads. With the incremental procedure, the creep strain increments are evaluated for small time intervals. By expanding these creep strain increments in Fourier series, the equivalent force amplitudes, which are regarded as pseudo loads, can be evaluated. A series of sets of problems are obtained with one set for each Fourier index that can be solved independently of each other.

The creep formulation based on the axisymmetric creep analysis and computer program developed by Emery (1971) has been incorporated into the excavation analysis as a subprogram after completing the necessary modifications. The analysis method and the computer program have been checked for the thick-walled cylinder given in Section 2.4 as an axisymmetric problem. The results are identical to the closed form plane strain, and Greenbaum (1966) finite element method, solutions.

The general procedure for the time-dependent analyses of axisymmetric structures subjected to non-axisymmetric initial in situ stress fields, using axisymmetric ring elements and the initial strain method, is given in simplified form in Figure 3.8. The procedure is repeated until the specified total elapsed time is reached.

Such time-dependent analysis can be performed after excavation and before and after support installation. Also, a plastic analysis as a

EVALUATION OF THE INITIAL STATE OF STRESS AND STRAIN AT PRESELECTED LOCATIONS WITH VARYING ANGLE OF ROTATION θ

DETERMINATION OF THE CREEP STRAIN INCREMENTS, DURING THE SELECTED TIME INTERVAL, AT THE SAME PRESELECTED LOCATIONS WITH VARYING ANGLE OF ROTATION θ

DETERMINATION OF THE CREEP STRAIN INCREMENTS AMPLITUDES BY EXPANDING THE CREEP STRAIN INCREMENTS INTO A NUMBER OF HARMONICS USING FOURIER SERIES APPROXIMATION

DETERMINATION OF THE NODAL FORCE AMPLITUDES FOLLOWING THE INITIAL STRAIN METHOD AND USING THE STRAIN AMPLITUDES PREVIOUSLY CALCULATED, FOR EACH FOURIER INDEX

DETERMINATION OF THE NODAL DISPLACEMENT AMPLITUDES BY IMPOSING THE EQUIVALENT NODAL FORCE AMPLITUDES AT THE CORRESPONDING NODES AND SOLVING THE EQUATIONS OF EQUILIBRIUM

DETERMINATION OF THE STRAIN AND STRESS INCREMENT AMPLITUDES USING THE COMPATIBILITY AND CONSTITUTIVE EQUATIONS

EVALUATION OF THE DISPLACEMENT, STRAIN AND STRESS INCREMENTS AT THE PRESELECTED LOCATIONS WITH VARYING ANGLE OF ROTATION θ, FOR EACH FOURIER INDEX

SUMMATION OVER THE HARMONICS FOR THE DISPLACEMENT, STRAIN AND STRESS INCREMENTS WITH THE INITIAL CORRESPONDING VALUES YIELDS THE FINAL SOLUTION AT THE END OF THE CURRENT CREEP ITERATION

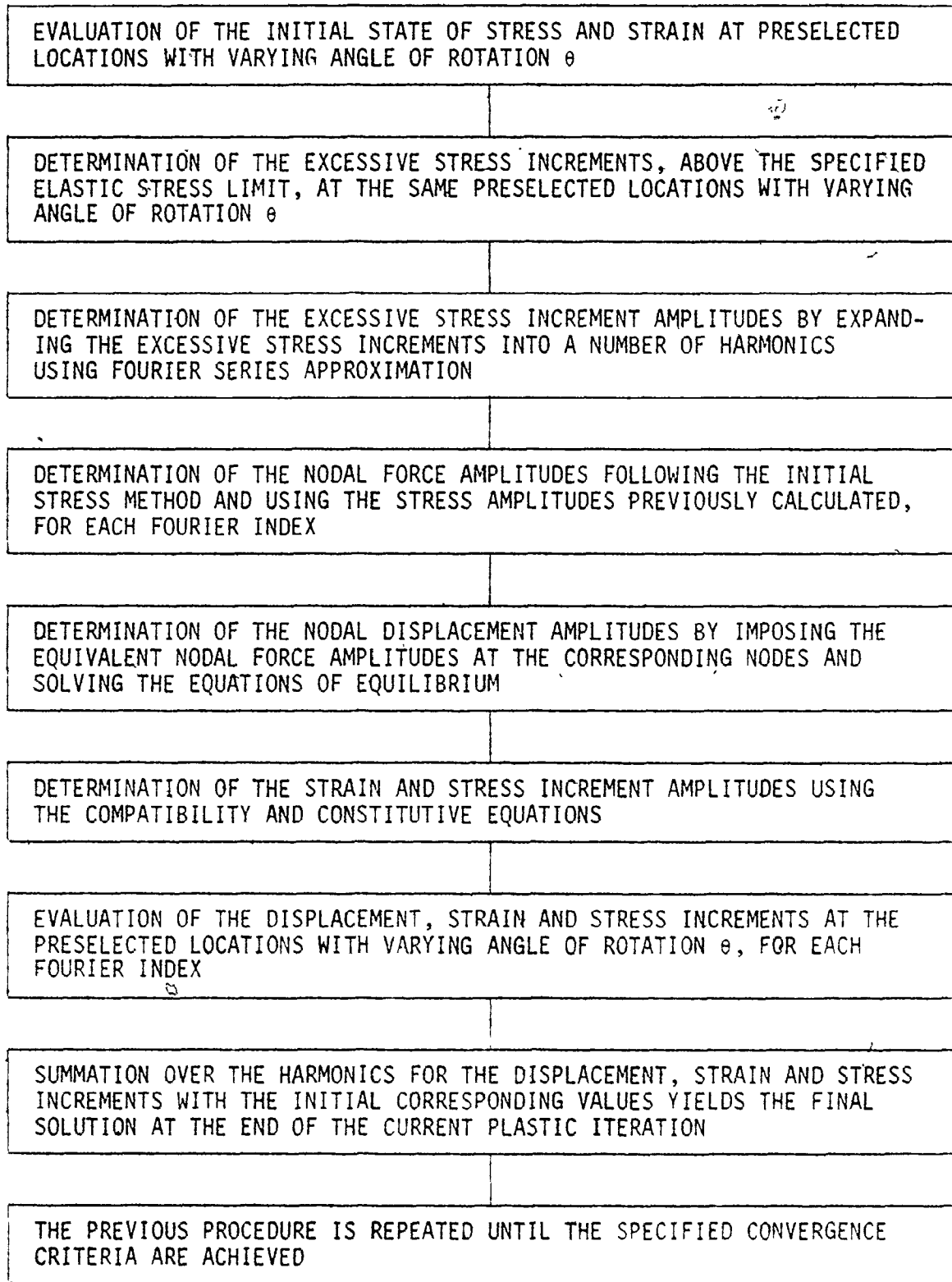THE PREVIOUS PROCEDURE IS REPEATED UNTIL THE SPECIFIED TOTAL ELAPSED TIME IS REACHED

FIGURE 3.8   SIMPLIFIED "FLOW" DIAGRAM FOR THE CREEP ANALYSIS OF AXISYMMETRIC STRUCTURES SUBJECTED TO NON-AXISYMMETRIC INITIAL IN SITU STRESS FIELD USING THE AXISYMMETRIC RING ELEMENT AND THE INITIAL STRAIN METHOD

limiting stress state can be performed after each time-increment during the creep analysis, or following several time-increments.

3.8 TUNNEL SUPPORT INSTALLATION

Tunnel liner support installation is simulated by the realistic assumption that the liner rings are axisymmetric structures made up of segments with respect to the tunnel axis and the support system is advanced by ring installation. In this formulation, complete compatibility is assumed between the support system and the ground and there is no slippage allowed at the interface. The analysis can be improved in this respect by introducing a frictional interface element such as joint elements (Goodman et al, 1968). This would of course require further program development. However, the simulation method allows for a soft backing between the support system concrete segments and ground that can take distorted deformations.

The procedure used to simulate the support system rings in the present approach is similar to the procedure described in Chapter 2. The reactivation process for the elements representing the liner rings at the current stage is utilized and this reactivation has to be carried through the global stiffness matrix for all harmonics. Stresses and strains within these elements and the nodal displacements, are initially set to zero. This is essential to obtain elements free of stresses, strains and displacements immediately after installation and before any stress redistribution has occurred. After a new excavation step, the equivalent nodal forces are applied at the corresponding ndoes and the response of both the

ground and support system can be obtained.

Typical examples are given in the following section to verify and check the analysis procedures and the computer program developed, and to demonstrate its capabilities.

3.9 SIMULATION EXAMPLES

To check the analysis procedures and the program developed, a typical elastic problem involving an underground excavation, considered by others in a three-dimensional finite element method analysis (Descoeudres, 1974), was examined. (No closed form analytical results are available.) The rock properties and initial stress assumptions are given in Figure 3.9 with the one and five step excavation simulations indicated. The general finite element mesh idealization is shown in Figure 3.10. This mesh and the computer input data were prepared by the mesh generation program which was developed for the finite element method analysis using the axisymmetric approach. Four harmonics were used throughout the analyses to represent the symmetric mode. The tunnel inward displacement results for both one and three excavation steps are given in Figures 3.11 and 3.12 for crown and springline, respectively. The tunnel closure curve obtained by Descoeudres (1974) using three-dimensional isoparametric finite elements is also shown in the same figure. Since a linear elastic material was assumed, all these solutions (one step, three step and three-dimensional) should yield the same predicted deformations if all of the excavation simulation approaches and programs are developed correctly. As shown in Figure 3.11 and 3.12, the predicted tunnel wall inward displacements in

ROCK PROPERTIES:

$E = 5 \times 10^6$ KPa
$\nu = 0.2$

IN-SITU INITIAL
STRESSES:

UNIFORM STRESS
  CONDITION = 8×10^3 KPa

A.
ONE-STEP EXCAVATION

35 m

5 m

40 m

25 m

65 m

ROCK PROPERTIES:

$E = 5 \times 10^6$ KPa
$\nu = 0.2$

IN-SITU INITIAL
STRESSES:

UNIFORM STRESS
  CONDITION = 8×10^3 KPa

B.
FIVE-STEP EXCAVATION

35 m

5 m

40 m

25 m
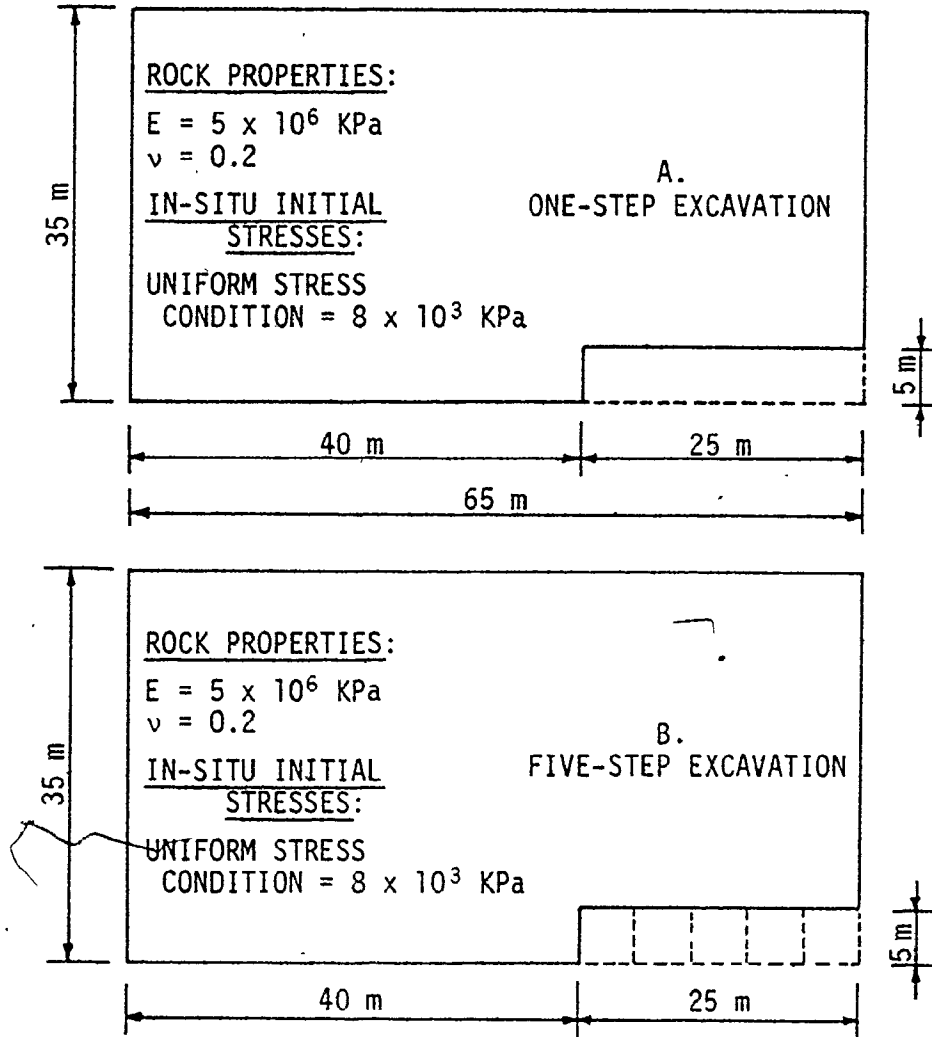
FIGURE 3.9   ONE AND FIVE-STEP EXCAVATIONS FOR THE TEST
PROBLEM USING THE AXISYMMETRIC APPROACH
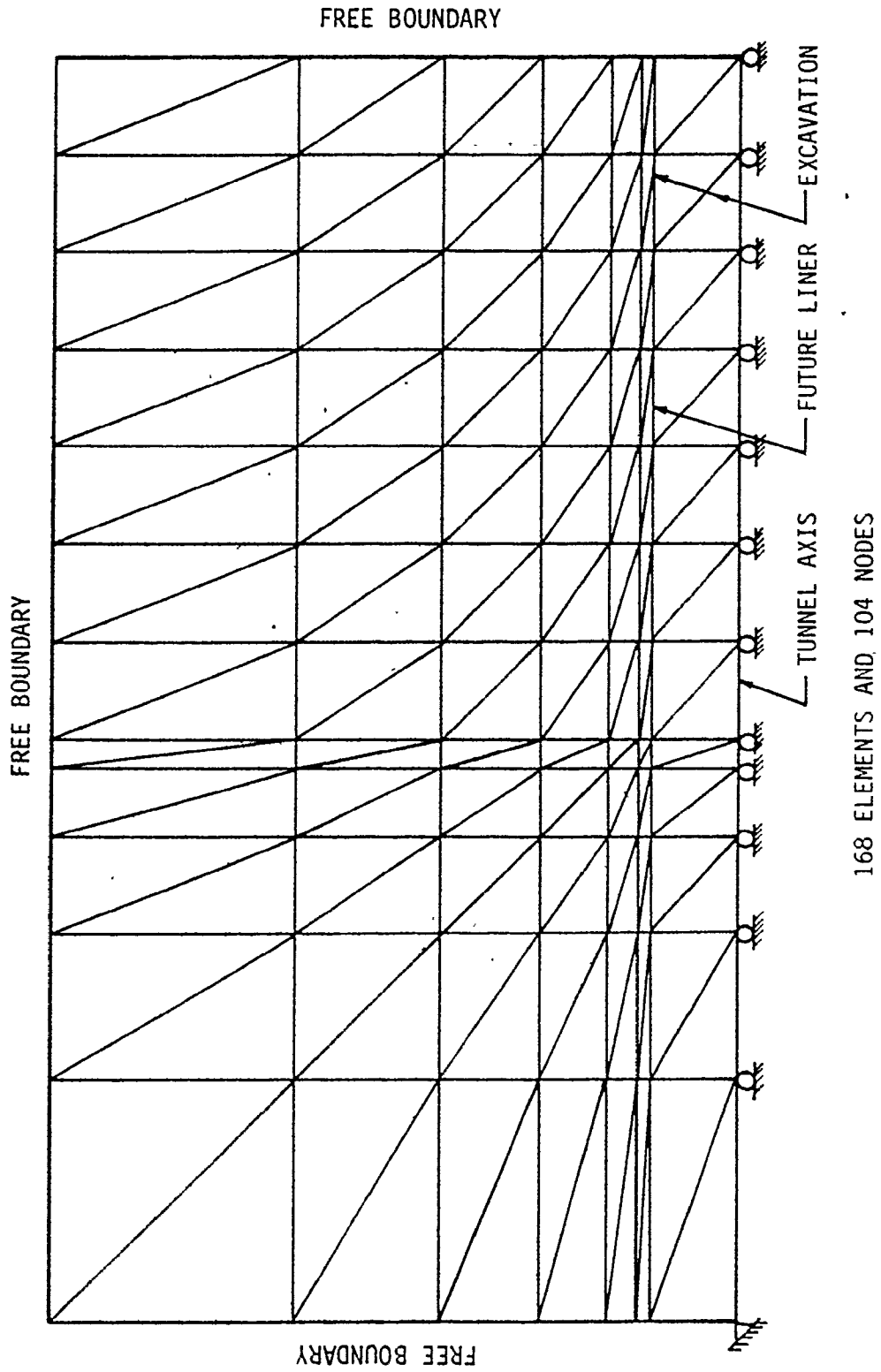
FIGURE 3.10   FINITE ELEMENT MESH REPRESENTATION OF A CYLINDRICAL OPENING WITH ADVANCING
             FACE (FIGURES 3.2 AND 3.3)
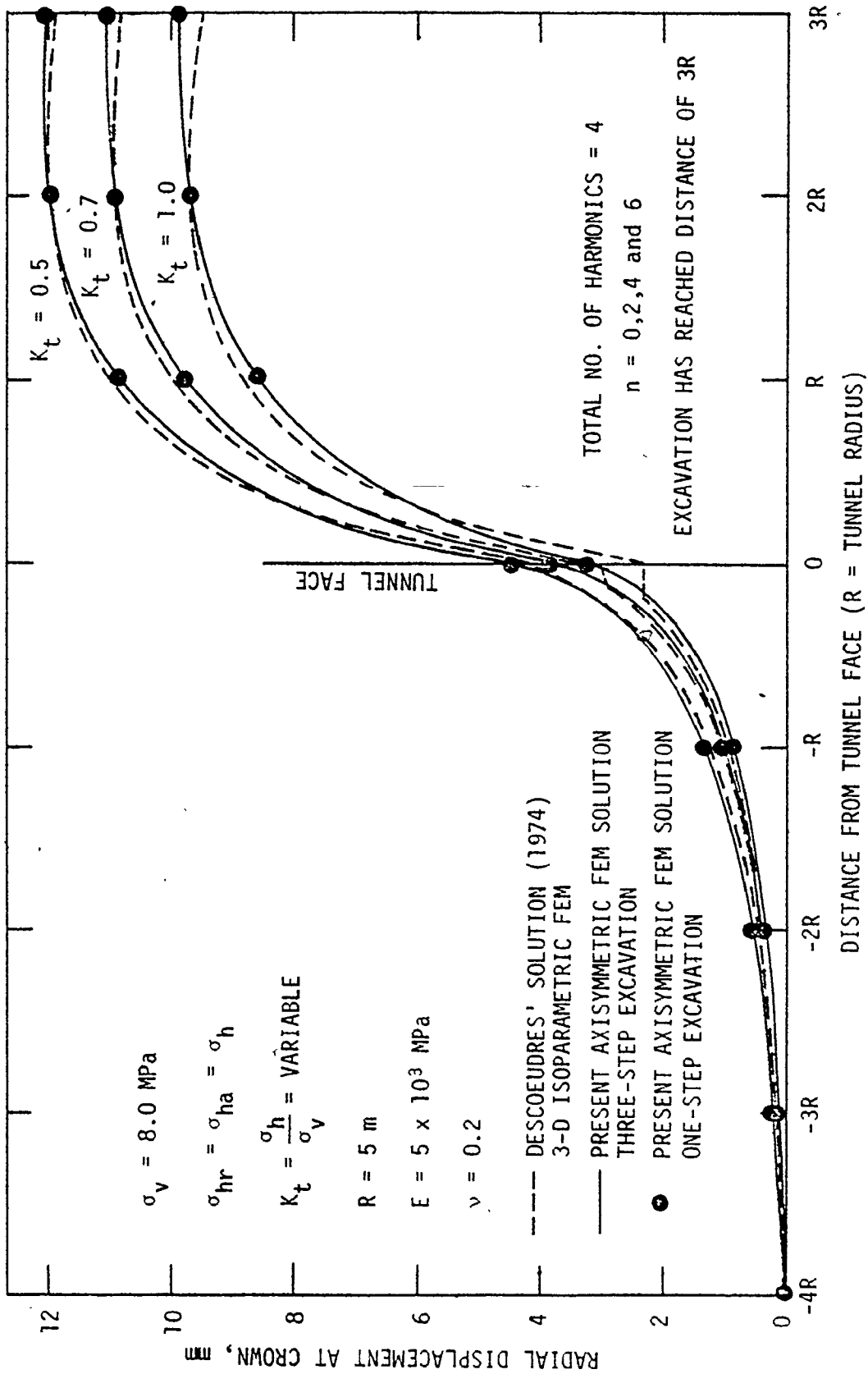
FIGURE 3.11 TUNNEL WALL RADIAL DISPLACEMENT AT CROWN NEAR THE FACE – COMPARISON OF AXISYMMETRIC AND THREE-DIMENSIONAL ISOPARAMETRIC FINITE ELEMENT METHOD ELASTIC SOLUTIONS
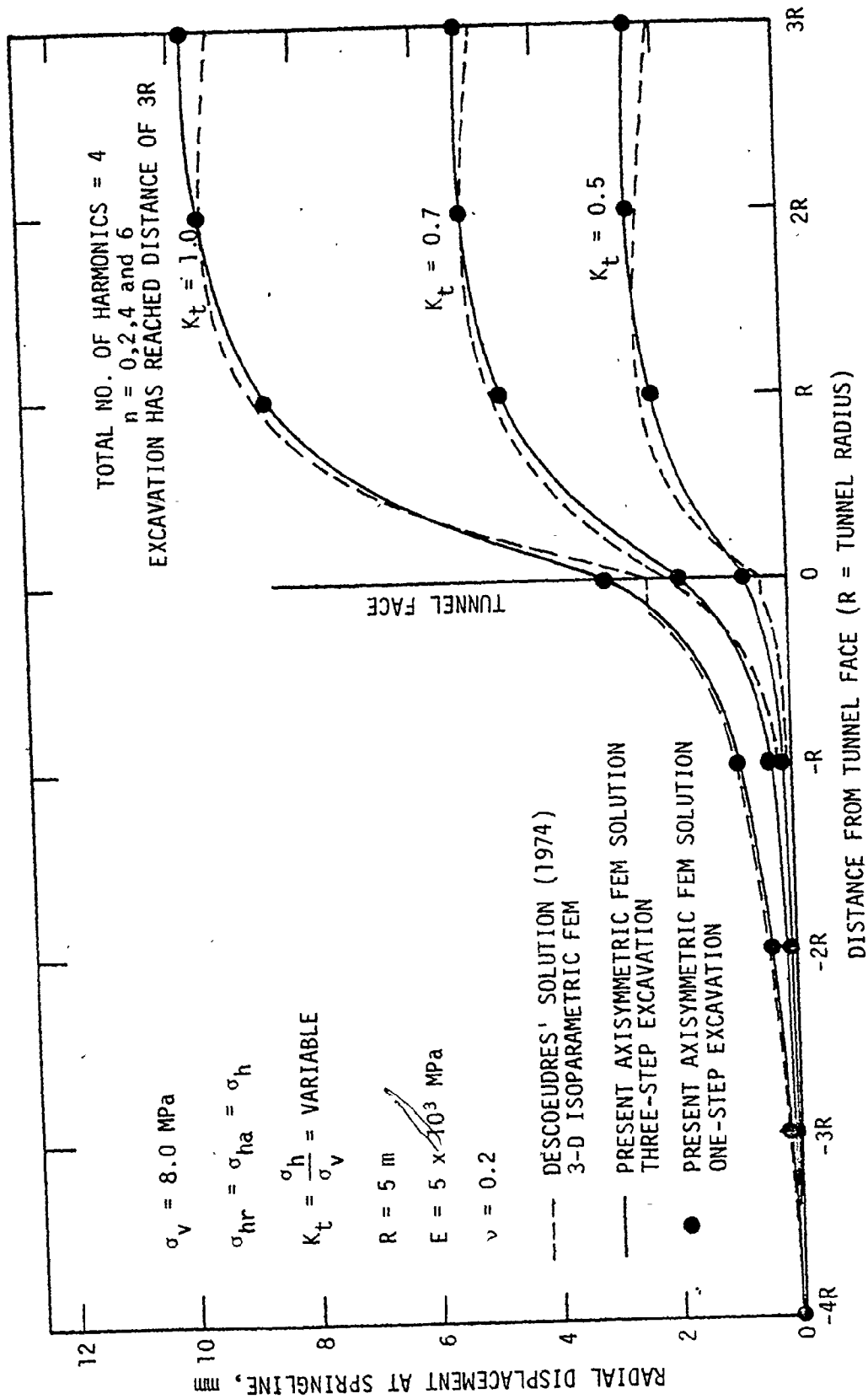
FIGURE 3.12 TUNNEL WALL RADIAL DISPLACEMENT AT SPRINGLINE - COMPARISON OF AXISYMMETRIC AND THREE-DIMENSIONAL ISOPARAMETRIC FINITE ELEMENT METHOD ELASTIC SOLUTIONS

the radial direction obtained by the one-step (instantaneous) and three-step (incremental) excavation simulations are identical as anticipated, and in good agreement with Descoeudres' published solution.

Figures 3.11 and 3.12 also show that radial displacements occur ahead of the face in the unexcavated ground along the tunnel wall. These movements gradually decrease with increasing distance ahead of the face.

Figure 3.13 shows the effect of a new excavation step on the radial displacements. The face is advanced by a distance of one diameter (2R) from the current position (at 5R). These incremental radial deformations are at a maximum at a distance of about one tunnel radius (R) from the new face and gradually decrease with increasing distance from the new face. At a distance of about twice the tunnel diameter (4R), no significant radial displacements occur due to the new advance.

In order to demonstrate the effect of face advancement on tunnel inward displacements, the radial elastic displacements at the reference point B shown in Figure 3.14 are tabulated in Table 3.1. Point B represents any reference point along the future tunnel wall that the tunnel face will advance and then pass. As shown in Table 3.1, when the tunnel face reaches the point of interest (i.e. point B), an accumulated radial displacement of more than 35 percent of the total displacement will already have occurred. When the tunnel face advances one radius ahead of the reference point, about 80 percent of the total displacement will have accumulated at the point of interest. More than 90 percent of the total displacement will have occurred at the same point (B) if the tunnel face advances to one diameter (2R) ahead of the reference point. It can also be seen that
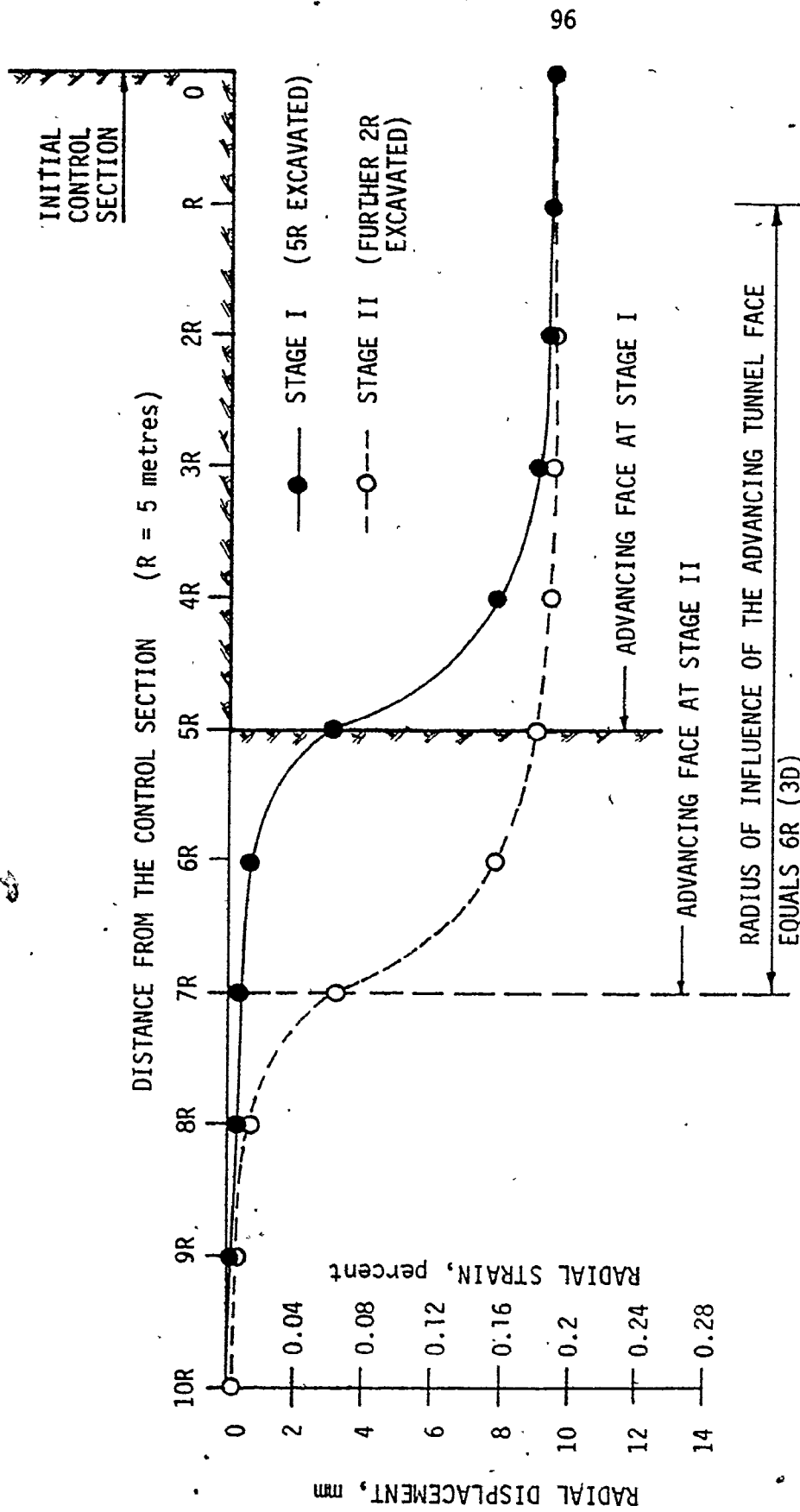
FIGURE 3.13   EFFECT OF NEW EXCAVATION STEP ON THE RADIAL DISPLACEMENTS
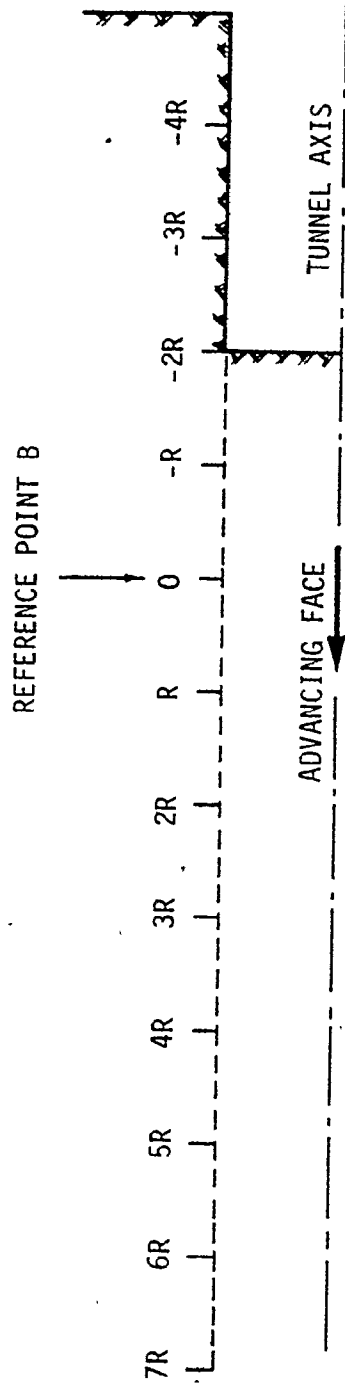
FIGURE 3.14   REFERENCE POINT FOR THE DISPLACEMENT RATIOS TABULATED IN TABLE 3.1

DISTANCE (L) FROM POINT OF INTEREST (B) TO THE ADVANCING FACE (SEE FIGURE 3.14)	RATIO BETWEEN THE INCREMENTAL AND FINAL RADIAL DISPLACEMENT AT POINT (B)	RATIO BETWEEN THE ACCUMULATIVE AND FINAL RADIAL DISPLACEMENT AT POINT (B)
-4R	0.007	0.007
-3R	0.008	0.015
-2R	0.019	0.034
-R	0.059	0.093
FACE AT THE POINT OF INTEREST (B)	0.284	0.377
R	0.431	0.808
2R	0.130	0.938
3R	0.031	0.969
4R	0.023	0.992
5R	0.003	0.995
6R	0.003	0.998
7R (APPROXIMATE DISTANCE OF INFLUENCE)	0.002	1.000

NOTE: R IS THE TUNNEL RADIUS

TABLE 3.1   EFFECT OF ADVANCING EXCAVATION ON THE ELASTIC RADIAL DISPLACEMENT RATIO AT A POINT B (FIGURE 3.14) ON THE TUNNEL WALL, UNDER UNIFORM INITIAL STRESS CONDITION

the complete elastic radial inward displacements are not achieved until the face has advanced approximately three diameters (6R) from the point under consideration. This example demonstrates quantitatively the percentage of the total predicted elastic displacement occurring before support system (liner) installation. Therefore, the load to be carried by the liner from any elastic excavation response depends on the distance between the advancing face and the location where the liner is pressed against the ground.

To demonstrate the applicability of the tunnel support system installation simulation method for considering the advancing face situation, two elastic cases were considered to show the effect of the support installation location on tunnel inward displacements and support stresses, and to compare these results with those predicted assuming a plane strain condition. Figure 3.15 shows these two cases where stiff liners (no soft backing) are used. In the first case, the liner is placed very near to the advancing face, while in the second case, the liner is placed at a distance of one radius (R) from the advancing face. The sequences of excavation and support placement are advanced in stages to a distance of seven R from the control section. The finite element mesh configuration shown previously in Figure 3.10 was used with the same rock properties and a uniform initial stress condition. The finite element mesh used for the plane strain assumption is shown in Figure 3.16 which represents a section remote from the advancing face. The support system modulus of elasticity used was in the practical range for precast concrete segmental liners of 6 times the rock modulus.
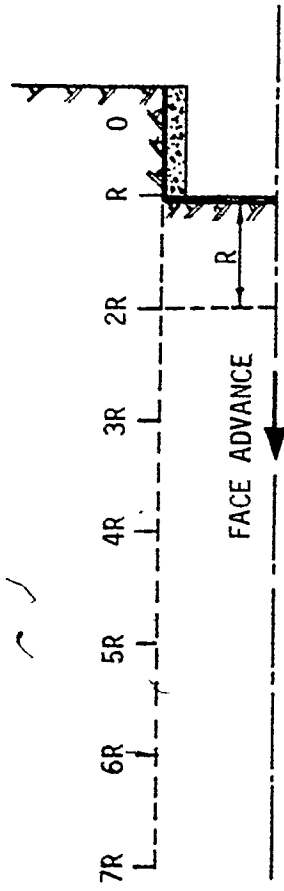
CASE 1: LINING SEGMENT PLACED VERY NEAR TO THE FACE
(R = TUNNEL RADIUS)
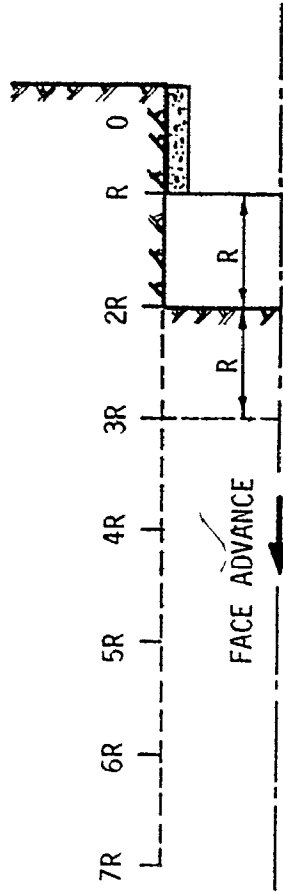
CASE 2: LINING SEGMENT PLACED AT DISTANCE R FROM THE
FACE (R = TUNNEL RADIUS)

FIGURE 3.15   LINING SEGMENT PLACEMENT CASES

14 ELEMENTS AND 16 NODES
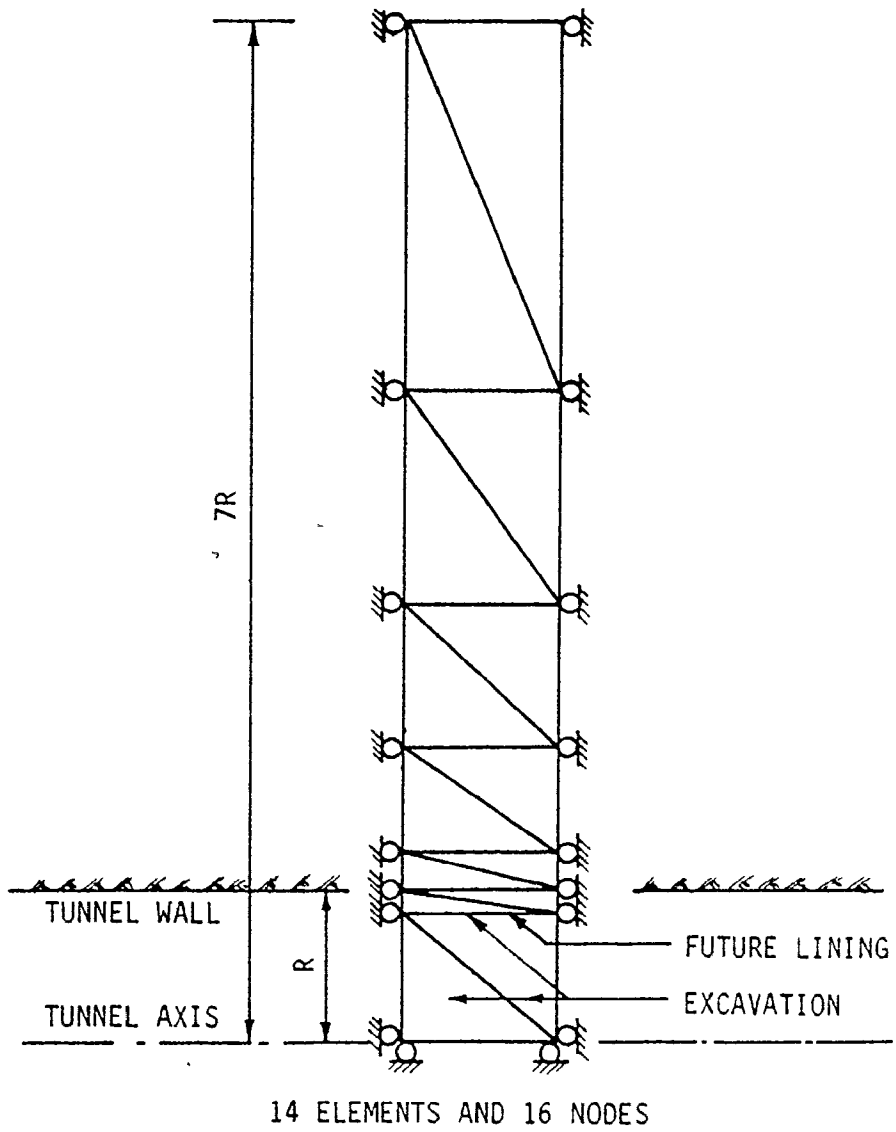
FIGURE 3.16   AXISYMMETRIC FINITE ELEMENT IDEALIZATION
(NO STRAIN IN AXIAL DIRECTION - REPRESENTS
SECTION REMOTE FROM ADVANCING FACE)

Figure 3.17 gives the elastic radial displacements along the tunnel wall which are plotted for both cases of support placements as well as for the unsupported tunnel for comparison. It can be seen that in the first case where the support is placed very near to the advancing face, the inward displacements have been reduced by about 25% of the total inward displacements for the unsupported tunnel, while in the second case of support placement, the tunnel inward displacements have been reduced by less than 10%. This indicates that if the support is placed far from the advancing face (i.e. 4 to 6 R), it will not result in any significant reduction in the tunnel elastic closure due to excavation and face progress. On the same figure, the results from the plane strain analysis are also plotted for both the unsupported and supported cases. The instantaneous excavation and liner placement case has been considered for the supported plane strain condition. This represents the extreme conditions for the rock displacements and support stresses (i.e. no consideration of displacements following excavation and prior support placement). From this comparison, it can be seen that the plane strain analysis cannot simulate the progressive excavation-support placement interaction near the advancing face. This is much clearer when comparing the stresses developed in the liner for both cases. Figure 3.18 shows the support system stresses as both the tunnel face and liner rings are advancing. The stresses developed in Case One where the liner is installed very near to the advancing face, represent about 46% of the plane strain case (i.e. instantaneous excavation and support placement). While in Case Two, where the support is installed at a distance of one radius (R) from the advancing face, the stresses in the liner are less than 20%. It can also be noted that when the face advances
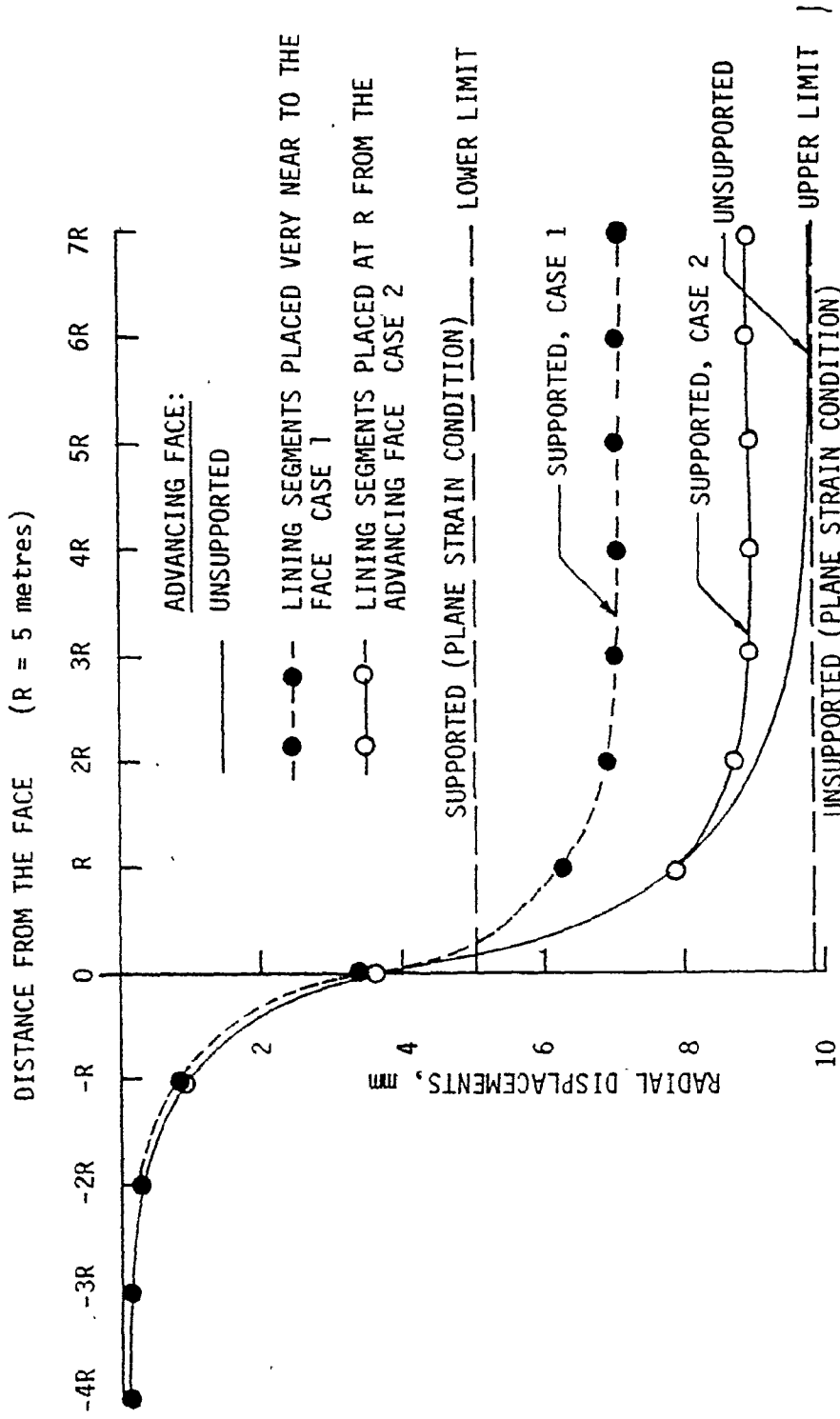
FIGURE 3.17   ELASTIC RADIAL DISPLACEMENTS ALONG THE TUNNEL WALL FOR BOTH SUPPORTED AND
UNSUPPORTED CASES (TUNNEL FACE AND LINING SEGMENTS PLACEMENT ARE ADVANCING)

DISTANCE FROM THE ADVANCING FACE TO THE LINING SEGMENT WHERE STRESSES ARE MONITORED

SUPPORT PLACED AT R FROM THE ADVANCING FACE
CASE 2

MAX. STRESS = 695 x 10³ Pa (18%)

SUPPORT PLACED VERY NEAR THE ADVANCING FACE
CASE 1

MAX. STRESS = 1740 x 10³ Pa (46%)

INSTANTANEOUS EXCAVATION AND LINING SEGMENT PLACEMENT
WITH PLANE STRAIN ASSUMPTION

MAX. STRESS = 3800 x 10³ Pa (100%)

TANGENTIAL STRESSES, x 10³ Pa
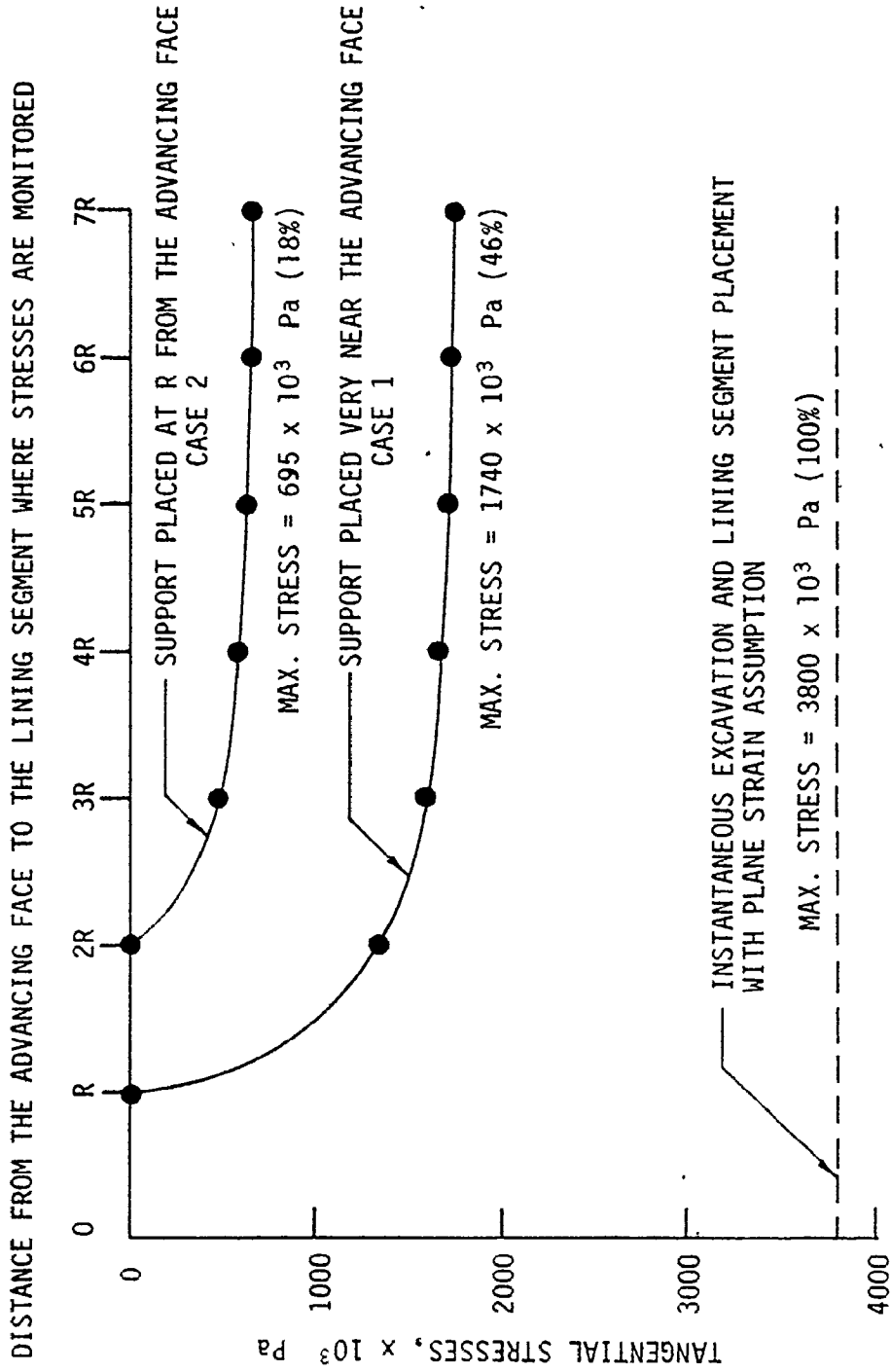
FIGURE 3.18 LINING SEGMENT STRESSES AS BOTH TUNNEL FACE AND LINING SEGMENTS PLACEMENT
ARE ADVANCING

three times the tunnel diameter (6R) ahead of the support ring of interest, the stresses reach their maximum value and no significant increases occur after further face advancement.

To demonstrate the effect of creep on tunnel inward displacements, the same design problem discussed in Section 3.3 was used with the same mesh configuration given in Figure 3.10. The rock properties and the uniform stress field were also kept the same. The simple creep relationship (Robertson, 1963) shown on Figure 3.19 was adopted since it is applicable for many soft rock types. The parameters for this creep relationship were adopted to be appropriate for the stress level involved (Robertson, 1963). The tunnel length of seven R was excavated instantaneously in a single step and then a time-dependent analysis was initiated. The tunnel was kept unsupported. Figure 3.19 shows the inward radial displacements of the tunnel wall for different creep times. The following observations can be made from Figure 3.19:

1. The creep has a great effect on increasing the tunnel inward displacements with the total inward displacements after about four days being more than four times the instantaneous elastic displacements at $t = 0$.

2. The creep increases the tunnel face influence zone. For example, the tunnel face influence zone has increased from 3R for the elastic case to at least 6R after about 4 days creep. This indicates that too much time-delay prior to liner placement for this example may result in excessive closure with potential failure,
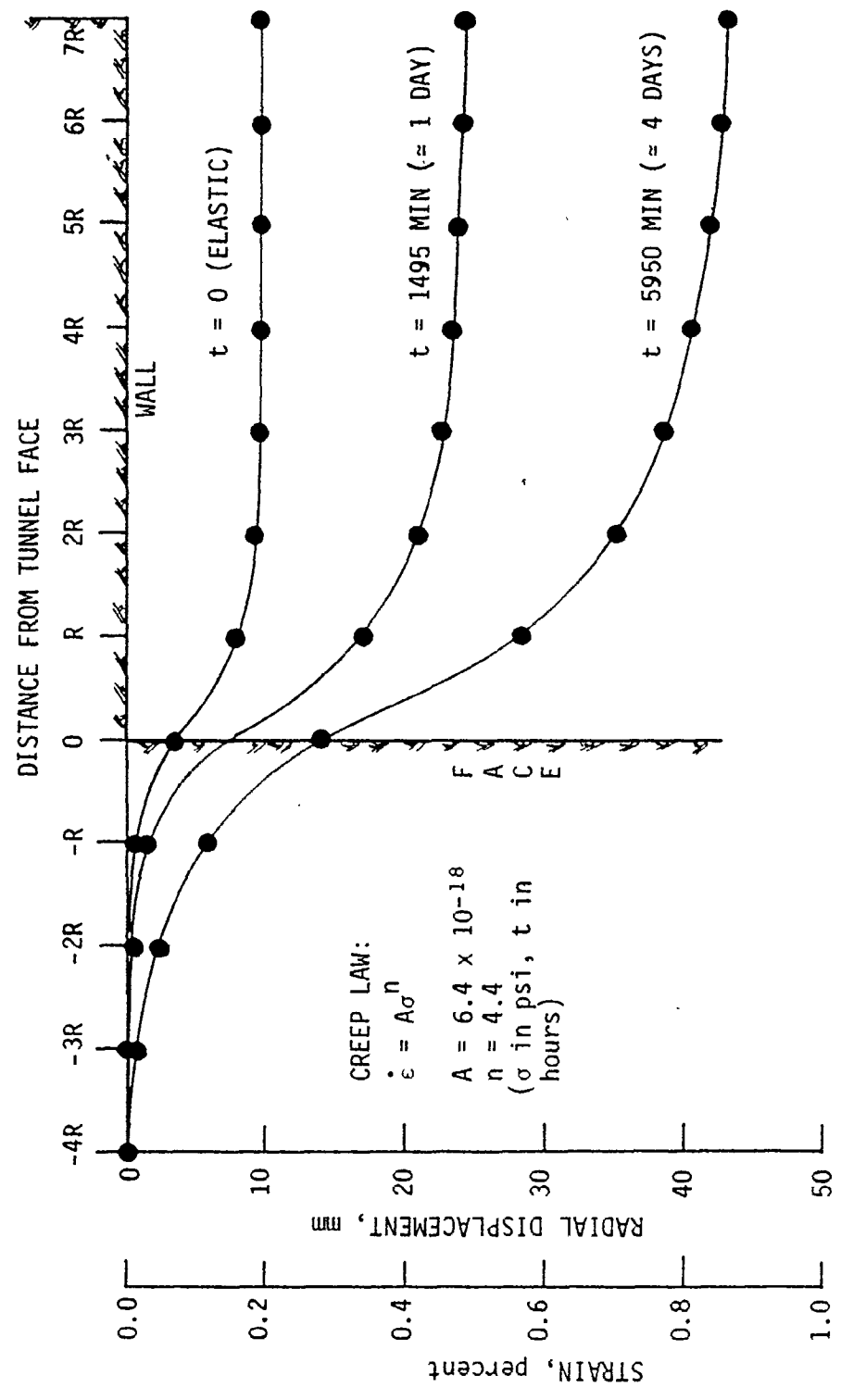
FIGURE 3.19   TUNNEL WALL CONVERGENCE WITH TIME (ELASTIC PLUS CREEP) – FEM SOLUTION

and the liner must be installed at an appropriate time-delay to prevent such a condition from developing.

The complete analysis considering different excavation and liner placement sequences, and the elastic-plastic creep responses, will be given in Chapter 5 where actual design problems are considered.

CHAPTER 4

PLANE STRAIN SIMULATION OF TYPICAL TUNNELS

4.1 INTRODUCTION

The excavation simulation procedures developed for the plane strain assumption (Chapter 2) have been applied to several design problems where fair materials and tunnel configuration data were available. The analyses and typical simulation results for two tunnels that are now constructed are summarized here to illustrate the capabilities of the method in assessing potential tunnel performance. The limitations of the available materials properties must be recognized at this stage as simulation capabilities often exceed characterization abilities. Further, the limitations of the plane strain assumption are recognized and dealt with in the next chapter. For the first example, a linear elastic analysis was required and considered adequate for the preliminary design. A complete elastic-plastic-creep analysis was required for the second design example. Some parametric studies were involved for each design.

4.2 ELASTIC ANALYSIS OF A TUNNEL CONSTRUCTED IN GLACIAL TILL

A 1310 m long storm water tunnel constructed at a depth of 31 m in Edmonton was selected as a typical example where a plane strain elastic analysis is considered adequate for preliminary design purposes. This tunnel had a circular cross section of diameter 2:57 m, and was constructed

with a tunnel boring machine entirely through a glacial till formation. A precast concrete segmental liner was used for the support system (Franklin Trow Associates Limited, 1979). Potential ground movements were of concern for the construction method and support system adopted.

The geometry, material properties and boundary conditions of the section analyzed using the finite element method are shown in Figure 4.1. The simulation considered a simplified two-layer soil stratigraphy: the upper layer representing the clay material with a modulus of 50 MPa and the lower layer representing the glacial till with a higher modulus of 140 MPa. The lateral stress ratio of unity (i.e. K_t = 1.0) was assumed to be the most likely value for the region from a review of available data on the till (Eisenstein and Morrison, 1973). However, K_t values of 0.7 and 1.3 were also considered to check the influence of lateral stresses on the elastic convergence as this range of K_t values might be involved. The available data for the till also indicated that any convergence (closure) due to tunnelling would be essentially elastic. Both effective and unit weight total stress analyses were completed for the K_t value of 1.0 as ground water data were minimal at the early design stages.

The finite element mesh used in the analysis to simulate excavation and support placement is shown in Figure 4.2. The first row of elements at the tunnel boundary were 'deactivated' to simulate excavation and then 'reactivated' to represent installation of the simplified precast concrete segmental liner. The results of the various simulations are presented in Tables 4.1 and 4.2. Table 4.1 gives the elastic displacements
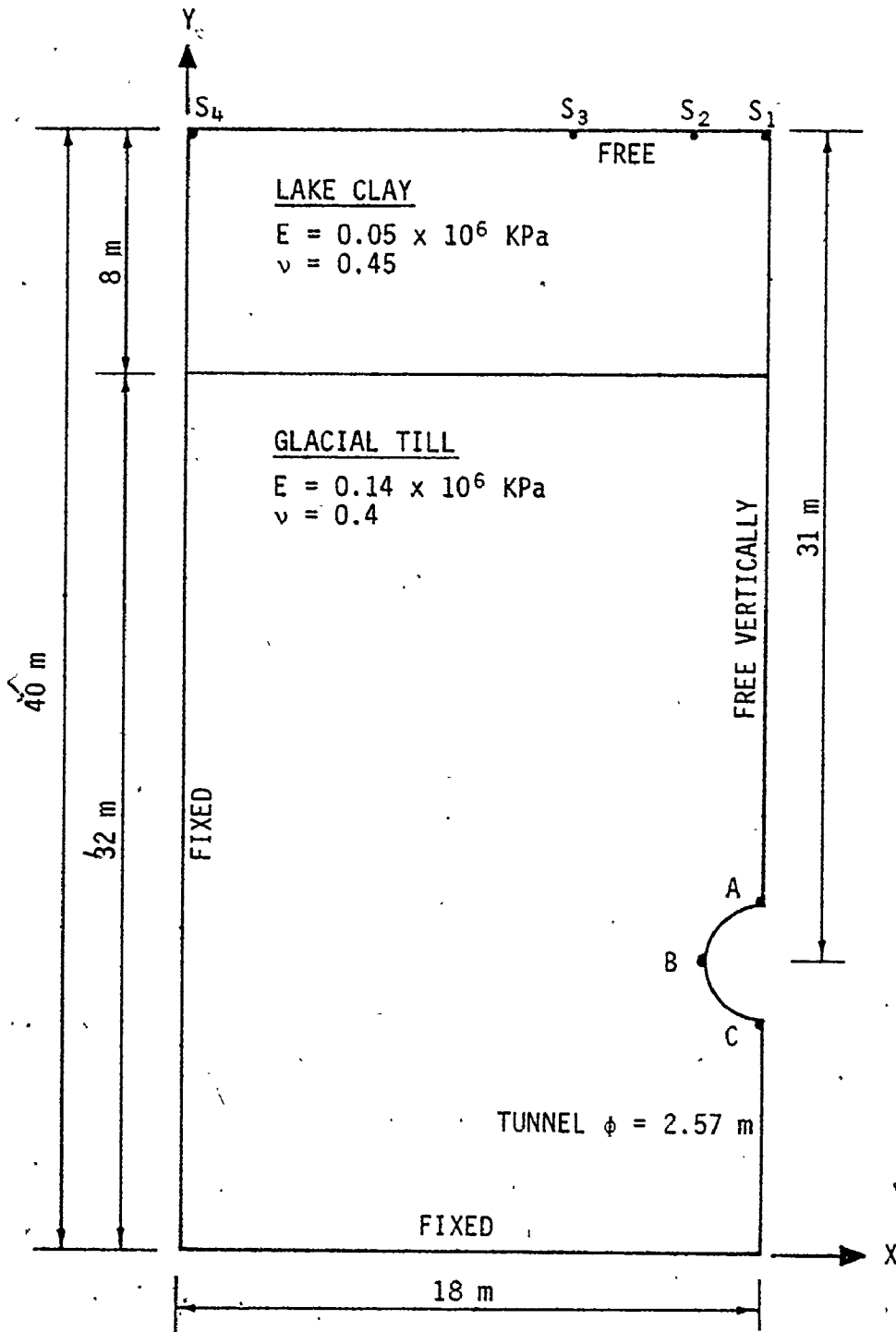
FIGURE 4.1   SIMPLIFIED GEOMETRY FOR THE LINEAR-
ELASTIC PLANE STRAIN ANALYSIS OF A
TUNNEL IN TILL
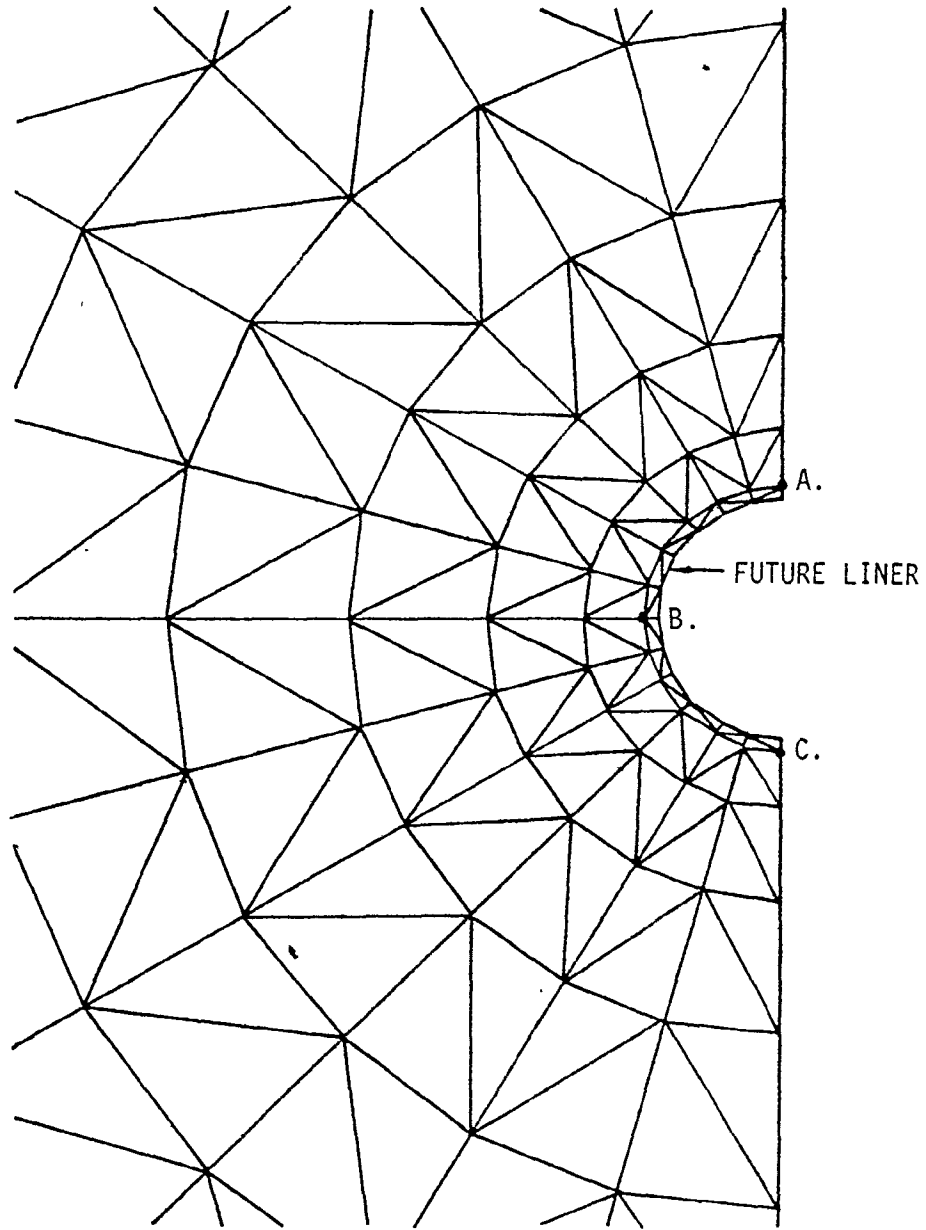
180 ELEMENTS AND 110 NODES

FIGURE 4.2   FINITE ELEMENT MESH FOR LINEAR ELASTIC
PLANE STRAIN ANALYSIS OF A TUNNEL IN
TILL

TABLE 4.1

ELASTIC DISPLACEMENTS AT TUNNEL AND GROUND SURFACES FOLLOWING EXCAVATION

PLANE STRAIN ANALYSIS OF TUNNEL IN TILL
(LINER NOT INSTALLED)

		Displacements, mm			
		Total Unit Weight Analyses			Effective Unit Weight Analysis
Location[a]		$K_t = 0.7$	$K_t = 1.0$	$K_t = 1.3$	$K_t = 1.0$
A.	Crown	8.01	8.01	8.01	4.31
B.	Spring line	5.34	7.65	9.96	4.12
C.	Invert	7.27	7.24	7.21	3.89
S1.	Ground	0.95	0.98	1.02	0.53
S2.	Ground	1.00	1.03	1.06	0.55
S3.	Ground	1.03	1.06	1.10	0.57
S4.	Ground	0.15	0.14	0.14	0.08

a. See Figure 4.1.

b. Positive values for points A,B, and C represent inward displace-
ments, and for points S1, S2, S3 and S4 represent downward
displacements.

TABLE 4.2

ELASTIC STRESSES IN CONCRETE SEGMENTAL LINER

PLANE STRAIN ANALYSIS OF TUNNEL IN TILL
(LINER INSTALLED INSTANTANEOUSLY)

| Location | Stresses in the Concrete Liner, MPa | | | |
| | Total Unit Weight Analyses | | | Effective Unit Weight Analysis |
	$K_t = 0.7**$	$K_t = 1.0*$	$K_t = 1.3***$	$K_t = 1.0*$
Crown	4.79	7.44	10.81	3.99
Springline (Average)	8.80	7.65	7.10	4.01
Invert	5.10	7.85	11.31	4.26

*No tensile stresses developed in the liner.

**Tensile stresses developed at spring line with maximum value = 440 kPa.

***Tensile stresses developed at both invert and crown with maximum value = 370 kPa.

at the tunnel and ground surfaces following excavation. For an initial uniform stress condition (i.e. K_t = 1.0), and total unit weight analysis, an approximately uniform tunnel diametrical closure of 15 mm was predicted with a maximum surface settlement of about 1 mm. Based on an effective unit weight analysis, these values were approximately 50% of the total unit weight values, as expected. The predicted displacements were affected comparatively little by changes in the assumed initial stress ratio.

~ Stresses in the precast concrete segmental liner were also determined. The liner had a thickness of 110 mm and elastic modulus of 2.1×10^3 MPa. The maximum compressive stresses at the locations corresponding to the crown, spring line and invert tabulated in Table 4.2 are based on the conservative assumption of instantaneous liner placement. These results indicate that for an assumed stress ratio of unity (i.e. K_t = 1.0), the liner stresses are entirely compressive with an average value of 7.65 MPa. However, for stress ratios of 0.7 and 1.3, tensile stresses developed in the liner with maximum values in the range of 440 and 370 kPa, respectively. These compressive and tensile stress levels are well within tolerable levels for 41 MPa compressive strength concrete.

Although the analyses assumed immediate liner placement and/or instantaneous excavation, the actual inward displacements do not occur immediately in the field due to the restraining effect of the tunnel face. The complete elastic displacements are not achieved until the face has advanced approximately 3 diameters from the point under consideration (see Table 4.1). The percentage of the total predicted elastic displace-

ments occurring before liner placement, and the load to be carried by the liner, will depend on the distance between the face and the location where the liner is actually installed. Moreover, no joints were used in the concrete liner representation in these analyses so that it is stiffer than the segmental concrete liner actually used. This aspect will be discussed further as part of the next design example. Even with these conservative assumptions, the stresses predicted are well within the anticipated compressive strength range for the concrete used (41 MPa), with minimal tensile stress development.

The tunnel has now been completed, and while detailed monitoring data are not currently available, the liner performance during and after construction was most satisfactory. Ground movements were well within tolerable levels, but somewhat greater than predicted as there was some movement of soil into voids behind the liner.

4.3 ELASTIC-PLASTIC-CREEP PLANE STRAIN ANALYSIS OF A TUNNEL CONSTRUCTED IN SILTSTONE

4.3.1 General Site Details and Constraints

The design example selected to illustrate a typical elastic-plastic-creep plane strain analysis involved a circular water intake tunnel to be constructed through a siltstone formation near Beulah, North Dakota. Overburden depths above the tunnel axis range from about 58 m at the inlet to 87 m at the outlet. The average lake elevation above the tunnel axis is 80 m. For the tunnelling machine design, a 2.667 m diameter leading edge (i.e. tunnel diameter) was required to allow for the recovery of parts of

the machine following completion of the contract. Previous experience in the area had indicated the siltstone to be in the squeezing ground classification and the existence of high lateral stress conditions.

4.3.2   Tunnel Liner and Mesh Idealization

A precast concrete segmental liner with each ring consisting of 4 segments flexibly joined at the 45°, 135°, 225°, and 315° positions was to be used. Each segment in the ring was also 'notched' at its mid-point to further reduce the flexural rigidity, giving an essentially flexible liner capable of withstanding fairly large ground movements. A soft backing behind the liner was also considered desirable for the following reasons:

1.   It allows for movements associated with squeezing ground conditions;

2.   It provides some tolerance for variations in tunnel diameter;

3.   It reduces localized stress concentrations;

4.   It introduces some waterproofing action; and

5.   It should eliminate the need for grouting.

The preliminary design data supplied for use during the excavation and liner installation simulation are given in Table 4.3 (R.V. Anderson Associates Limited, personal communication). Compressive properties of the Ethafoam soft backing are given in Table 4.4 (R.V. Anderson Associates Limited, personal communication).

The finite element mesh used in the analyses to simulate excavation and support system placement is shown in Figure 4.3, with fixed boundaries

TABLE 4.3

PRELIMINARY TUNNEL DESIGN DATA

Outside Tunnel Diameter	2.667 m
Ethafoam Soft Backing Thickness	45 mm
Precast Concrete Segmental Lining Thickness	171 mm
Inside Tunnel Diameter	2.235 m

TABLE 4.4

COMPRESSIVE PROPERTIES OF THE ETHAFOAM SOFT BACKING

Compression, Percent	Stiffness, kPa
5	300
25	370
50	520
80	2070

located more than 7 radii away from the tunnel axis. The left boundary representing the line of symmetry was taken to be free vertically and fixed horizontally. The first two rows of elements at the tunnel boundary were deactivated to simulate excavation and then reactivated to represent support system installation. The thin element layer in Figure 4.3 represents the Ethafoam soft backing, while the thick element layer represents the precast concrete segmental tunnel liner. Both the joints between segments and notches at their midpoints were presented in a very simplified way to give some reduction in the flexural rigidity. These
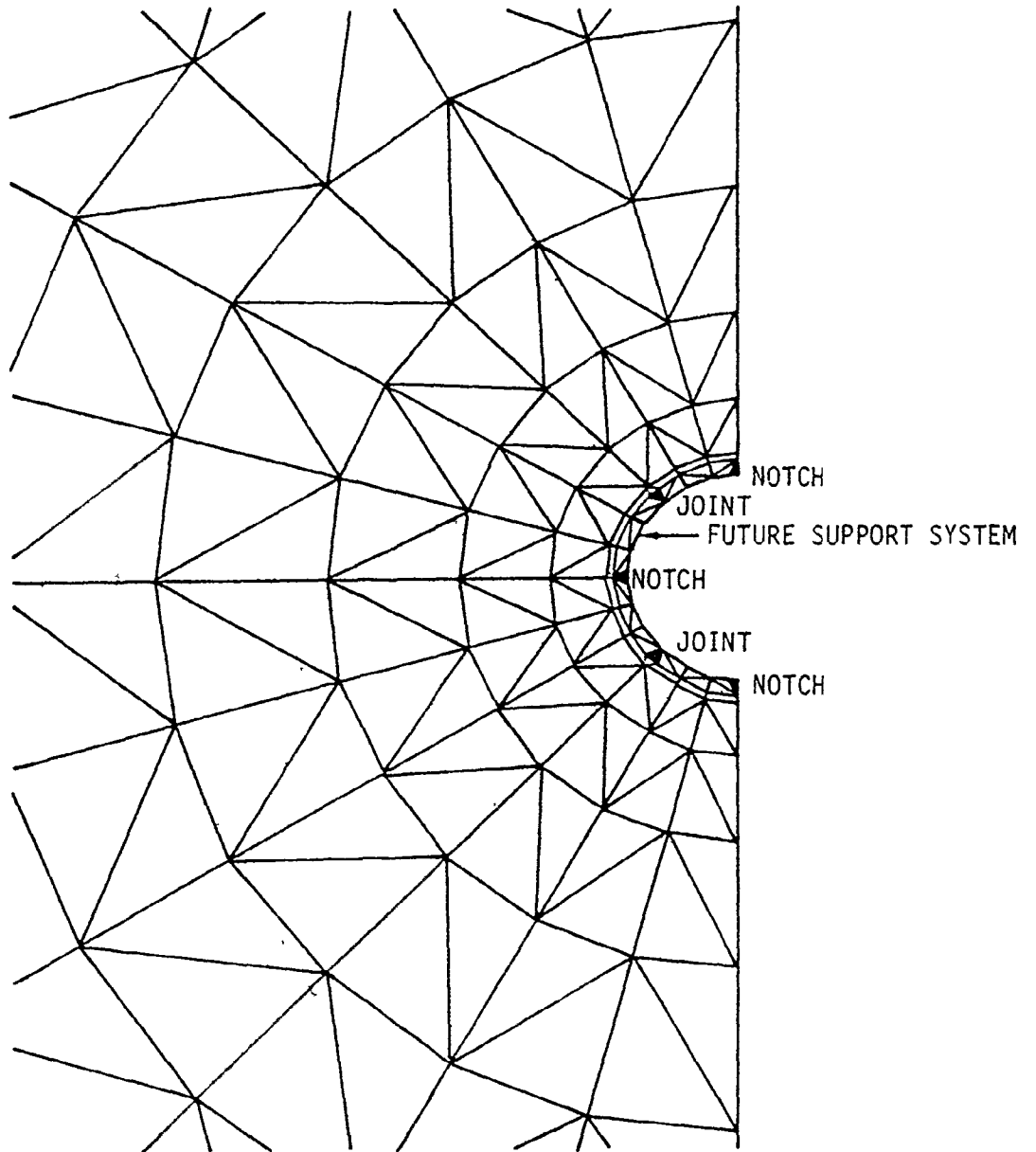
211 ELEMENTS AND 128 NODES

FIGURE 4.3   FINITE ELEMENT MESH REPRESENTATION OF
TUNNEL EXCAVATION AND SUPPORT SYSTEM
PLACEMENT, ELASTIC-PLASTIC-CREEP PLANE
STRAIN ANALYSIS

simplifications could be much improved in supplemental detailed stress analyses for the support system (i.e. refined mesh and/or bending elements) using displacement boundary conditions at any time from the elastic-plastic-creep simulation.

4.3.3   Properties Adopted for the Analysis

It was difficult to select appropriate properties for the siltstone as the available laboratory data were limited. No information on appropriate creep relationships was available, and the initial in situ stress ratio (K_t) estimate required refinement. Given these limitations, estimates of properties were made where necessary that appear reasonable from the available data and technical literature. Since the siltstone probably behaves like a soft rock or a heavily preconsolidated hard clay (R.V. Anderson Associates Limited, personal communication), the creep properties for London Clay (Bishop and Lovenbury, 1969) were used in the Singh and Mitchell three parameter creep relationship (1969). This equation is discussed in detail in Appendix C. The properties used in the analysis for the siltstone and tunnel support system are given in Tables 4.5 and 4.6 respectively, with supplemental comments on the values adopted. The precast concrete segmental liner joint stiffness was assumed to be 1/100 of the liner stiffness, while the soft backing stiffness was obtained by linearizing the Ethafoam compressive stiffness data.

4.3.4   Cases Considered and Typical Results

The following cases were considered:

1.   Elastic, no liner, K_t = 0.75, 1.0, 1.25, 1.5 and 2.0.

TABLE 4.5

SILTSTONE PROPERTIES USED IN THE ANALYSIS

Properties	Value	Comments
Modulus of Elasticity	210 MPa	May be somewhat low since the field moduli are typically 2 to 3 times those determined in the laboratory.
Poisson's Ratio	0.4	
Unit Weight	20 kN/m^3	Assumed uniform with depth for all strata.
Yield Stress	a. 0.7 MPa	Represents 90% of maximum laboratory compressive strength.
	b. 1.0 MPa	Represents 90% of two times average laboratory compressive strength to allow for sample disturbance.
Depth	87 m	Maximum depth considered.
Initial Stress Field Ratio	K_t = 0.75, 1.25, 1.5 and 2.0	K_t seems to be between 1.0 and 1.5 for site.
Uniform Vertical Pressure (Depth)	87 m	Taken equal to the overburden depth.
Creep Properties	A=0.1255x10^{-3} α=0.4815x10^{-3} m=1.03 (t in days, D in psf)	London clay parameters for Singh and Mitchell's creep relationship: $\dot{\varepsilon} = Ae^{\alpha D}(\frac{1}{t})^m$

TABLE 4.6

TUNNEL SUPPORT PROPERTIES USED IN THE ANALYSIS

Properties		
Structural Concrete		
Modulus of Elasticity	21×10^3 MPa	Modulus of elasticity is relatively low, as 41 MPa concrete may be used with modulus of elasticity of 31×10^3 MPa.
Poisson's Ratio	0.2	
Compressive Strength	41 MPa	
Joints and Notches in the Liner		
Modulus of Elasticity	210 MPa	Stiffness reduced to 1/100, but this probably does not introduce much compressibility.
Poisson's Ratio	0.2	
Soft Backing		
Modulus of Elasticity	1.0 MPa	Obtained from the Ethafoam compression properties.
Poisson's Ratio	0.45	

TABLE 4.7

ELASTIC INWARD DISPLACEMENTS AFTER EXCAVATION FOR UNLINED AND LINED CASES WITH DIFFERENT INITIAL STRESS CONDITIONS

Case \ Location	Inward Displacements, mm		
	Crown	Spring Line	Invert
Unlined K_t = 0.75	6.41	4.83	6.62
Unlined K_t = 1.0	6.38	6.49	6.59
Unlined K_t = 1.25	6.34	8.15	6.55
Unlined K_t = 1.50	6.30	9.81	6.51
Unlined K_t = 2.0	6.23	13.12	6.44
Lined, 45 mm Soft Backing, K_t = 1.0	3.97	4.11	4.17
Lined, 45 mm Soft Backing K_t = 2.0	2.72	9.45	2.92
Lined, 20 mm Soft Backing, K_t = 1.0	2.62	2.69	2.75

2. Elastic, liner, K_t = 1.0, 2.0.

3. Elastic-plastic, no liner, 0.7 MPa yield stress, K_t = 1.0 and 2.0.

4. Elastic-plastic, no liner, 1.0 MPa yield stress, K_t = 1.0 and 2.0.

5. Elastic-plastic, liner, K_t = 1.0, 2.0.

6. Elastic-creep, no liner, K_t = 1.0, 2.0.

7. Elastic-creep, liner, K_t = 1.0, 2.0.

8. Elastic-plastic, liner (backing reduced to 20 mm), K_t = 1.0 and 2.0.

9. Elastic-creep, liner (backing reduced to 20 mm), K_t = 1.0.

All of the cases were based on the effective unit weights for an overburden depth of 87 m at the outlet. For full water pressure acting at a depth equal to the overburden depth, the final stresses can be simply obtained as the summation of the effective and hydrostatic stresses. The plastic analyses are based on an elastic-perfectly plastic material behaviour following the von Mises yield criterion with the loading due to excavation applied incrementally. The major constraint in the analyses was of course the selection of an appropriate creep relationship (i.e. Singh and Mitchell creep relationship with London Clay parameters).

a. Elastic Analysis

Table 4.7 gives the elastic inward displacements after excavation for the unlined and lined cases for various initial stress conditions. For the unlined tunnel with a uniform in situ stress field (i.e. K_t = 1.0) uniform inward displacements were found as anticipated, with an average value of 6.5 mm. For K_t equal to 2.0, the horizontal inward displacement of 13.13 mm was approximately twice the average vertical inward displacement

of 6.35 mm. For both K_t equal to 1.0 and 2.0, the elastic inward displacements were quite small giving maximum elastic strains of 0.51% and 1.02%, respectively. In the case of the lined tunnel, the precast concrete segmental liner reduced the inward displacements somewhat as anticipated since it was considered to be placed immediately following excavation. Uniform inward displacements were found for K_t equal to 1.0 with an average value of 4.08 mm for the 45 mm soft backing and 2.69 mm for the 20 mm soft backing. The horizontal inward displacement of 9.45 mm for the 44 mm soft backing was more than three times the average vertical inward displacement of 2.82 mm for the higher lateral stress ratio of K_t equal to 2.0.

The maximum elastic compressive stresses developed at three locations corresponding to the crown, spring line and invert of the precast concrete segmental liner are given in Table 4.8. A uniform stress distribution developed in the liner for K_t equal to 1.0, and the stress distribution was fairly uniform even for K_t equal to 2.0. This is due to the soft backing and its effect in reducing any stress concentrations. The liner is acting essentially as a compression member, even for K_t equal to 2.0 where small tension zones developed with a maximum value of 190 kPa. The effect of reducing the thickness of the soft backing was a corresponding increase in the liner stresses.

b.   Elastic-Plastic Analysis

To select a realistic number of increments of loading in the elastic-plastic analyses, one, five and ten increments were considered.

TABLE 4.8

MAXIMUM COMPRESSIVE STRESSES DEVELOPED IN
THE PRECAST CONCRETE SEGMENTAL TUNNEL LINER

Location Case	Maximum Compressive Stress, MPa		
	Crown	Spring Line (Average)	Invert
Lined, 45 mm Soft Backing, $K_t = 1.0$	2.52	2.62	2.56
Lined, 45 mm Soft Backing, $K_t = 2.0$	3.75	3.94	3.81
Lined, 20 mm Soft Backing, $K_t = 1.0$	4.00	4.18	4.14

The results showed that there was no significant difference between five
and ten increments of loading, while there was a substantial difference
between one and ten increments of loading as shown in Table 4.9 for the
inward displacements. Therefore, most of the results given here are based
on one excavation step with ten increments of loading. Tables 4.9 and
4.10 give the total (elastic plus plastic) inward displacements for un-
lined and lined tunnel cross sections, respectively. For the case of the
unlined tunnel, yield stresses of 0.7 MPa and 1.0 MPa were considered for
K_t values of 1.0 and 2.0. For K_t equal to 1.0 there was minimal plastic
yielding and the inward displacements were fairly uniform at 8.27 mm and

6.84 mm for the lower and higher yield stresses, respectively. However, for K_t equal to 2.0, the entire region surrounding the excavation yielded for both yield stresses. It should be noted that the yield stresses adopted are probably somewhat low for the formation involved.

For the lined tunnel analyses, the liner was constructed immediately following excavation and the one-step excavation loads were again applied in 10 increments. The yield stress was assumed to be 1.0 MPa for initial stress conditions of K_t equal to 1.0 and 2.0. (Compressible soft backing thicknesses of 45 mm and 20 mm were considered to determine backing influences.) The results for the various analyses are summarized in Tables 4.9 and 4.10. For K_t equal to 1.0, there was no plastic yielding and the inward displacements were fairly uniform at 4.11 mm and 2.68 mm for the 45 mm and 20 mm soft backing thicknesses, respectively. Uniform compressive stresses developed in the liner for both backings. For K_t equal to 2.0, there was minimal plastic yielding in the crown and invert zones as anticipated since the high lateral stresses tend to be redistributed. The plastic zone developed is shown in Figure 4.4. The horizontal inward movements were much greater than the vertical movements, and uniform compressive stresses developed in the liner with only small tension zones (150 kPa and 270 kPa for 45 mm and 20 mm backing, respectively). The liner is acting essentially in the desired compressive mode throughout. Comparing the performance of the thin soft backing with the thick soft backing (Table 4.11), the liner stresses increased by only about 60% for K_t equal to 1.0 and 50% for K_t equal to 2.0, which indicates that the thicker backing has distinct advantages in reducing the design stresses for the

b. LINED (171 mm CONCRETE WITH 20 mm SOFT BACK-ING), $K_t = 2.0$
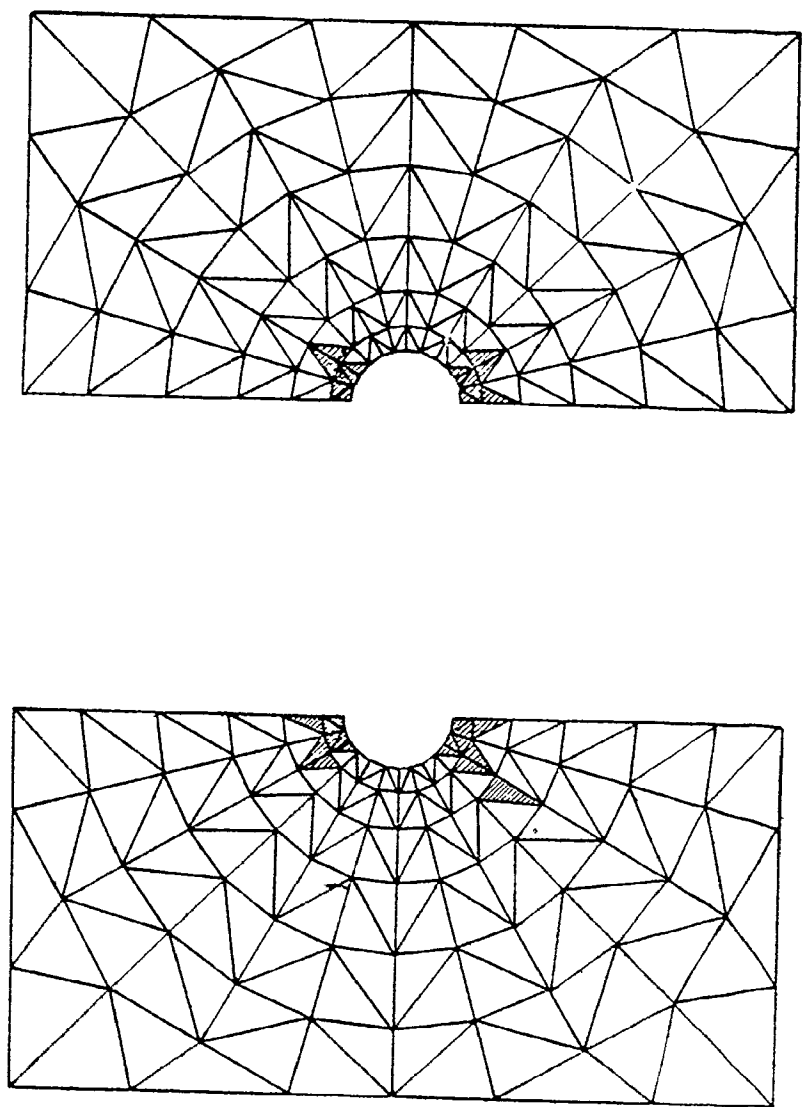
a. LINED (171 mm CONCRETE WITH 45 mm SOFT BACK-ING), $K_t = 2.0$

FIGURE 4.4   PLASTIC YIELDING ZONES FOR LINED TUNNEL WITH DIFFERENT SOFT BACKING THICKNESSES, YIELD STRESS = 1.0 MPa, $K_t = 2.0$

TABLE 4.9

ELASTIC PLUS PLASTIC INWARD DISPLACEMENTS FOR UNLINED TUNNEL

Loading Condition	K_t Value	Location	Total Inward Displacements, mm	
			Yield Stress 1.0 MPa	Yield Stress 0.7 MPa
One step excavation, one increment of loading	1.0	Crown		7.90
		Spring Line		8.02
		Invert		8.19
One step excavation, 10 increments of loading	1.0	Crown	6.73	8.13
		Spring Line	6.84	8.27
		Invert	6.97	8.41
	2.0	Crown	Failure condition occurred at load increment No. 4, entire region yielded	Failure condition occurred at load increment No. 4, entire region yielded
		Spring Line		
		Invert		

TABLE 4.10

ELASTIC PLUS PLASTIC INWARD MOVEMENTS FOR LINED TUNNEL

YIELD STRESS = 1.0 MPa

Loading Condition	K_t Value	Location	Total Inward Displacements, mm	
			Soft Backing 45 mm	Soft Backing 20 mm
One step excava-tion, 10 increment of loading,	1.0	Crown	3.97*	2.69*
		Spring Line	4.11*	2.69*
		Invert	4.17*	2.75*
Yield Stress 1.0 MPa	2.0	Crown	3.89	0.73
		Spring Line	10.10	7.65
		Invert	4.24	0.82

*Same as the elastic solution since no yielding occurred

TABLE 4.11

STRESSES IN THE LINER FOR THE ELASTIC-PLASTIC ANALYSIS

Loading\Condition	K_t Value	Location	Liner Stresses, MPa	
			Soft Backing 45 mm	Soft Backing 20 mm
One step excavation, 10 increments of loading	1.0	Crown	2.52	4.00
		Spring Line	2.62	4.02
		Invert	2.56	4.14
Yield Stress = 1.0 MPa	2.0	Crown	4.37	6.53
		Spring Line	4.50	6.58
		Invert	4.45	6.78

elastic-plastic response. It should be noted again that the effect of the hydrostatic pressure at the site of 780 kPa would be added to the computed liner stresses in each case to obtain the final design stresses.

c.   Elastic-Creep Analysis

    While an elastic-plastic-creep analysis would yield more complete information, given the small amount of yielding, an elastic-creep analysis was considered adequate for design purposes. (The elastic-plastic-creep analysis with advancing face is applied in the next chapter.) After excavation, creep analyses were carried out for both the unlined and lined cases using the Singh and Mitchell creep relationship with Bishop and Lovenbury's constants for London Clay. For the unlined tunnel there was a noticeable stress redistribution around the opening with time. The tangential, radial and equivalent stresses near the opening decreased with time until they approached a steady state condition in about four days as shown in Figure 4.5 for the K_t equal to 1.0 case. Four initial stress conditions (K_t = 0.75, 1.0, 1.25 and 1.5) were considered to study this influence on the tunnel inward displacements with time. After about seven days, primary creep was completed and the secondary creep was showing up for the initial stress conditions considered. The creep displacements around the opening increased with increasing lateral stresses. In spite of the nonuniform elastic displacements that occurred following excavation for the nonuniform stress cases ($K_t \neq$ 1.0), uniform displacements developed with time due to creep stress redistribution. This stress redistribution behaviour observed in creep simulations occurs along the lines suggested by Peck in his state-of-the-art report to the ICSMFE in Mexico (1969) that
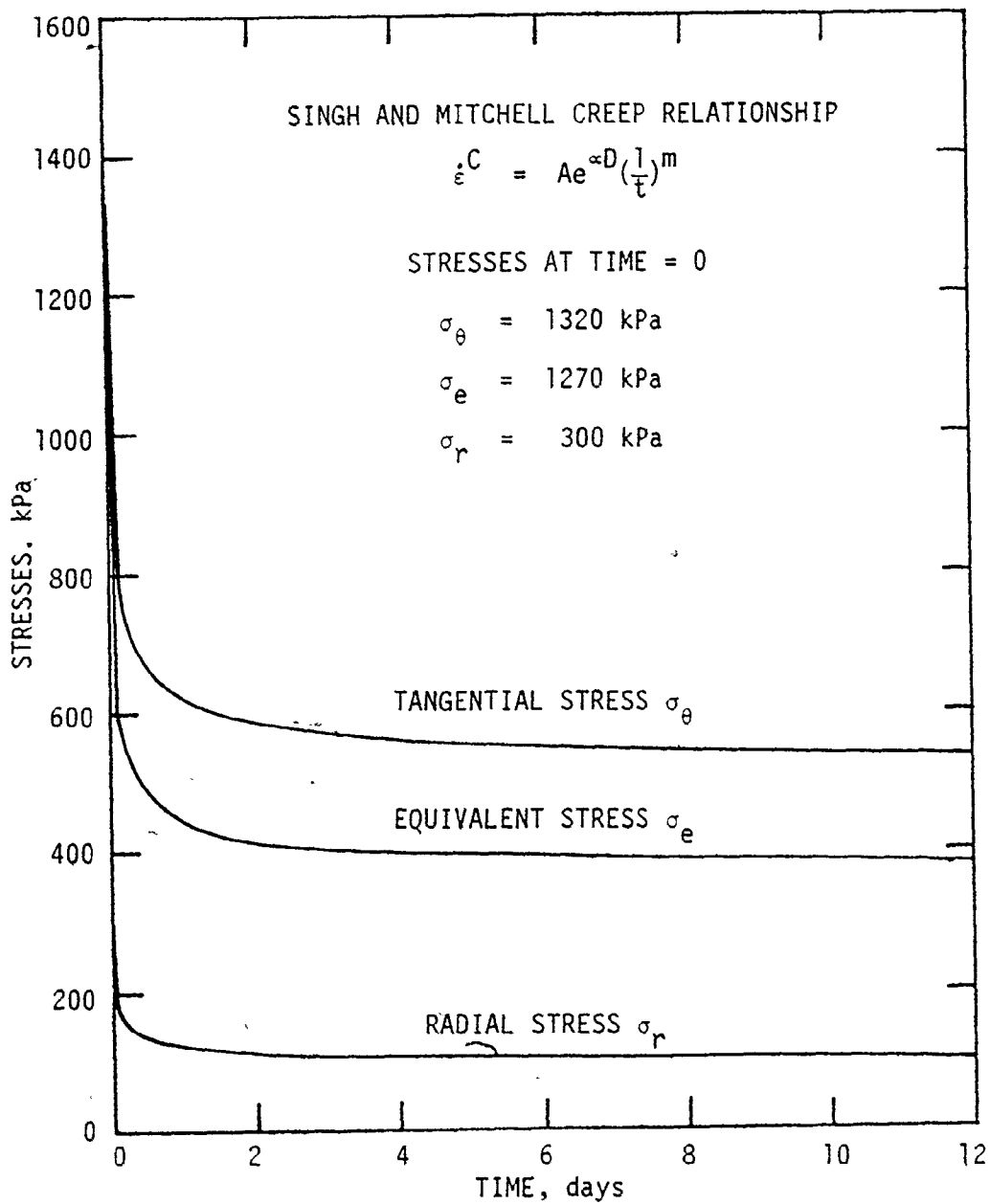
FIGURE 4.5   CREEP INFLUENCE ON THE STRESSES NEAR THE UNLINED
TUNNEL WALL AT THE CROWN, K_t = 1.0, SINGH AND
MITCHELL CREEP RELATIONSHIP

forms the basis for many empirical design procedures. The total inward displacements at the crown, spring line and invert after two months creep are given in Table 4.12. A comparison of these values with the displacements after about 12 days in Figures 4.6 and 4.7, and field experience with subway tunnels in London Clay (Ward, 1978), indicates that creep should be minimal for design purposes after about one month.

TABLE 4.12

ELASTIC PLUS CREEP INWARD DISPLACEMENTS FOR
UNLINED TUNNEL AFTER 2 MONTHS CREEP,
SINGH AND MITCHELL CREEP RELATIONSHIP

K_t Value	Elastic Plus Creep Inward Displacements, mm		
	Crown	Spring Line	Invert
0.75	30.91	30.24	31.09
1.00	37.54	38.08	38.35
1.25	44.52	45.79	45.99
1.50	52.41	54.38	54.51

For the case of the unlined tunnel analyses, the support system with 20 mm of Ethafoam backing was assumed to be constructed one hour after excavation. This was based on a stand-up time estimate of one hour for the site and conditions involved. The analysis used took into consideration the initial state of stress in the rock mass (K_t = 1.0 assumed to be appropriate), the displacements and stress redistribution occurring during tunnel excavation, and the behaviour of the precast concrete segmental
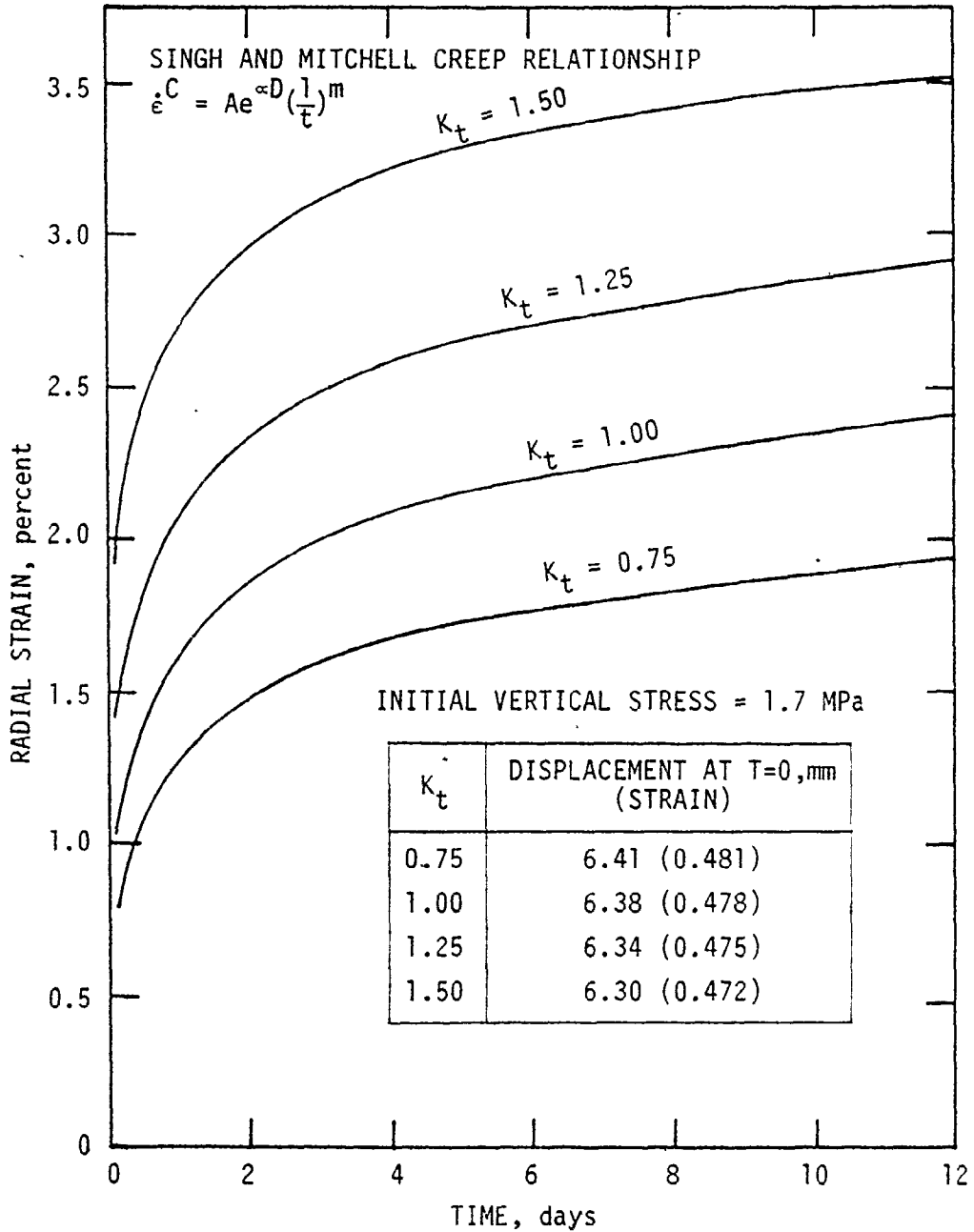
FIGURE 4.6   CROWN DOWNWARD RADIAL STRAIN WITH TIME FOR DIFFERENT STRESS CONDITIONS
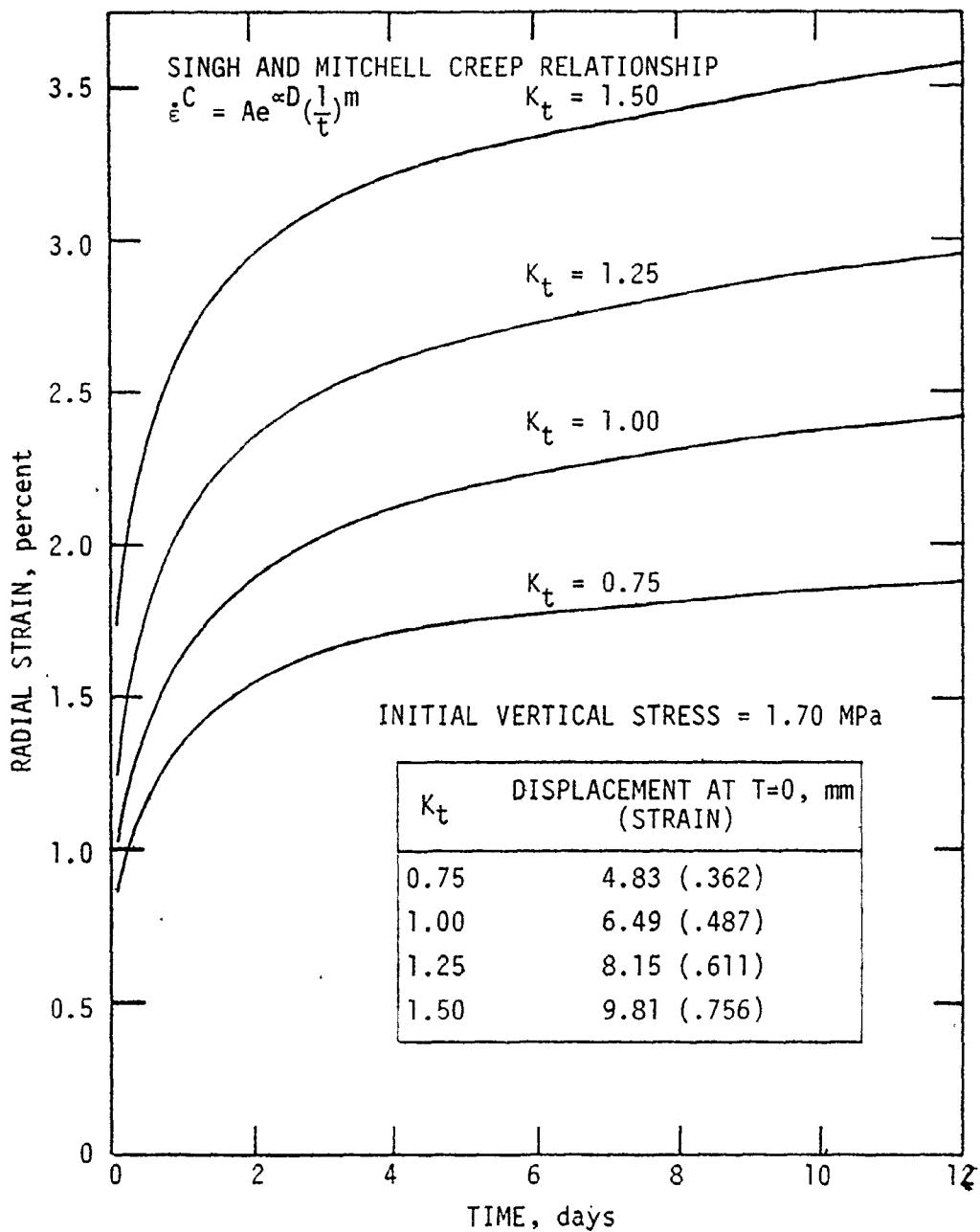
FIGURE 4.7   SPRING LINE INWARD RADIAL STRAIN WITH TIME
FOR DIFFERENT STRESS CONDITIONS

liner and deformable interface material following its installation in the opening. The support system was assumed to have no time-dependent behaviour as this is a conservative assumption in terms of liner stress development due to creep. However, the analysis can allow support creep if desired. A summary of the key results from these analyses is given in Table 4.13. The inward displacements increased from 6.49 mm to 13.44 mm (i.e. more than 100%) in three days due to creep, but in the period between three to eighteen days, the displacement increases occurred at a decreasing rate and would not get significantly larger. After three days, the liner's maximum compressive stress was 2.71 MPa, but again the liner stresses did not increase significantly after about eighteen days.

It is important to note the overall scope and limitations on the design example described which was based on several simplifying assumptions: plane strain; one step excavation (i.e. no advancing face excavation); instantaneous or delayed support placement (i.e. no advancing liner placement); and the assumed creep relationship and rock properties. In order to consider fully any proposed support system and tunnel construction procedure, further analyses based on the more detailed advancing face and liner placement simulation would be required. This full simulation is described with examples in the next chapter. Also, testing to characterize the rock and determine the creep properties would be of considerable value in improving the reliability of any simulation. Finally, confirmation of the tunnel and liner response predictions, and liner performance, by monitoring during construction is considered essential. This monitoring is in progress for the tunnel as its construction is now at an advanced

TABLE 4.13

CREEP INFLUENCE ON TUNNEL WALL INWARD DISPLACEMENTS

(AT LINER-ROCK INTERFACE) AND CONCRETE LINER STRESSES,

$K_t = 1.0$

Location	Inward Movements, mm			Concrete Liner Stresses, MPa		
	$T^* = 0$	T = 3 days	T = 18 days	T = 0	T = 3 days	T = 18 days
Crown	6.38	13.39	13.72	0	2.52	3.03
Spring Line	6.49	13.44	13.72	0	2.71	3.26
Invert	6.59	13.54	13.73	0	2.63	3.16

*T = Time from support installation

stage. No problems have been encountered with the excavation and liner design based on the plane strain simulation and more detailed simulation is given in the next chapter.

CHAPTER 5

THREE-DIMENSIONAL ANALYSIS OF TUNNEL EXCAVATIONS NEAR
THE ADVANCING FACE - RESULTS AND DISCUSSION

5.1 INTRODUCTION

The results given in Chapter 4 showed the capability of the finite element method program developed for tunnel excavation and liner placement simulation for the plane strain assumption. In this chapter, the program developed for the three-dimensional tunnel excavation and liner placement simulation with both tunnel face and support advance (described in Chapter 3) is applied to an actual tunnel design problem. The analyses were completed to indicate the capabilities of the simulation method developed, and to show typical results for an actual tunnel. In these analyses, the effects of the longitudinal stress ratio K_ℓ and transverse stress ratio K_t on tunnel wall convergence are presented to show the influence of the pre-existing in situ stresses prior to excavation. The effects of free advancement rate and time-delays (stationary time) on tunnel wall convergence are also presented. Other typical results are given for the elastic-plastic-creep response of both lined and unlined tunnel sections. The tunnel wall convergence and the lining stresses are presented for these cases as these displacements and stresses are important considerations during design.

The tunnel chosen for the three-dimensional analysis (axisymmetric analysis) was the second example presented in the previous chapter, now

under construction in a siltstone formation with high lateral stresses and a tendency to squeeze. The site and formation properties given in Table 4.5, and the precast concrete segmental liner properties given in Table 4.6, were used in the analyses. The soft Ethafoam backing was not considered in the axisymmetric analyses in order to obtain the maximum stresses developed in the precast concrete segmental liner as a limiting condition. The properties and tunnel dimensions were kept constant in order to allow comparisons with the results predicted from the previous two-dimensional plane strain analyses (Chapter 4).

The finite element mesh idealization used in the axisymmetric analysis to model the longitudinal tunnel section was the same as that given in Figure 3.10. The mesh (168 elements and 104 nodes) and input data were prepared using the mesh generating program for a tunnel radius R of 1.334 m. The boundary conditions are shown in Figure 3.10 along with the selected excavation and face advance of one tunnel radius (1R) per excavation step. A total excavation distance of 6R was used for both the unlined and lined tunnel sections. This finite element mesh was used in all of the axisymmetric excavation and liner placement simulations summarized in this chapter.

For the general case of nonaxisymmetric in situ stress fields, Fourier series expansions have been used with a total of four harmonics in the symmetric mode, i.e. 0, 2, 4 and 6. This number of harmonics is considered a realistic and sufficient number from trial analyses to give accurate results to approximate the in situ stress conditions.

Throughout this chapter, strains rather than displacements are employed to facilitate the comparison of deformations for tunnels of different size. In this way, a better understanding may be gained of the increasing in deformations with increasing tunnel size that are often observed in the field.

5.2 EFFECT OF PRE-EXCAVATION-LONGITUDINAL STRESS COMPONENT ON TUNNEL CONVERGENCE

In the design of an underground opening using the plane strain analysis, the question of the effect of the pre-excavation longitudinal (axial) stress component on tunnel convergence cannot be considered. It is a particular advantage that the axisymmetric simulation can deal with the actual field in situ stresses and consider the influences of the axial component. To examine these influences, a total of five simulations were completed in which the axial stress ratio was varied, i.e. K_ℓ was taken as 0.0, 0.5, 1.0, 1.5 and 2.0. A radially uniform in situ stress equal to the vertical stress at the tunnel axis (i.e. $K_t = 1.0$) was assumed for these five cases. An elastic analysis was adopted to simulate quick excavation of a tunnel length of 6R. These results are shown in Figure 5.1 where it is clear that the longitudinal stress ratio K_ℓ has a significant effect on the tunnel convergence, and the convergence increases with increasing K_ℓ. However, to fully consider this influence, it is necessary to vary the transverse (lateral) stress ratio K_t value for the same range of K_ℓ values.
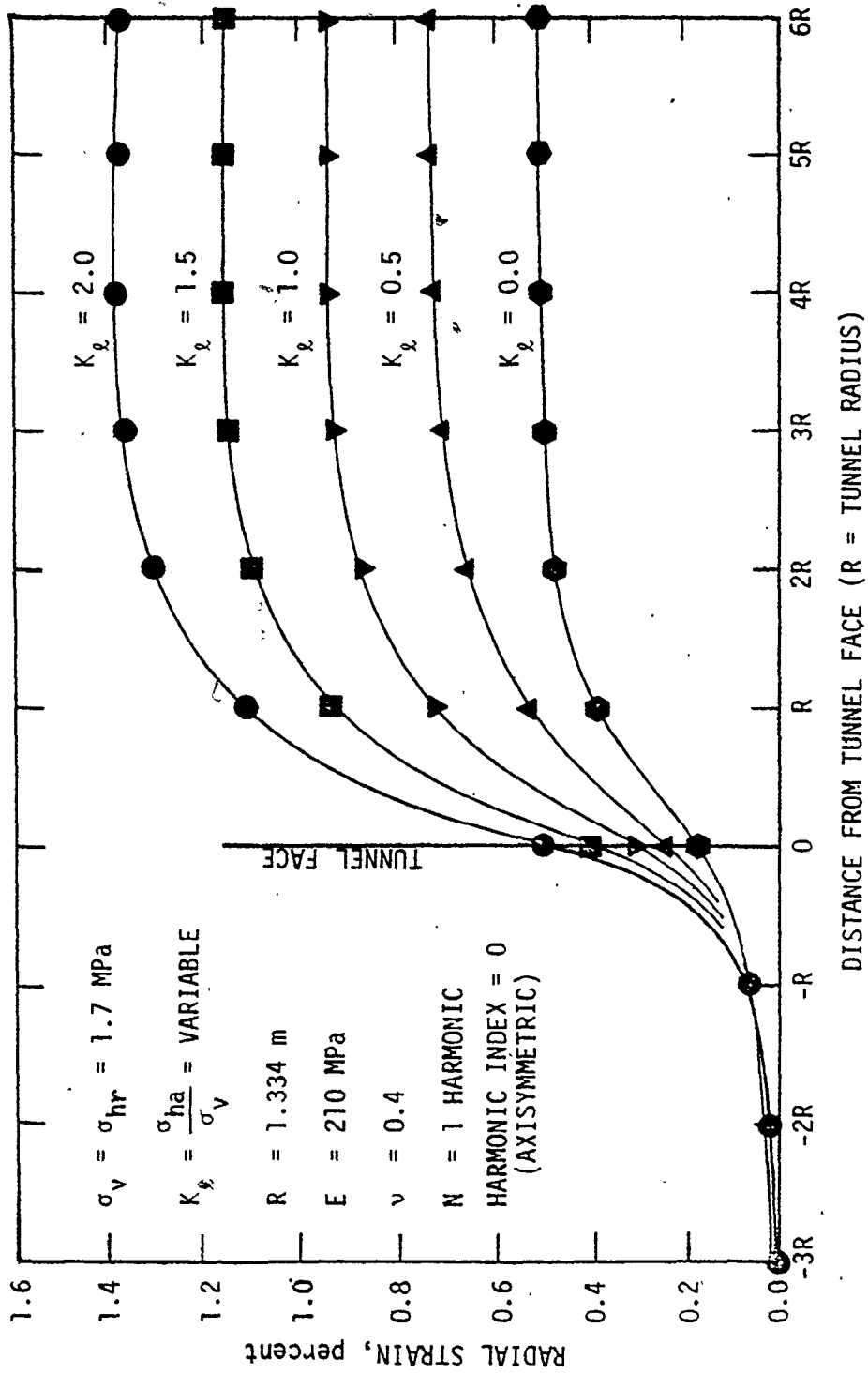
FIGURE 5.1   EFFECT OF THE LONGITUDINAL STRESS RATIO K_ℓ ON THE TUNNEL RADIAL ELASTIC WALL CONVERGENCE – UNLINED CASES, 6R EXCAVATION

5.3 EFFECT OF PRE-EXCAVATION LATERAL STRESS COMPONENT ON TUNNEL CONVERGENCE

Three cases were considered in which the lateral stress component was varied to examine convergence influences. The transverse stress ratio K_t was taken as 0.75, 1.0 and 1.25, with the longitudinal stress ratio equal to the transverse stress ratio (i..e. $K_\ell = K_t$) for each case. The radial convergence results for these cases are shown in Figures 5.2 and 5.3 for both the crown and spring line, respectively. As expected, for K_t less than 1.0, the spring line convergence was less than the crown convergence, while for K_t greater than 1.0, the spring line convergence was higher than the crown convergence. It can also be seen in Figures 5.2 and 5.3 that the crown convergence changes over a narrow range, while the spring line convergence changes over a wider range for the K_t values considered.

These three cases were then considered for lined tunnel sections. The excavation was completed as an incremental operation with the tunnel face advanced by one radius (R) for each step. A rigid concrete liner installed at a distance one radius (R) back from the face at each step was also simulated in the advancing face analyses. The face was advanced a total distance of 6R. The radial convergences for these advancing face cases are also plotted in Figures 5.2 and 5.3. The results show that the rigid liner is completely capable of sustaining the elastic radial displacements due to face advancement with maximum lining stresses of 4.5, 5.45 and 6.4 MPa at the crown, and 5.0, 5.45 and 6.0 MPa at the spring line, for the three K_t values of 0.75, 1.0 and 1.25, respectively. These
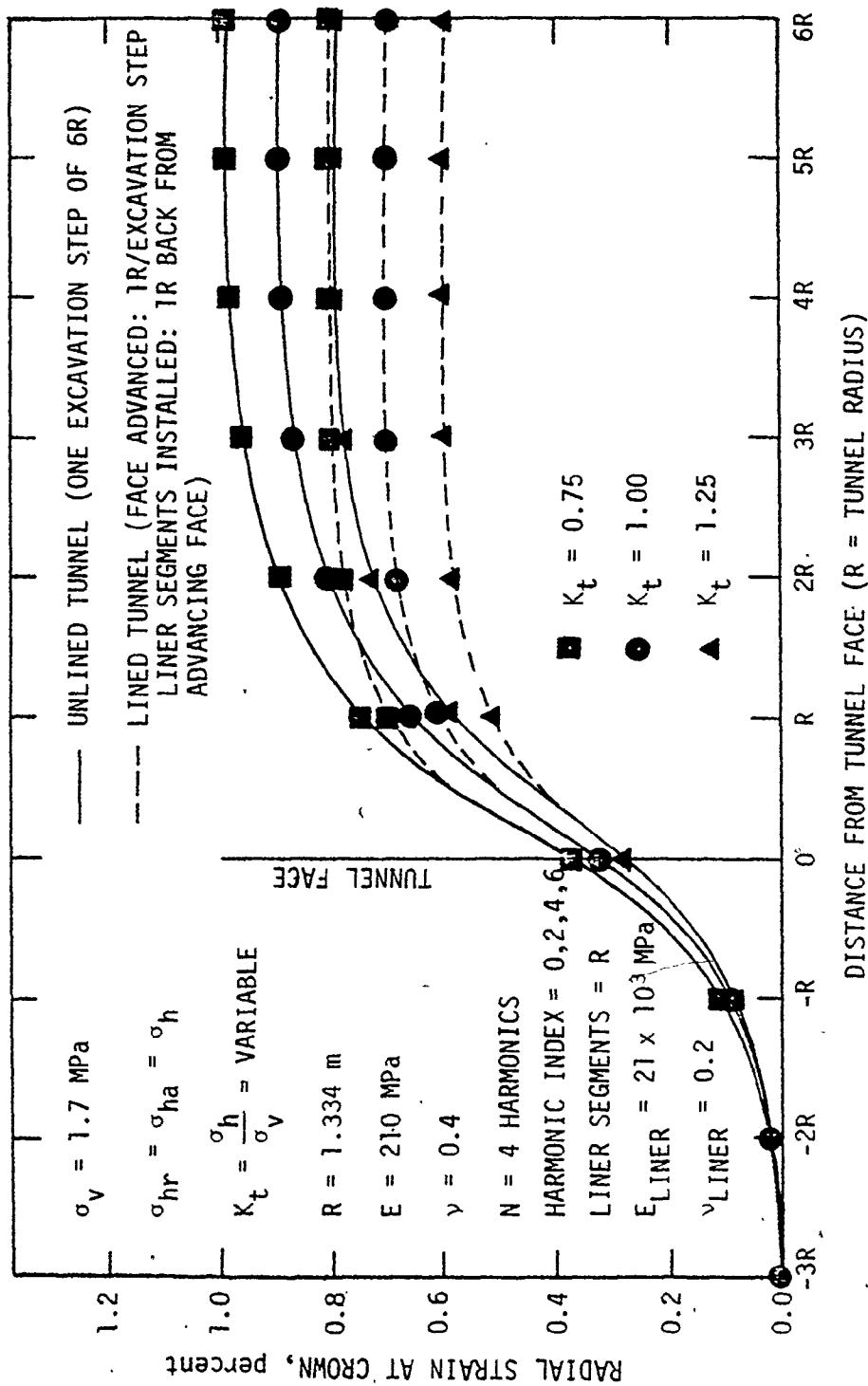
FIGURE 5.2 RADIAL ELASTIC STRAIN AT CROWN NEAR THE TUNNEL FACE FOR VARIOUS TRANSVERSE (LATERAL) STRESS RATIO K_t, UNLINED AND LINED CASES
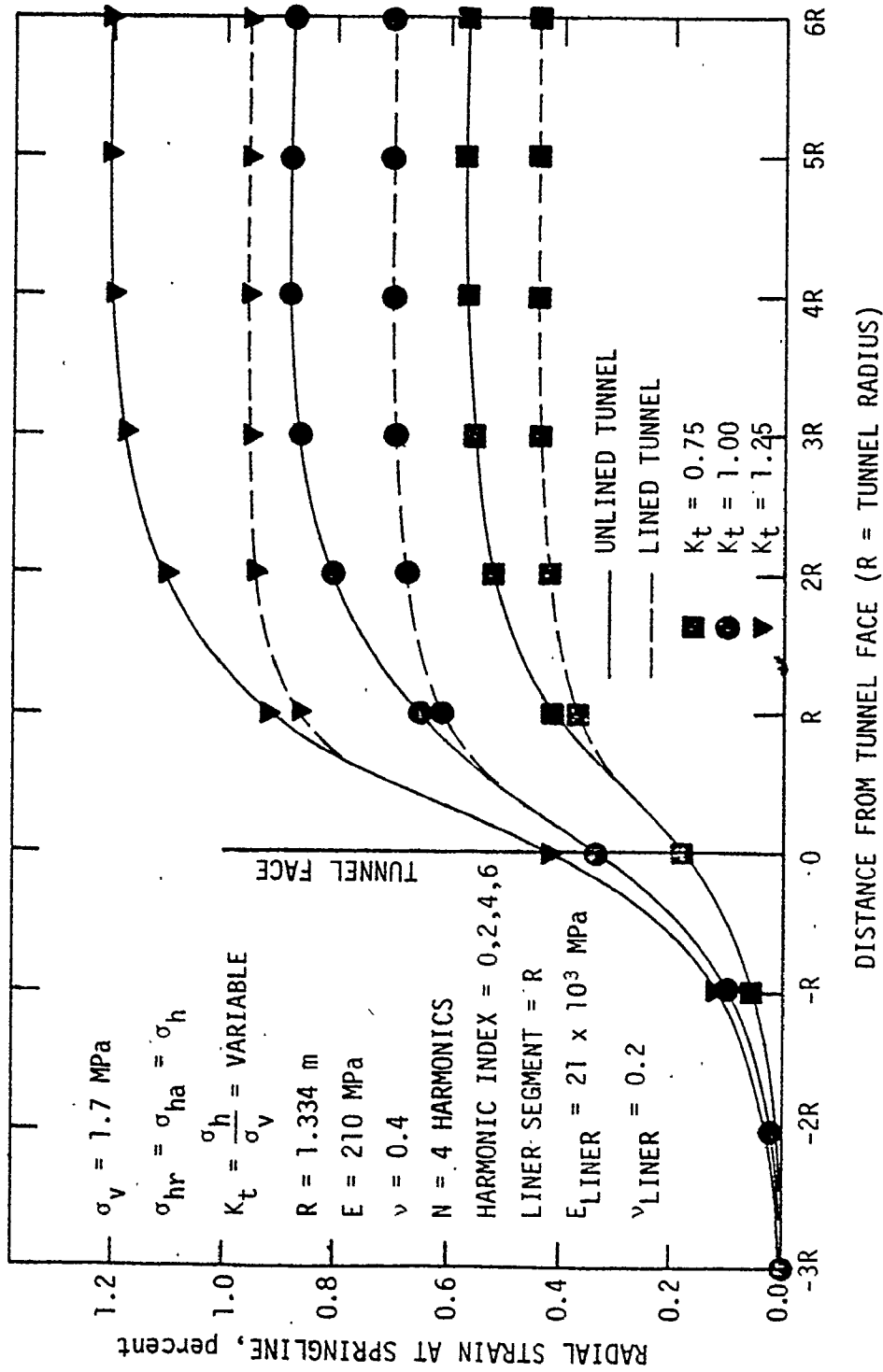
FIGURE 5.3   RADIAL ELASTIC STRAIN AT SPRINGLINE NEAR THE TUNNEL FACE FOR
VARIOUS TRANSVERSE (LATERAL) STRESS RATIO K_t, UNLINED AND
LINED CASES

'conservative' stresses are well within the allowable range for the 41 MPa compressive strength precast concrete segmental liner involved. A comparison of these results with the results given in Table 4.8 obtained for the plane strain analyses for sections with a soft backing, it can be concluded that the soft backing both reduces the liner stresses and gives uniform stresses.

5.4 EFFECT OF FACE ADVANCEMENT RATE ON TUNNEL CONVERGENCE

To demonstrate the effect of face advancement rate on tunnel convergence, five cases were simulated in which the rate of advance was varied. Since a reasonable advance rate for a medium size tunnel construc-in squeezing ground might be one to two tunnel diameters (2 to 4R) per 8 hour shift, the rate was assumed to be 2R per 1,2,8 and 12 hours for each excavation step. In these simulations, the face was advanced to represent actual tunnel construction practice, i.e. advancement in discrete rounds during which the face is advanced very quickly during the shift and then left stationary for a period of time during liner placement and shift changes/maintenance. The advance rate is defined as the distance advanced divided by the stationary time. A fifth case representing a continuous excavation operation without stationary times was also considered to give the limiting advance rate case. The results from these analyses are given in Figure 5.4. They show that decreasing the rate of advance in squeezing ground leads to increased tunnel wall convergence by the end of excavation. It can also be seen that the radial strains for an advance rate of 2R per 2 hours are about twice those for the quick excavation operation for the example problem considered.
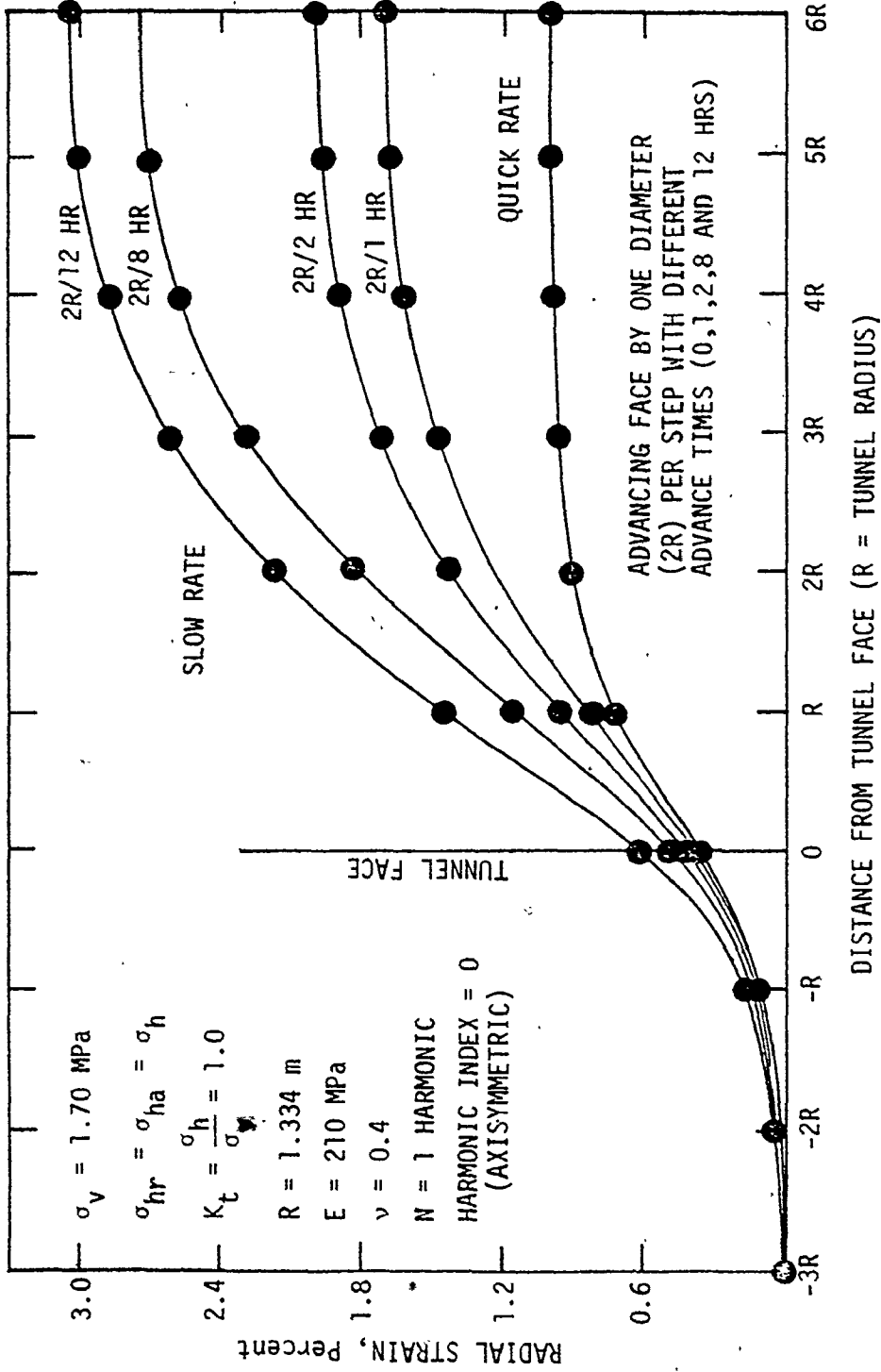
FIGURE 5.4   EFFECT OF THE FACE ADVANCEMENT RATE ON THE TUNNEL CONVERGENCE - COMPARED AT THE END OF EXCAVATION (6R)

To show the effect of the time-delay following excavation for various advancement rates, creep analyses were completed for the previous five cases. A total elapsed time of 3 days following the start of excavation was assumed. In all of these cases, the tunnel section was kept completely unsupported. The resulting radial strains are shown in Figure 5.5 for the different excavation rates. The information summarized in the figures indicates that the previous conclusion that a decrease in advance rate leads to an increase in the tunnel wall convergence is still valid, even with such a time delay. But, it can also be seen that the time delay reduces the wide range in convergence due to the face advance rate, i.e. increasing the unsupported time delay following excavation increases the convergence, and reduces the advantage of high advance rates in reducing tunnel convergence.

5.5 GENERAL ELASTIC-PLASTIC-CREEP ANALYSIS CASES

In order to demonstrate more fully the effect of the transverse stress ratio, K_ℓ, on the tunnel wall convergence and liner stresses, a complete elastic-plastic-creep analysis was performed using the axisymmetric approach for the same tunnel section previously described. Three cases were considered with different initial stress conditions. The vertical overburden stress was taken to be 1.70 MPa with transverse stress ratios of 0.75, 1.0 and 1.25, and an axial stress ratio of 1.0, i.e. horizontal principal stress components assumed to be equal for the three cases. In these cases, the incremental excavation operation was simulated as shown in Figure 3.10, with excavation steps of R. Following excavation of a 6R tunnel section length, a stationary time of 3 hours was allowed in order
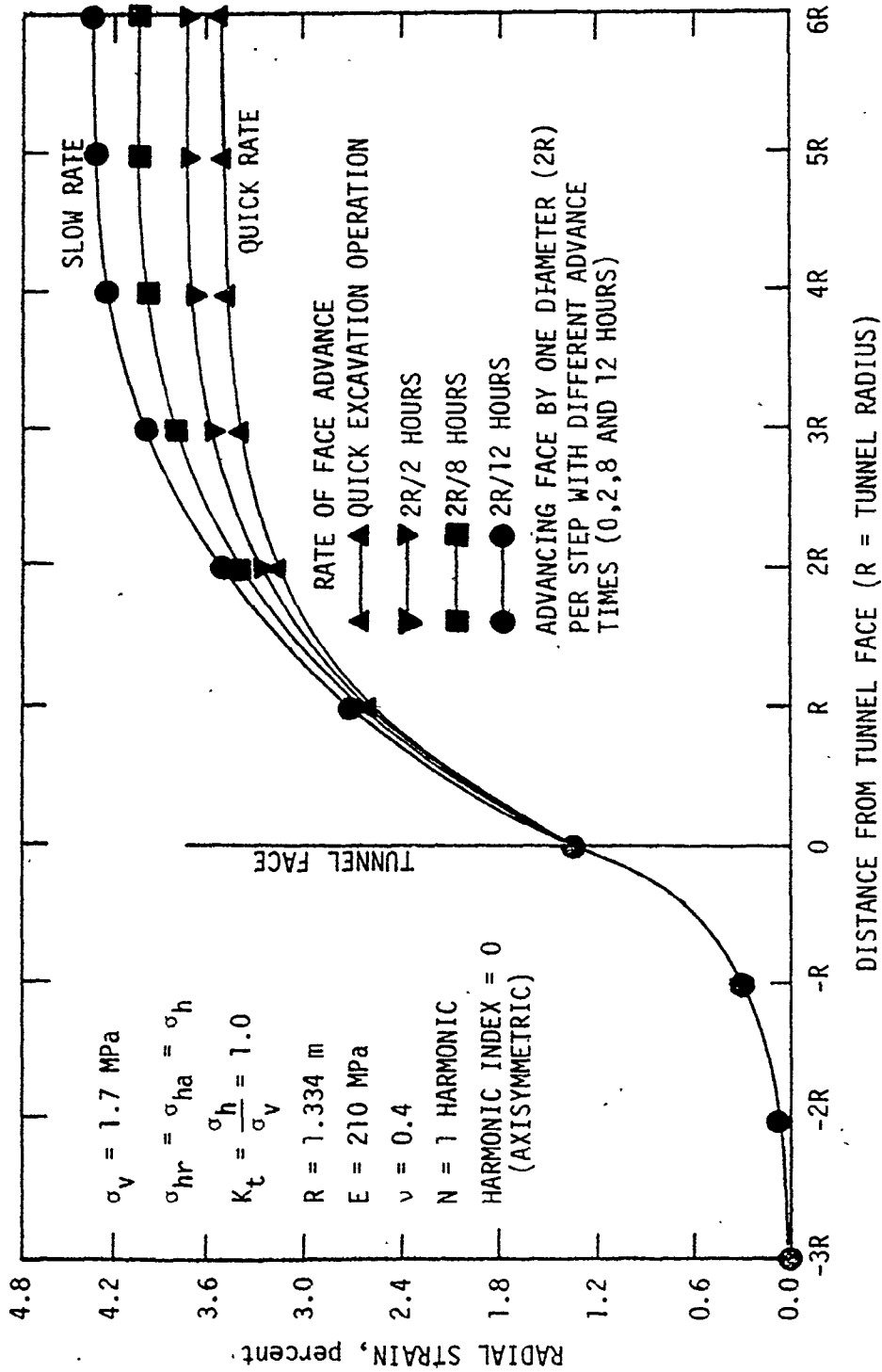
FIGURE 5.5   EFFECT OF THE FACE ADVANCEMENT RATE ON THE TUNNEL
CONVERGENCE – COMPARED AT THE EQUAL ELAPSED TIME
OF THREE DAYS SINCE EXCAVATION STARTED

to simulate a rate of face advancement and excavation of approximately one diameter per hour. Following this 3 hours, during which creep occurred, liner installation for the total excavated 6R was simulated. This liner was assumed to be a precast concrete segmental liner with no soft backing in order to obtain the maximum stress developed in the liner. The creep analysis was then continued for 10 hours to show the effect of the time-delay on the liner stresses and on the inward displacements, and to compare these results with those predicted for the unlined section. These results are shown for both the tunnel wall convergence and lining stresses in Figures 5.6, 5.7 and 5.8.

Figures 5.6 and 5.7 give the total elastic-plastic-creep radial strains along the tunnel wall which were plotted for both the case of support placement after 10 hours time delay, as well as for the unsupported tunnel following excavation completion. For the unsupported tunnel section, yielding occurred at the wall-face corner at every excavation step while the face was advancing. This indicates the position of high stress concentrations anticipated during design. While yielding was minor for K_t equal to 1, it was of larger extent for the case of K_t equal to 0.75 and 1.25. As previously mentioned, due to the creep response, there is a continuous adjustment of the stresses around the opening as the stresses move towards a uniform radial condition. For this reason, and since a time-delay following each excavation stage was allowed, the stresses in the few yielding elements were reduced, and the yielding was eliminated. After liner placement, and tunnel section support placement, the radial strains stopped increasing as shown in Figures 5.6 and 5.7. The lining compressive

151

FIGURE 5.6 RADIAL ELASTIC-PLASTIC-CREEP STRAIN AT CROWN NEAR THE TUNNEL FACE FOR VARIOUS TRANSVERSE (LATERAL) STRESS RATIO K_t - UNLINED AND LINED CASES
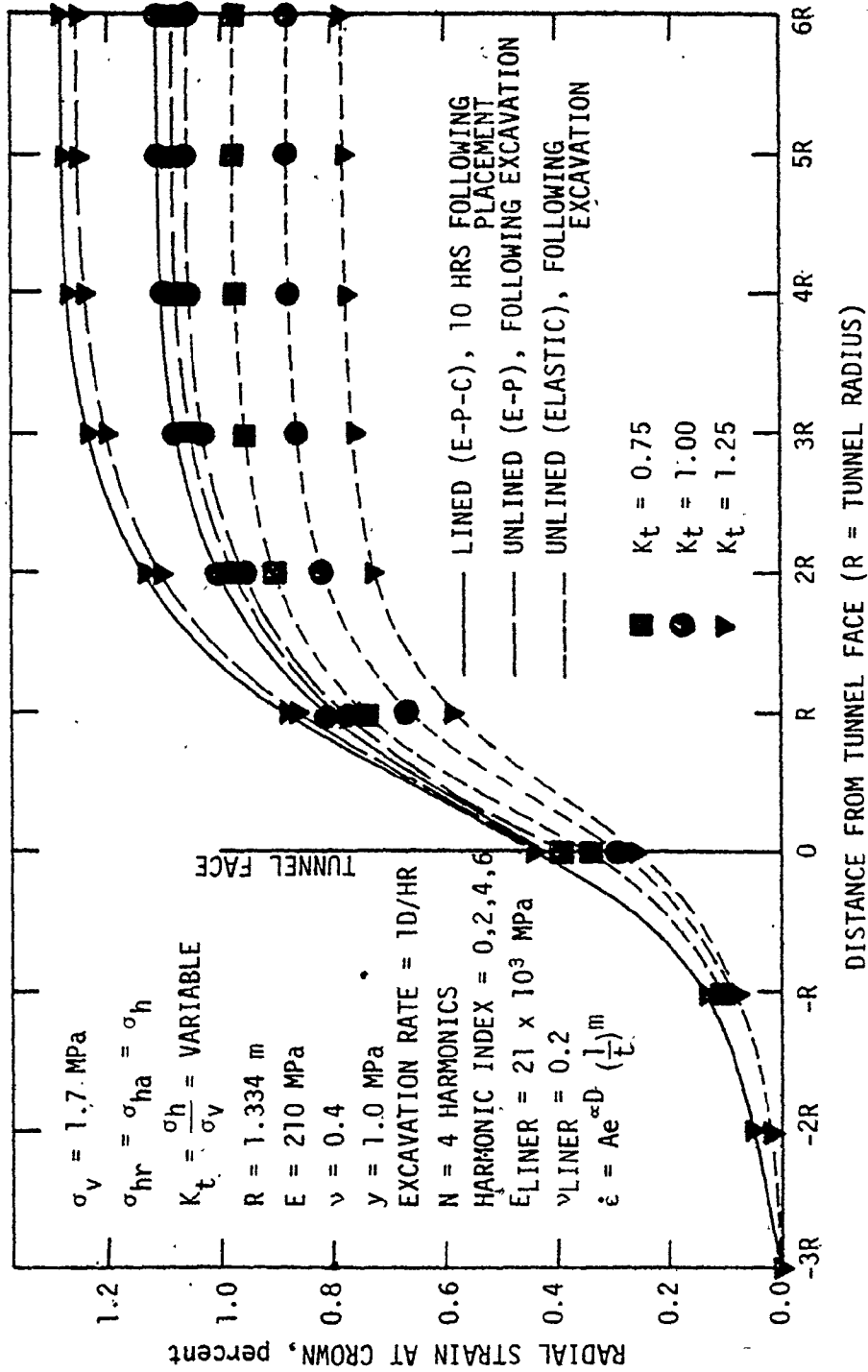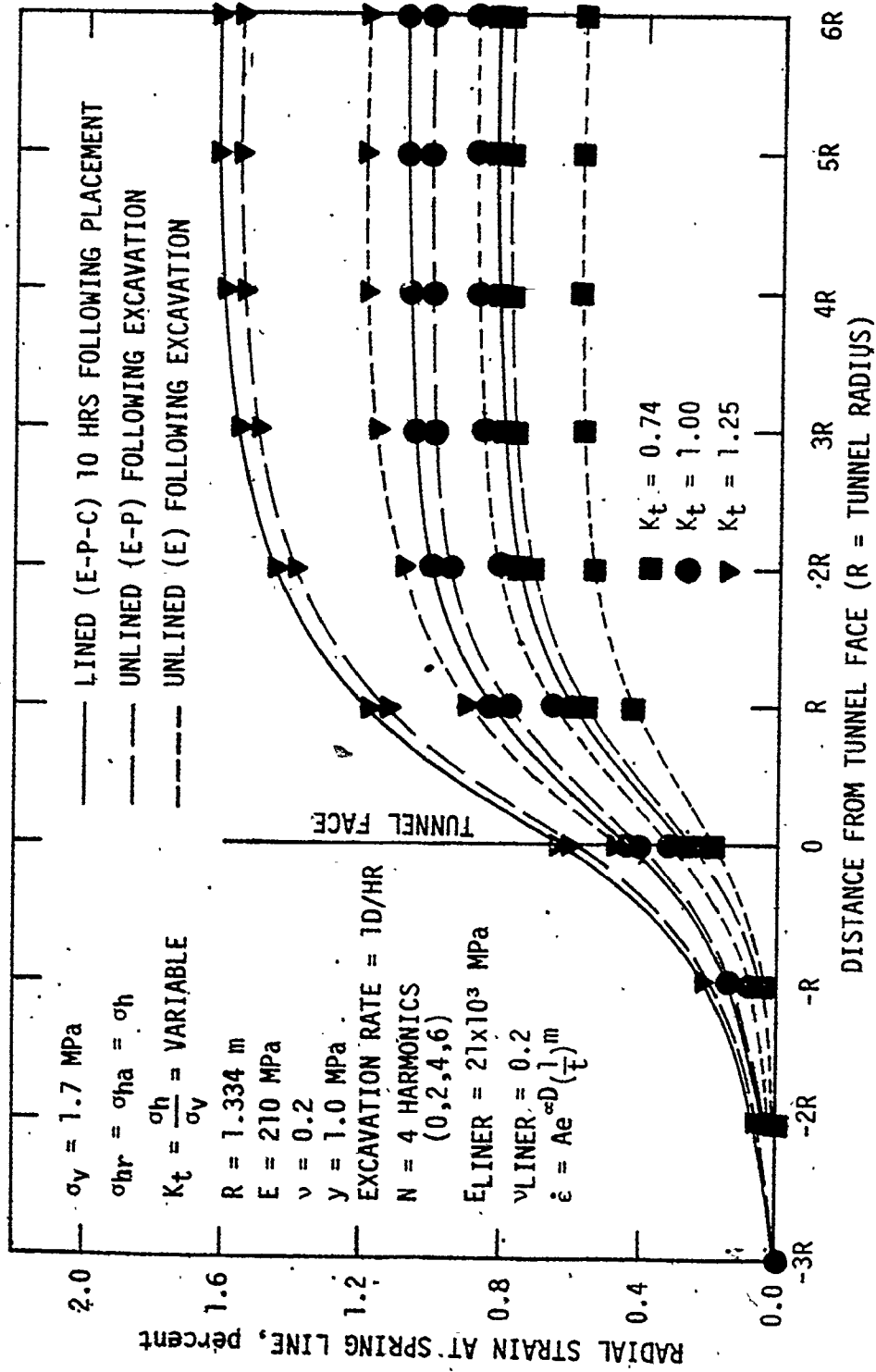
FIGURE 5.7   RADIAL ELASTIC-PLASTIC-CREEP STRAIN AT SPRING LINE NEAR THE TUNNEL FACE FOR VARIOUS TRANSVERSE (LATERAL) STRESS RATIO K_t — UNLINED AND LINED CASES
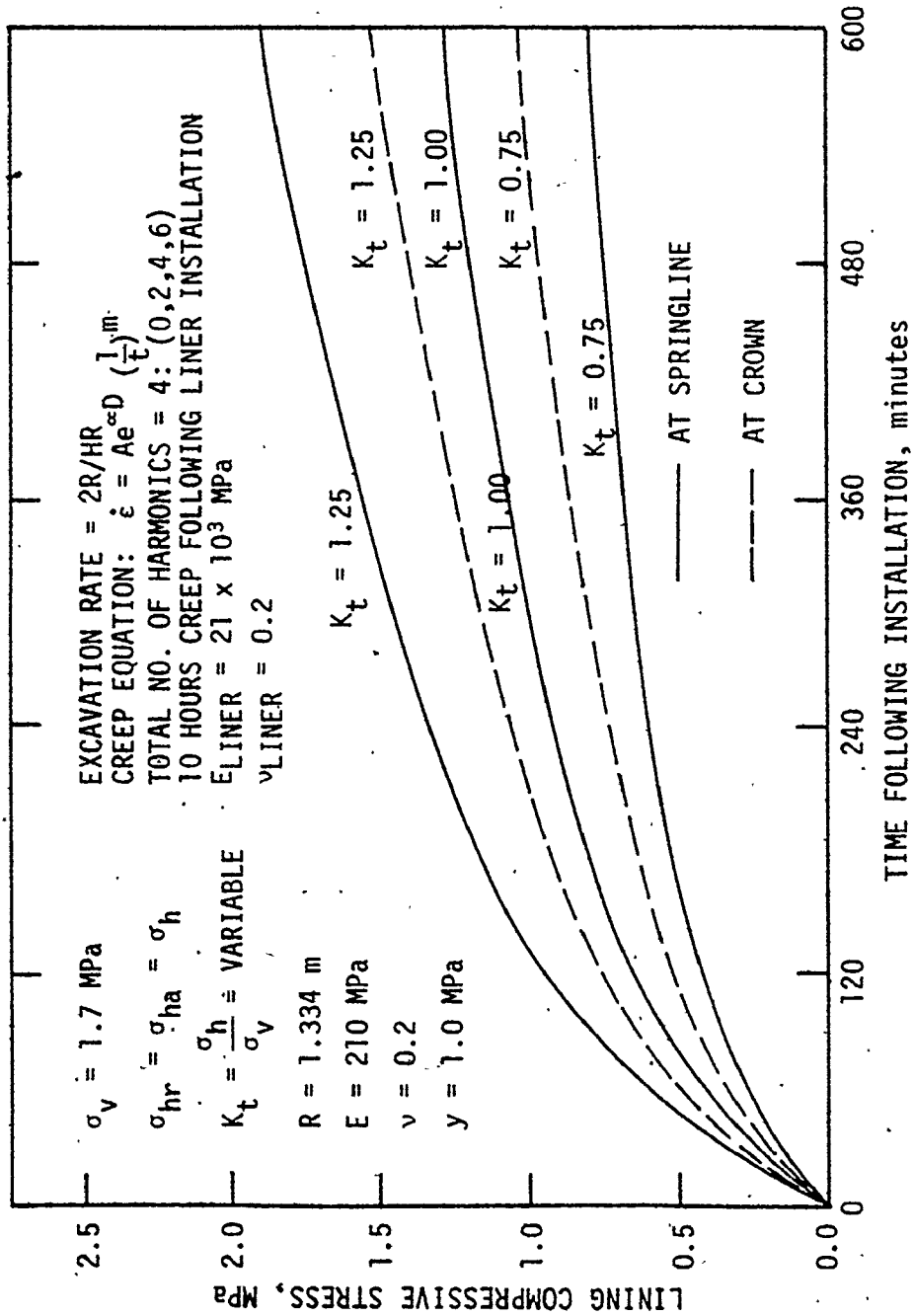
FIGURE 5.8   LINING STRESSES WITH TIME FOLLOWING INSTALLATION –
SPRINGLINE AND CROWN

stresses due to ground squeeze increased with time, but at a decreasing rate that eventually stabilizes as shown in Figure 5.8.

CHAPTER 6

SUMMARY, CONCLUSIONS, AND RECOMMENDATIONS FOR FURTHER RESEARCH AND DEVELOPMENT

6.1 SUMMARY

Empirical, analytical, and semi-rational design methods for analy-
zing the stability of underground openings and designing their support
systems are not adequate to consider the majority of the required stability
and design parameters for tunnels constructed in squeezing ground conditions.
Semi-rational design methods, which are widely used in practice, do not
necessarily distinguish conservative work, or even perhaps unsatisfactory
practice. They take no account of the fact that the support system can be
both satisfactory and unsatisfactory in the same ground condition, depend-
ing on the construction procedures. For squeezing ground conditions, the
support system can be damaged if adequate design provisions such as liner
placement delay or soft backings are not made. Several examples of such
failures and damage are well known in Southern Ontario.

A general procedure that takes into account most of the parameters
involved with the design of excavations in squeezing ground, such as ground
condition and mechanical properties, primary state of stress and high
lateral stress conditions, excavation-support construction sequences and
progressive interaction, construction procedures and new construction
methods, such as precast concrete segmental liners, three-dimensional
effects near the advancing face, and the elastic-plastic-creep behaviour

of the ground as excavation progresses, is not currently available.

The prime objective of this study was to develop a general method of analysis to be used in practice as a design proeedure for underground openings taking into account most of these design parameters. The finite element method was adopted to develop the necessary excavation and liner placement plane strain and axisymmetric simulations. The incremental approach was also adopted to simulate the construction sequences of excavation and support placement. Incorporation of inelastic behaviour for both ground yielding and time-dependent deformations was based on the initial stress and initial strain methods, respectively. The general three-dimensional stress analysis for anisotropic in situ stress field conditions was also formulated using an axisymmetric approach and Fourier series expansions. This axisymmetric approach was also extended to include inelastic behaviour.

Typical problems were analyzed using both the two-dimensional (plane strain) and three-dimensional (axisymmetric) stress methods with emphasis on the advantages and limitations of each simualtion technique. The results were reported in a tabular and graphical format to be useful for design purposes. Several parametric studies were also involved.

In order to improve the simulations and their applicability to support system design, incorporation of creep properties based on testing the actual material are considered essential. Field stress and displacement monitoring during and after construction to confirm and improve the predicted values is also considered important. On the other hand, a number

of projects are currently in progress that provide an opportunity for back

analysis in order to assess the characteristics of the ground and in situ

stresses, and to check the validity of the simulation methods.

6.2 CONCLUSIONS

The availability of large computers allows numerical techniques,

such as the finite element method simulation of tunnelling developed in

this study, to be applied to a wide range of geotechnology problems in

order to determine displacements and stresses.for design purposes. The

methods developed can be generally applied to underground excavations to

simulate the major steps in excavation and support system placement. Such

stress analyses can be regularly used to determine both ground and support

system displacements and stresses during and after excavation and support

construction sequences. This was done by simulation of excavation and

support placement in stages, as well as ground yielding and time-dependent

behaviour. The ground-support system interaction, which plays an import-

ant role in udnerground constructions, is simulated as closely as possible

to the actual conditions. In the study, these stress analyses can be

performed near the advancing face as well as at plane strain sections

(i.e. far from the tunnel face).

The two-dimensional plane strain and three-dimensional longitudinal

sections are two cases which have been presented for the analysis of

underground excavations. For both of them, an attempt was made to simulate

the mechanics of the interactive nature of the problem and emphasis was

·put on the development of methods that take into account the construction

sequences influencing the progressive interaction between them. This required simulation of both time-independent ground yielding and time-dependent creep behaviour. The techniques used were consistent with the finite element formulation.

Since tunnelling through squeezing ground is one of the most troublesome and least understood areas in underground construction, the simulation methods presented were used to gain some information on in situ stress influences to advance the design state-of-the-art for tunnelling in squeezing ground. This information, while requiring extension, if implemented should allow for more effective and economic design and construction procedures.

On the basis of the study, the following points can be summarized:

1. Excellent agreement was found between the finite element results and closed form solutions.

2. Results from the incremental simulation of single and multi-step excavations for linear elastic materials were identical as expected for the same loading and boundary conditions.

3. The excavation and support placement simulations and the idealization of both ground yielding and creep behaviour adopted, are suitable for predicting ground behaviour during all phases of excavations and support placements.

4. Since incremental techniques were adopted throughout, nonlinear constitutive relationships for both yielding and creep analyses

could be modelled using the initial stress and initial strain methods, respectively.

5. The simulation methods developed can be used in conjunction with field monitoring to predict the actual initial insitu stress conditions and creep properties of the materials involved.

6. There are many problems in geotechnology where the simulation methods can be applied. One application, for example, is the stabilization of underground openings by grouting. The finite element method program developed for both plane strain and axisymmetric analyses can be used without any additional modifications to study grout stabilized tunnels. Problems such as groundwater inflow, loss of ground and surface settlements, time-dependent creep response and reduced support thickness are usually associated with tunnelling. Injection of stabilizers is now used to minimize such problems for pervious soil and weathered rock. Stress analyses can be completed to determine the influence of different sizes and strengths of grouted zones on surface settlements or tunnel convergence.

Based on the analyses and results presented throughout this study, the following conclusions concerning tunnelling through squeezing ground can be made:

1. There is stress relief due to tunnelling as an instantaneous response. In squeezing ground, this stress relief will continue for several months, or more, depending upon the strength and deformation

characteristics of the ground. Such stress relief can be monitored during construction to check the simulation results.

2. In order to allow this stress relief to occur without damaging any support system, some radial deformations must be allowed to occur. Such radial deformations can be accommodated by a time-delay before the support system is installed, and/or by a flexible support system which allow for the rest of the required deformations, but prevent loosening as much as possible. This normally can be done in practice by leaving a suitable gap or installing a soft backing between the ground and support system, and/or by leaving narrow longitudinal gaps or packing between the support system segments.

3. The stresses developed in the support system, if installed as suggested above, will build up gradually and be kept to a minimum. Such support systems will also tend to be more economic than mono-lithic systems.

4. If it is intended to only permit small deformations (i.e. not sufficient time-delay, no soft backing, and/or no gap or packing) the stresses in any support system will increase dramatically and may result in rapid failure. On the other hand, sufficient support must be provided to avoid ground failure.

5. It was found in three-dimensional (axisymmetric) simulations that the pre-excavation longitudinal in situ stress component has a great effect on the convergence values. It was shown that with

increasing longitudinal stress ratio K_ℓ, the convergence increases. It was also found that increasing face advancement rate for tunnels constructed in squeezing ground resulted in decreased tunnel convergence by the end of the excavation period.

Finally, it would appear that the simulation methods are fully suited for application to practical geotechnical design work where reliable predictions of ground deformations and support stresses during excavation and construction are required. It is also important to mention that the reliability of any deformation and stress predictions based on numerical analyses is largely a function of the adequacy of the input data (initial state of stress and ground characteristics) and a realistic representation of the excavation and construction procedures. The computer has not replaced the significant engineering judgement required at all stages of tunnel design, as changed conditions are almost the rule during tunnelling.

6.3 FURTHER RESEARCH AND DEVELOPMENT

Distinct possibilities for development, improvement and refinement exist for continuing the study. Necessary further research and development includes:

1. Incorporation of orthotropic material properties into the analysis to include bedding effects.

2. Incorporation of pore water pressure effects into the analysis of excavations.

3. Incorporation of more realistic idealizations, such as improved strain-hardening laws, for the material behaviour.

Also, there are potential improvements and refinements of the present simulation methods such as:

1. Adopting an implicit scheme for the nonlinear plastic and creep analysis rather than the explicit scheme to give better efficiency in the iterations.

2. Using a refined element such as an isoparametric element rather than the constant strain element. This will reduce the number of elements and computer capacity required to achieve the same accuracy.

The axisymmetric approach used for the advancing tunnel face simulation is restricted to the simple geometry of circular openings and simulation of full-face excavations. Fortunately, this is often the case in tunnelling. If a different case is requried, a full three-dimensional stress analysis will be needed. This requires the development of an efficient three-dimensional finite element method simulation to allow the consideration of realistic problems with computers of the size generally available to designers.

These areas, as well as several suggested throughout the study, appear to be logical extensions for future work.

BIBLIOGRAPHY

Afrouz, A. and Harvey, J.M., 1974. "Rheology of Rocks Within the Soft to Medium Strength Range", Int. J. Rock Mech. Min. Sci., Vol. 11, No. 7, pp. 281-290.

Bishop, A.W., and Lovenbury, H.T., 1969. "Creep Characteristics of Two Undisturbed Clays", Proc. 7th Int. Conf. Soil Mech. Found. Eng., Vol. 1, pp. 29-37.

Boresi, A.P. and Deere, D.U., 1963. "Creep Closure of a Spherical Cavity in an Infinite Medium, with Special Application to Project Dribble, Tatum Salt Dome, Mississippi", for Holmes Narver Inc., Las Vegas Division.

Brebbia, C.A. and Conner, J., 1974. Fundamental of Finite Element Techniques for Structural Engineers, John Wiley and Sons Inc., New York.

Brown, E.T. and Hoek, E., 1978. "Trends in Relationships between Measured In-Situ Stresses and Depth", Int. J. Rock Mech. Min. Sci. and Geomech. Abstr., Vol. 15, No. 4, pp. 211-215.

Christian, J.T. and Wong, I.H., 1973. "Errors in Simulating Excavation in Elastic Media by Finite Elements", Soils and Foundations, Vol. 13, No. 1, March, pp. 1-10.

Clough, G.W. and Duncan, J.M., 1969. "Finite Element Analyses of Port Allen and Old River Locks", Contract Report S-69-6, U.S. Army Engineer Waterways Experiment Station, Corps of Engineers, Vicksburg, Mississippi.

Clough, G.W. and Mana, A.I., 1976. "Lessons Learned in Finite Element Analyses of Temporary Excavations in Soft Clay", Proc. 2nd Int. Conf. on Numerical Methods in Geomechanics, Blacksburg, Virginia, Vol. 1, pp. 596-510.

Conte, S.D. and Boor, C., 1972. Elementary Numerical Analysis, An Alogorithmic Approach, McGraw Hill Company, Toronto.

Daemen, J.J., 1975. "Tunnel Support Loading Caused by Rock Failure", Ph.D. Thesis, University of Minesota.

Dahlquist, G. and Bjorck, A., 1974. Numerical Methods, Translated by Anderson, N., Prentice-Hall Inc., Englewood Cliffs, New Jersey.

Davis, E.H., 1968. "Theory of Plasticity and the Failure of Soil Masses", Soil Mechanics: Selected Topics, Edited by I.L. Lee, pp. 341-380.

Deere, D.U., Peck, R.B., Monsees, J.E. and Schmidt, B., 1969. "Design of Tunnel Liners and Support Systems". University of Illinois, Report for Office of High Speed Ground Transportation, U.S. Department of Transportation.

Desai, C.S. and Abel, J.F., 1972. Introduction to the Finite Element Method, Van Nostrand Reinhold Company, New York.

Descoeudres, F., 1974. "Three-Dimensional Analysis of Tunnel Stability Near the Face in an Elasto-Plastic Rock", Advances in Rock Mechantics, Proceedings of the Third Congress of the Int. Soci. Rock Mech., Denver, Vol. II, pp. 1130-1135.

Donath, F.A., 1970. "Some Information Squeezed out of Rock", American Scientist, Vol. 58, No. 1, pp. 54-72.

Drucker, D.C. and Prager, W., 1952. "Soil Mechanics and Plastic Analysis or Limit Design", Q.J. Appl. Math., Vol. 10, No. 2, pp. 157-165.

Egger, P., 1974. "Underground Openings - Principles of Design", A Lecture in Rock Mechanics, Edited by M. Müller, Springer-Verlag Wien, New York, pp. 283-297.

Einstein, H.H. and Schwartz, C.W., 1978. "Improvement of Ground Support Performance by Full Consideration of Ground Displacements", Draft of Paper for Tunnelling and Underground Structures Symposium, TRB Meeting.

Eisenstein, Z. and Morrison, N.A., 1973. "Prediction of Foundation Deformations in Edmonton Using an In Situ Pressure Probe", Canadian Geotechnical Journal, Vol. 10, pp. 139-210.

Emery, J.J., 1971. "Finite Element Analysis of Creep Problems in Soil Mechanics", Ph.D. Thesis, University of British Columbia.

Emery, J.J., 1978. "Simulation of Slope Creep", Rockslides and Avalanches, Vol. 1, Natural Phenonema, Edited by B. Voight, pp. 669-691, Developments in Geotechnical Engineering, 14A, Elsevier, Amsterdam.

Fairhurst, C., 1979. "Improved Tunnel Support Design Possibilities Using 'Characteristic-Lines' Approach Discussed in AFTES Symposium (Paris)", Underground Space, Vol. 3, No. 4, pp. 207-217.

Farmer, I.W., 1968. Engineering Properties of Rocks, Spon, London.

Florence, A.L. and Schwer, L.E., 1978. "Axisymmetric Compression of a Mohr-Coulomb Medium Around a Circular Hole", Int. J. Numerical and Analytical Methods in Geomechanics, Vol. 2, No. 4, pp. 367-379.

Franklin, J.A. and Hungr, O., 1978. "Rock Stresses in Canada; Their Relevance to Engineering Projects", Rock Mechanics, Suppl. 6, pp. 24-46.

Franklin-Trow Associates Ltd., Rock Engineering Consultants, 1978. "Supplementary Study Easterly Filtration Plant Intank Tunnel, Scarborough, Ontario", Personal Communication, Rexdale, Ontario.

Fung, Y.C., 1965. Foundations of Solid Mechanics, Prentice-Hall Inc., New Jersey.

Goodman, R.E., Taylor, R.L. and Brekke, J.L., 1963. "A Model for the Mechanics of Jointed Rock", J. Soil Mech. Found. Div., ASCE, Vol. 94, No. SM3, Proc. Paper 5937, May, pp. 637-659.

Greenbaum, G.A., 1966. "Creep Analysis of Axisymmetric Bodies", Ph.D. Thesis, University of California, Los Angeles.

Hanafy, E.A., 1976. "Finite Element Simulation of Tunnel Excavations in Creeping Rock", M. Eng. Thesis, McMaster University, Hamilton, Ontario.

Herget, G., 1974. "Ground Stress Determination in Canada", Rock Mechanics, Vol. 6, pp. 53-64.

Hill, R., 1950. The Mathematical Theory of Plasticity, Clarendon Press, Oxford.

Hirst, T.J. and Mitchell, J.K., 1968. "Compositional and Environmental Influences on the Stress-Strain-Time Behaviour of Soils", Report No. TE-68-4, Department of Civil Eng., Institute of Transportation and Traffic Eng., University of California, Berkeley.

Hobbs, D.W., 1970. "Stress-Strain-Time Behaviour of a Number of Coal Measure Rocks", Int. J. Rock Mech. Min. Sci., Vol. 7, pp. 149-170.

Hocking, G., 1976. "Three-Dimensional Elastic Stress Distribution Around the Flat End of a Cylindrical Cavity", Int. J. Rock Mech. Min. Sci., Vol. 13, No. 12, pp. 331-337.

Hocking, G., Brown, E.T. and Watson, J.O., 1976. "Three-Dimensional Elastic Stress Analysis of Underground Openings by the Boundary Integral Equation Method", Proc. 3rd Symp. Eng. Applications of Solid Mechanics, University of Toronto, June, pp. 203-217.

Jaeger, J.C. and Cook, N.G.W., 1976. Fundamentals of Rock Mechanics, John Wiley and Sons Inc., New York.

Krenk, S., 1978. "Internally Pressurized Spherical and Cylindrical Cavities in Rock Salt", Int. J. Rock Mech. Min. Sci. and Geomech. Abstr., Vol. 15, No. 5, pp. 219-224.

Kulhawy, F.H., 1974. "Finite Element Modelling Criteria for Underground Openings in Rock", Int. J. Rock. Mech. Min. Sci., Vol. 11, No. 12, pp. 465-472.

Ladanyi, B., 1976. "Quasi-Static Expansion of a Cylindrical Cavity in Rock", Proc. 3rd Symp. Eng. Applications of Solid Mechanics, University of Toronto, June, pp. 219-240.

Lane, K.S., 1975. "Field Test Sections Save Cost in Tunnel Support", Report from Underground Construction Research Council, ASCE, October.

Lee, C.F. and Lo, K.Y., 1976. "Rock Squeeze Study of Two Deep Excavations at Niagara Falls", Proc. Conf. Rock Engineering for Foundations and Slopes, University of Colorado, August 16-18.

Lo, K.Y. and Morton, J.D., 1976. "Tunnels in Bedded Rock with High Horizontal Stresses", Can. Geotechn. J., Vol. 13, No. 3, pp. 216-230.

Lombardi, G.A., 1973. "Dimensioning of Tunnel Lining with Regard to Constructional Procedure", Tunnels and Tunneling, Vol. 5, No. 4, July, pp. 340-351.

Lombardi, G.A., 1974. "Tunnel Support", Advances in Rock Mechanics, Proceedings of the Third Congress of the Int. Soci. Rock Mech., Denver, Vol. I, pp. 1518-1529.

Love, A.E.H., 1927. The Mathematical Theory of Elasticity, University Press, Cambridge.

Lubahn, J.D. and Felgar, R.P., 1961. Plasticity and Creep of Metals, John Wiley and Sons Inc., New York.

Marcal, P.V. and King, I.P., 1967. "Elastic-Plastic Analysis of Two Dimensional Stress System by the Finite Element Method", Int. J. Mech. Sci., Vol. 9, pp. 143-155.

Meek, J.L., 1973. "Excavation in Rock; An Application of the Finite Element Method of Analysis", Proceedings of the Tokyo Seminar on Finite Element Analysis, University of Tokyo Press, Tokyo, pp. 195-213.

Meissner, H.E., "Laterally Loaded Pipe Pile in Cohesionless Soil", in Numerical Methods in Geomechanics, Vol. 3, Edited by C.S. Desai, 1976, pp. 1353-1365.

Mendelson, A., 1970. Plasticity: Theory and Application, MacMillan Company, New York.

Mroz, Z., 1963. "Non-Associated Flow Laws in Plasticity", J. de Mechanique, Vol. 2, No. 1, pp. 42-63.

Myer, L.R., Brekke, T.L., Korbin, G.E., Kavazanjian, E. and Mitchell, J.K., 1977. "Stand-up Time of Tunnels in Squeezing Ground - Part I: Physical Model Study", Report No. DOT-TST-77-59, Department of Civil Eng., University of California, Berkeley; June.

Nair, G.P., 1975. "Response of Soil-Pile Systems to Seismic Waves", Ph.D. Thesis, McMaster University, Hamilton, Ontario.

Obert, L. and Duvall, W.I., 1967. Rock Mechanics and the Design of Structures in Rocks, John Wiley and Sons Inc., New York.

Pariseau, W.G., 1972. "Discussion on Papers by Gates, Chang, et al., and Lu and Scott", Proc. Applications of the Finite Element Method in Geotech. Eng., U.S. Army Eng. Waterways Exp. Stat. Vicksburg, Miss., Sept., pp. 1223-1224.

Pariseau, W.G., Voight, B. and Dahl, H.D., 1970. "Finite Element Analyses of Elastic-Plastic Problems in the Mechanics of Geologic. Media: An Overview", Proc. 2nd Int. Soc. Rock Mech., Beograd, Vol. 2, pp. 311-323.

Peck, R.B., 1969. "Deep Excavations and Tunnelling in Soft Ground", Proc. 7th Int. Conf. Soil Mech. and Found. Eng., Mexico City, State-of-the-Art Volume, pp. 225-290.

Peck, R.B., Hendron, A.J. and Mohraz, B., 1972. "State of the ARt of Soft Ground Tunnelling", Proc. North America Rapid Excavation and Tunnelling Conf., Chicago, P. 259. Published by AIME, Lane and Garfield, Editors.

Prager, W. and Hodge, P.G., 1951. Theory of Perfectly Plastic Solids, John Wiley and Sons Inc., New York.

Rabcewicz, L.V., 1964. "The New Austrian Tunnelling Method", Water Power, Nov., pp. 453-457, December, pp. 511-516, and Jan. 1965, pp. 19-25.

Reyes, S.F. and Deere, D.U., 1966. "Elasto-Plastic Analysis of Underground Opening by the Finite Element Method", Proc. 1st Int. Cong. Rock Mech., Vol. 3, Lisbon.

Robertson, E.C., 1963. "Viscoelasticity of Rocks", Int. Conf. on the State of Stress in the Earth's Crust, Santa Monica, California, May, pp. 181-220.

R.V. Anderson Associates Limited, Consulting Engineers and Planners, 1979. Geotechnical and Pre-Cast Segmental Lining Design Data, Personal Communications, January, Willowdale, Ontario.

Sakurai, S., 1978. "Approximate Time-Dependent Analysis of Tunnel Support Structure Considering Progress of Tunnel Face", Int. J. Numerical and Analytical Methods in Geomechanics, Vol. 2, No. 2, pp. 159-175.

Samuelson, L.A., "Creep Buckling of A Cylindrical Shell Under Non-Uniform External Loads", Int. J. Solids Structures, 1970, Vol. 6, pp. 91-116.

Sbar, M.L. and Sykes,L.R., 1973. "Contemporary Compressive Stress and Seismicity in Eastern North America, An Example of Intra-Plate Tectonics", Bulletin of the Geological Society of America, Vol. 84, pp. 1861-1882.

Shieh, W.Y.J. and Sandhu, R.S., 1970. "Application of Elastic-Plastic Analysis in Earth Structures", Proc. Nat. Meeting on Water Resources Eng., ASCE, Memphis, Tenn., January.

Singh, A. and Mitchell, J.K., 1968. "A General Stress-Stress-Time Function for Soils", J. Soil Mech. Found. Div., ASCE, Vol. 94, No. SM1, pp. 21-46.

Singh, A. and Mitchell, J.K., 1969. "Creep and Long-Term Strength of Soils Subjected to Variable Load", Proc. 7th Int. Conf. Soil Mech. and Found. Eng., Mexico City, Vol. 1, pp. 423-431.

Szechy, K., 1973. The Art of Tunnelling, Akadémiai Kiadó, Budapest.

Terzaghi, K., 1946. "Rock Defects and Loads on Tunnell Supports", in Rock Tunnelling with Steel Supports, by R.V. Proctor and T.L. White,. the Commercial Shearing and Stamping Co., Yongstown, Ohio.

Tunnelling Technology, 1976. An Appraisal of the State of the Art for Application to Transit Systems, The Ontario Ministry of Transportation and Communications, Ontario.

Ward, W.H., 1978. "Ground Supports for Tunnels in Weak Rocks", Geotechnique, Vol. 28, No. 2, pp. 133-171.

Wilson, E.L., 1965. "Structural Analysis of Axisymmetric Solids", AIAA Journal, pp. 2269-2274.

Wittke, W. and Pierau, B., 1976. "3-D Stability Analysis of Tunnels in Jointed Rock", The Second Int. Conf. Numerical Methods in Geomechanics, Virginia, Vol. III, pp. 1401-1418.

Yamada, Y., Yoshimura, N. and Sakurai, T., 1968. "Plastic Stress-Strain Matrix and its Application for the Solution of Elastic-Plastic Problems by the Finite Element Method", Int. J. Mech. Sci., Vol. 10, No. 5, pp. 343-354.

Zienkiewicz, O.C., 1968. "Continuum Mechanics as an Approach to Rock Mass Problems", Chapter 8 in Rock Mechanics in Engineering Practice, Edited by K.G. Stagg and O.C. Zienkiewicz, John Wiley and Sons Inc., New York.

Zienkiewicz, O.C., 1977. The Finite Element Method, McGraw-Hill Co., London.

Zienkiewicz, O.C. and Cormeau, I.C., 1974. "Visco-plasticity and Creep in Elastic Solids -- A Unified Numerical Solution Approach", Int. J. Numerical Methods in Engineering, Vol. 8, No. 4, pp. 821-845.

ELASTICITY AND PLASTICITY MATRICES

The general elasticity matrix, expressing the stress-strain relationship in which the material is assumed to be linear, isotropic, and elastic, is (Desai and Abel, 1972):

$$[D^E] = \frac{E}{(1+\nu)(1-2\nu)} \begin{bmatrix} 1-\nu & \nu & \nu & 0 & 0 & 0 \\ & 1-\nu & \nu & 0 & 0 & 0 \\ & & 1-\nu & 0 & 0 & 0 \\ & & & \frac{1-2\nu}{2} & 0 & 0 \\ & & & & \frac{1-2\nu}{2} & 0 \\ & & & & & \frac{1-2\nu}{2} \end{bmatrix} \quad (A.1)$$

where E is the modulus of elasticity and ν is the Poisson's ratio.

The general plasticity matrix $[D^P]$ adopting the von Mises yield criterion is (Desai and Abel, 1972):

$$[D^P] = C \begin{bmatrix} \sigma_{Dx}^2 & \sigma_{Dx}\sigma_{Dy} & \sigma_{Dx}\sigma_{Dz} & \sigma_{Dx}\tau_{xy} & \sigma_{Dx}\tau_{yz} & \sigma_{Dx}\tau_{zx} \\ & \sigma_{Dy}^2 & \sigma_{Dy}\sigma_{Dz} & \sigma_{Dy}\tau_{xy} & \sigma_{Dy}\tau_{yz} & \sigma_{Dy}\tau_{zx} \\ & & \sigma_{Dz}^2 & \sigma_{Dz}\tau_{xy} & \sigma_{Dz}\tau_{yz} & \sigma_{Dz}\tau_{zx} \\ \text{Symmetrical} & & & \tau_{xy}^2 & \tau_{xy}\tau_{yz} & \tau_{xy}\tau_{zx} \\ & & & & \tau_{yz}^2 & \tau_{yz}\tau_{zx} \\ & & & & & \tau_{zx}^2 \end{bmatrix} \quad (A.2)$$

in which:
$$C = \frac{2G}{\frac{2}{3}\sigma_e^2(1 + \frac{H'}{3G})}$$

where G is the shear modulus, σ_D are the deviatoric stress components and H' is the slope of the equivalent stress-equivalent strain curve (equal to zero for an elastic-perfectly plastic material). The term 'equivalent' is used instead of 'effective' to prevent any misunderstanding since the term 'effective' has a different, general meaning (i.e. intergranular stress) in geotechnology. With the von Mises yield criterion, the equivalent stress is:

$$\sigma_e = \frac{1}{\sqrt{2}}[(\sigma_1-\sigma_2)^2 + (\sigma_2-\sigma_3)^2 + (\sigma_3-\sigma_1)^2]^{\frac{1}{2}} \qquad (A.3)$$

and the equivalent strain is:

$$\varepsilon_e = \frac{\sqrt{2}}{3}[(\varepsilon_1-\varepsilon_2)^2 + (\varepsilon_2-\varepsilon_3)^2 + (\varepsilon_3-\varepsilon_1)^2]^{\frac{1}{2}} \qquad (A.4)$$

APPENDIX B

MATRICES AND INTEGRALS FOR ANALYSIS OF AXISYMMETRIC STRUCTURES

Some of the important matrices and axisymmetric integrals used in the analysis of axisymmetric structures under symmetric and nonsymmetric initial in situ stress conditions are given in this appendix.

B-1 MATRICES RELATING DISPLACEMENTS, STRAINS AND STRESSES

The matrices $[D^E]$, $[\bar{B}]$, $[C^{-1}]$, and $([\bar{B}]^T[D^E][\bar{B}])$ used in the axisymmetric structure analysis are defined as follows:

$[D^E]$ is the elasticity matrix defined in Appendix A.

$$[C]^{-1} = \frac{1}{|A|} \begin{bmatrix} (r_j z_k - r_k z_j) & (r_k z_i - r_i z_k) & (r_i z_j - r_j z_i) \\ (z_j - z_k) & (z_k - z_i) & (z_i - z_j) \\ (r_k - r_j) & (r_i - r_k) & (r_j - r_i) \end{bmatrix} \quad (B.1)$$

where $|A| = r_i(z_j - z_k) + r_j(z_k - z_i) + r_k(z_i - z_j)$

$$[\bar{B}] = \begin{bmatrix} 0 & 1 & 0 & 0 & 0 & 0 & 0 & 0 & 0 \\ 0 & 0 & 0 & 0 & 0 & 1 & 0 & 0 & 0 \\ \frac{1}{r} & 1 & \frac{z}{r} & 0 & 0 & 0 & \frac{n}{r} & n & \frac{nz}{r} \\ 0 & 0 & 1 & 0 & 1 & 0 & 0 & 0 & 0 \\ -\frac{n}{r} & -n & -\frac{nz}{r} & 0 & 0 & 0 & -\frac{1}{r} & 0 & -\frac{z}{r} \\ 0 & 0 & 0 & -\frac{n}{r} & -n & -\frac{nz}{r} & 0 & 0 & 1 \end{bmatrix} \tag{B.2}$$

where r and z are the nodal coordinates and n is the harmonic index.

NOTE: The matrix $[\bar{B}]$ given in Equation B.2 is applicable for symmetric modes only.

$$\{[\bar{B}]^T[D][\bar{B}]\} = \frac{\nu E}{(1+\nu)(1-2\nu)} \times$$

$$
\begin{bmatrix}
(m_1+m_2n^2)\dfrac{1}{r^2} & (\tfrac{1}{\nu}+m_2n^2)\dfrac{1}{r} & (m_1+m_2n^2)\dfrac{z}{r^2} & 0 & m_1\dfrac{n}{r} & (m_1+m_2)\dfrac{nz}{r^2} \\[8pt]
 & \dfrac{2}{\nu}+m_2n^2 & (\tfrac{1}{\nu}+m_2n^2)\dfrac{z}{r} & 0 & \dfrac{n}{\nu} & (\tfrac{1}{\nu}+m_2)\dfrac{nz}{r} \\[8pt]
 & & \dfrac{m_2^2+}{(m_1+m_2n^2)\dfrac{z^2}{r^2}} & m_2 & (m_1+m_2n^2)\dfrac{n}{r^2} & (m_1+m_2)\dfrac{nz}{r^2} \\[8pt]
 & & & m_2\dfrac{n^2}{r^2} & m_2\dfrac{n^2}{r} & -m_2\dfrac{n}{2r} \\[8pt]
 & & & & m_2(1+n^2) & -m_2\dot{n} \\[8pt]
 & & & & \left(m_1n^2+m_2\right)\dfrac{1}{r^2}\Big| & (1-m_1)\dfrac{nz}{r} \\[8pt]
 & & & & m_1\dfrac{n^2}{r} & (m_1n^2+m_2)\dfrac{z}{r^2} \\[8pt]
 & & & & m_1n^2 & m_1n^2\dfrac{z}{r} \\[8pt]
 & & & & & \dfrac{m_2+}{(m_1n^2+m_2)\dfrac{z^2}{r^2}}
\end{bmatrix}
$$

$$\text{(B.3)}$$

where ν = Poisson's ratio, n = harmonic index, $m_1 = (1-\nu)/\nu$ and $m_2 = (1-2\nu)/2\nu$

NOTE: The matrix given in Equation B.3 is applicable for symmetric modes only.

B-2 AXISYMMETRIC INTEGRALS

There are eight axisymmetric integrals λ_1 to λ_8 which are used in this analysis of axisymmetric structures. The expression for these integrals which are evaluated using Green's Lemma are as follows:

$$\lambda_1 = \iint r\,dr\,dz = -\oint rz\,dr = -\left[\frac{a_1}{2}(r_j^2 - r_i^2) + \frac{b_1}{3}(r_j^3 - r_i^3) + \frac{a_2}{2}(r_k^2 - r_j^2)\right.$$

$$\left. + \frac{b_2}{3}(r_k^3 - r_j^3) + \frac{a_3}{2}(r_i^2 - r_k^2) + \frac{b_3}{3}(r_i^3 - r_k^3)\right]$$

$$\lambda_2 = \iint dr\,dz = -\oint z\,dr = -\left[a_1(r_j - r_i) + \frac{b_1}{2}(r_j^2 - r_i^2) + a_2(r_k - r_j)\right.$$

$$\left. + \frac{b_2}{2}(r_k^2 - r_j^2) + a_3(r_i - r_k) + \frac{b_3}{2}(r_i^2 - r_k^2)\right]$$

$$\lambda_3 = \iint z\,dr\,dz = -\oint \frac{z^2}{2}\,dr = -\left[\frac{a_1^2}{2}(r_j - r_i) + \frac{a_1 b_1}{2}(r_j^2 - r_i^2)\right.$$

$$+ \frac{b_1^2}{6}(r_j^3 - r_i^3) + \frac{a_2^2}{2}(r_k - r_j) + \frac{a_2 b_2}{2}(r_k^2 - r_j^2)$$

$$+ \frac{b_2^2}{6}(r_k^3 - r_j^3) + \frac{a_3^2}{2}(r_i - r_k) + \frac{a_3 b_3}{2}(r_i^2 - r_k^2)$$

$$\left. + \frac{b_3^2}{6}(r_i^3 - r_k^3)\right]$$

$$\lambda_4 = \iint \frac{1}{r} \, dr dz = - \oint \frac{z}{r} \, dr = - \left[a_1 \ln(\frac{r_j}{r_i}) + b_1(r_j - r_i) + a_2 \ln(\frac{r_k}{r_j}) \right.$$

$$\left. + b_2(r_k - r_j) + a_3 \ln(\frac{r_i}{r_k}) + b_3(r_i - r_k) \right]$$

$$\lambda_5 = \iint \frac{z}{r} \, dr dz = - \oint \frac{z^2}{2r} \, dr = - \left[\frac{a_1^2}{2} \ln(\frac{r_j}{r_i}) + a_1 b_1(r_j - r_i) + \frac{b_1^2}{4}(r_j^2 - r_i^2) \right.$$

$$+ \frac{a_2^2}{2} \ln(\frac{r_k}{r_j}) + a_2 b_2(r_k - r_j) + \frac{b_2^2}{4}(r_k^2 - r_j^2)$$

$$\left. + \frac{a_3^2}{2} \ln(\frac{r_i}{r_k}) + a_3 b_3(r_i - r_k) + \frac{b_3^2}{4}(r_i^2 - r_k^2) \right]$$

$$\lambda_6 = \iint \frac{z^2}{r} \, dr dz = - \oint \frac{z^3}{3r} \, dr = - \left[\frac{a_1^3}{3} \ln(\frac{r_j}{r_i}) + a_1^2 b_1 \ (r_j - r_i) \right.$$

$$+ \frac{a_1 b_1^2}{2}(r_j^2 - r_i^2) + \frac{b_1^3}{9}(r_j^3 - r_i^3)$$

$$+ \frac{a_2^3}{3} \ln(\frac{r_k}{r_j}) + a_2^2 b_2 \ (r_k - r_j) + \frac{a_2 b_2^2}{2}$$

$$(r_k^2 - r_j^2) + \frac{b_2^3}{9}(r_k^3 - r_j^3) + \frac{a_3^3}{3} \ln$$

$$(\frac{r_i}{r_k}) + a_3^2 b_3 \ (r_i - r_k) + \frac{a_3 b_3^2}{2}(r_i^2 - r_k^2)$$

$$\left. + \frac{b_3^3}{9}(r_i^3 - r_k^3) \right]$$

$$\lambda_7 = \iint r^2\,drdz = -\oint r^2 z\,dr = -\left[\frac{a_1}{3}(r_j^3-r_i^3)+\frac{b_1}{4}(r_j^4-r_i^4)+\frac{a_2}{3}(r_k^3-r_j^3)\right.$$

$$\left.+\frac{b_2}{4}(r_k^4-r_j^4)+\frac{a_3}{3}(r_i^3-r_k^3)+\frac{b_3}{4}(r_i^4-r_k^4)\right]$$

$$\lambda_8 = \iint zr\,drdz = -\oint \frac{rz^2}{2}\,dr = -\left[\frac{a_1^2}{4}(r_j^2-r_i^2)+\frac{a_1 b_1}{3}(r_j^3-r_i^3)\right.$$

$$+\frac{b_1^2}{8}(r_j^4-r_i^4)+\frac{a_2^2}{4}(r_k^2-r_j^2)+\frac{a_2 b_2}{3}(r_k^3-r_j^3)$$

$$+\frac{b_2^2}{8}(r_k^4-r_j^4)+\frac{a_3^2}{4}(r_i^2-r_k^2)+\frac{a_3 b_3}{3}(r_i^3-r_k^3)$$

$$\left.+\frac{b_3^2}{8}(r_i^4-r_k^4)\right]$$

where

$$a_1 = z_i - b_1 r_i \qquad b_1 = \frac{z_j - z_i}{r_j - r_i}$$

$$a_2 = z_j - b_2 r_j \qquad b_2 = \frac{z_k - z_j}{r_k - r_j}$$

$$a_3 = z_k - b_3 r_k \qquad b_3 = \frac{z_i - z_k}{r_i - r_k}$$

However, there are simplified expressions for these integrals which are approximate in the case of λ_4, λ_5, λ_6 and λ_9 to λ_{11}. These approximations are valid under the assumption that the dimension of the cross section of the element is small compared to its radius of revolution. The simplified forms are:

$$\lambda_1 = A \bar{r}$$

$$\lambda_2 = A$$

$$\lambda_3 = A \bar{z}$$

$$\lambda_4 = A/\bar{r}$$

$$\lambda_5 = A \bar{z}/\bar{r}$$

$$\lambda_6 = \frac{A}{12 \bar{r}} [(z_i + z_j)^2 + (z_j + z_k)^2 + (z_k + z_i)^2]$$

$$\lambda_7 = \frac{A}{12} [(r_i + r_j)^2 + (r_j + r_k)^2 + (r_k + r_i)^2]$$

$$\lambda_8 = A\bar{z}\bar{r}$$

where

$$2A = r_i (z_j - z_k) + r_j(z_k - z_i) + r_k(z_i - z_j)$$

$$\bar{r} = \frac{1}{3} (r_i + r_j + r_k)$$

and

$$\bar{z} = \frac{1}{3} (z_i + z_j + z_k)$$

APPENDIX C

USE OF SINGH AND MITCHELL'S EMPIRICAL CREEP LAW

Singh and Mitchell's Creep Law

Singh and Mitchell (1968, 1969) have developed a very useful generalized stress-strain-time function for cohesive soils which is based on the study of creep curves for many cohesive soils over a range of sustained deviatoric stresses:

$$\dot{\varepsilon} = Ae^{\alpha D} \left(\frac{t_1}{t}\right)^m \qquad (C.1)$$

The parameters in Equation C.1 are explained with the aid of Figure C.1.

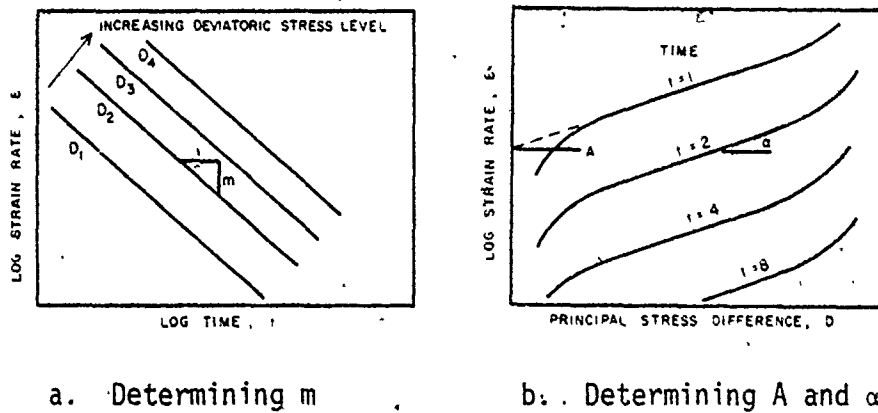a. Determining m   b. . Determining A and α

FIGURE C.1   STRAIN RATE EQUATION PARAMETERS
(Singh and Mitchell, 1968)

where:

$\dot{\varepsilon}$ is the strain rate at time t and is a function of the deviatoric stress D;

A   is the projected value of strain rate at time t_1 (t_1 usually

takes as unity) and $D = 0$, i.e. $A = \dot{\varepsilon}(t_1, D = 0)$;

α is the slope of the mid-range linear portion of the log strain rate - deviatoric stress plot, all points corresponding to the same t, i.e. slope of log $\dot{\varepsilon}$ - D plot;

m is the slope of the straight lines on the log strain rate - log time plot, i.e. slope of log $\dot{\varepsilon}$ - log t plot.

This simple three-parameter relationship (Equation C.1) appears approximately valid irrespective of whether the clays are undisturbed or remolded, wet or dry, normally consolidated or overconsolidated, or tested drained or undrained. The parameters A, α and m can be readily determined from creep tests on two identical samples subjected to different deviatoric stresses. The 'fictitious' nature of the parameter A is apparent in Figure C.1. However, Singh and Mitchell feel that parameter A is meaningful in that it indicates the order of magnitude of the creep rate for the particular cohesive soil, and reflects the structure, composition and stress history. The parameter α indicates the stress level effect on creep rate and, from analogy with rate process theory, it may be hypothesized that α reflects the number of bonds per unit area resisting the creep movement. The parameter m provides a measure of the creep potential: soils with $m < 1$ eventually fail in creep rupture (strain softening); soils with $m = 1$ seem to exhibit the same strength before and after creep; and soils with $m > 1$ exhibit cessation of creep with time under constant load (strain hardening). It has been observed that m is not-unique for a given cohesive soil and depends on the consolidation history. Thus, it is critical that the A, α and m parameters for Equation C.1 be developed for the appropriate soil   and

anticipated in the field. On the basis of its simplicity and adequacy in describing the creep deformations of a wide range of soils, Equation C.1 was adopted during the analysis of the tunnel in siltstone.

The strain can then be obtained for a given deviatoric stress level D. Integrating Equation C.1 results in two solutions:

a. <u>If $m \neq 1$</u> $\varepsilon = Ae^{\alpha D}(t_1)^m(\frac{1}{1-m})t^{1-m}$ + Constant (C.2)

b. <u>If $m = 1$</u> $\varepsilon = Ae^{\alpha D}(t_1)\ln t$ + Constant (C.3)

Considering the first solution case ($m \neq 1$) with $t_1 = 1$, and taking $M = 1-m$

$$\varepsilon = C + \frac{A}{M} e^{\alpha D}(t)^M \quad (m \neq 1, t_1 = 1) \quad (C.4)$$

At $t = 1$, $\varepsilon = \varepsilon_1$ = strain at unit time $t = 1$,

therefore, $C = \varepsilon_1 - \frac{A}{M} \varepsilon^{\alpha D}$ (C.5)

Equation C.4 then becomes:

$$\varepsilon = \varepsilon_1 + \frac{A}{M} e^{\alpha D}(t^M - 1) \quad (C.6)$$

ε_1 is considered to be the 'initial elastic strain', i.e. at time $t = 1$, the initial elastic strain is known, assuming $\varepsilon^c = 0$ at $t = 1$ where the subscript c designates a creep strain or creep strain rate.

Therefore, $\varepsilon^c = \frac{A}{M} e^{\alpha D}(t^M - 1)$ (C.7)

giving the desired creep strain equation, or substituting $M = 1 - m$

$$\varepsilon^c = \frac{A}{1-m} e^{\alpha D}(t^{1-m} - 1) \quad (C.8)$$

Equation c.7 will be considered the basic form of the creep law for the analysis:

$$\dot{\varepsilon}^C = \frac{A}{M} e^{\alpha D}(t^M - 1) \tag{C.9}$$

with the limitations $m \neq 1$ and where $M = 1 - m$. If $m > 1$; M will be - ve and ε^C will be + ve with $\dot{\varepsilon}$ decreasing. If $m < 1$; M will be + ve and ε^C will be + ve with $\dot{\varepsilon}$ increasing.

Function TM1

Determination of the first time increment in computer program

Δt_1 is taken from $t = 1$ for the first increment and $\varepsilon^C = \frac{\varepsilon^E}{25}$ (where ε^E is the elastic strain), therefore

$$\Delta \varepsilon^C = \frac{A}{M} e^{\alpha D}[(1 + \Delta t_1)^M - 1] \tag{C.10}$$

$$(1 + \Delta t_1)^M = \frac{M \varepsilon^C}{A e^{\alpha D}} + 1$$

$$1 + \Delta t_1 = [\frac{M \varepsilon^C}{A e^{\alpha D}} + 1]^{1/M}$$

$$\Delta t_1 = [\frac{M \varepsilon^C}{A e^{\alpha D}} + 1]^{1/M} - 1 \tag{C.11}$$

therefore the first time increment Δt_1 can be computed based on

$$\varepsilon^C = \frac{\varepsilon^E}{25}$$

which is a limit to ensure solution stability (Emery, 1978).

Function TMCL

Determinations of the creep strain increments and the fictitious time t_f for further increments

$$\varepsilon^C = \frac{A}{M} e^{\alpha D}[t^M - 1] \tag{C.12}$$

For the strain hardening cumulative creep rule (Emery, 1978):

$$\Delta\epsilon^C = \frac{A}{M} e^{\alpha D}\{[(t_f + \Delta t)^M - 1] - [t_f^M - 1]\}$$

$$\Delta\epsilon^C = \frac{A}{M} e^{\alpha D}[(t_f + \Delta t)^M - (t_f)^M]$$

Also, for $t = t_f$ Equation C.12 is:

$$\epsilon^C = \frac{A}{M} e^{\alpha D}[t_f^M - 1] \qquad\qquad (C.13)$$

and
$$t_f = [\frac{M\epsilon^C}{Ae^{\alpha D}} - 1]^{1/M}$$

where ϵ^C is the previous total creep strain.